Master's Thesis

Daniel Sadra, B.Eng.

Contact-free Vibration Measurements with Particle Velocity Probes

Fakultät Technik und Informatik
Department Fahrzeugtechnik und Flugzeugbau

Faculty of Engineering and Computer Science
Department of Automotive and Aeronautical Engineering

Daniel Sadra, B.Eng.

Contact-free Vibration Measurements with Particle Velocity Probes

Masterarbeit eingereicht im Rahmen der Masterprüfung

im Studiengang Flugzeugbau / Entwurf und Leichtbau
am Department Fahrzeugtechnik und Flugzeugbau
der Fakultät Technik und Informatik
der Hochschule für Angewandte Wissenschaften Hamburg

in Zusammenarbeit mit:
Microflown Technologies
Tivolilaan 205
6824 BV Arnhem
The Netherlands

Erstprüfer:	Prof. Dr.-Ing. habil. Thomas Kletschkowski
Zweitprüfer :	Emiel Tijs, PhD
Industrieller Betreuer:	Emiel Tijs, PhD
Abgabedatum:	12. September 2013

Abstract

Daniel Sadra, B.Eng.

Title of the master's thesis

Contact-free Vibration Measurements with Particle Velocity Probes

Keywords

Vibroacoustics, structural dynamics, measurement technique, Microflown

Abstract

This master's thesis reports on the contact-free vibration measurements with particle velocity probes. The aim of this thesis is to determine, if it is possible to measure a structural oscillation using particle velocity probes. The 3-D probe in the investigations can be applied to measure both the particle velocity (in all three directions (x,y,z)) and sound pressure.

A big advantage of contact-free vibration measurement is the accuracy in measurement results compared to conventional methods, because it is not necessary to de-tune the structure by the attachment of sensors. Even for carbon fibre structures no damage of the surface has to be taken into account.
Nowadays it is essential to have a measurement technique which can be used at any time, inflight or on ground.

The investigation has been carried out at the University of Applied Sciences Hamburg under the chair of Prof. Dr.-Ing. (habil.) Thomas Kletschkowski and in cooperation with Microflown Technologies, Arnhem, the Netherlands.

In the first part of the thesis, the vibro-acoustic test environment is described. The acoustic and structural resonances have been calculated theoretically first and then have been measured to control if the results can be matched. Furthermore some investigations on the self-noise of the used measurement technique have been performed in order to get a general idea about a good signal-to-noise ratio and the minimum level of excitation.

In the second part the measurement of the structural vibration with particle velocity probes is described. This thesis describes a coherence based approach and proves that it is not necessary to use structural sensors, such as accelerometers.
A parameter variation to proof this method has been performed. According to that, the influence of background noise has been examined. Moreover a method for the qualification of the signal-to-noise ratio using the transfer function and the auto spectral density is illustrated.

Finally some guidelines for an appropriate use of the acoustic sensor have been formulated and the results summarized.

Kurzfassung

Daniel Sadra, B.Eng.

Thema der Masterthesis

Kontaktfreie Vibrationsmessung mit Hilfe von Schallschnelle-Sonden

Stichworte

Vibroakustik, Strukturdynamik, Messtechnik, Microflown

Kurzfassung

Die vorliegende Masterarbeit beschreibt die kontaktfreie Vibrationsmessung mit Hilfe von Schallschnelle-Sonden. Das Ziel dieser Arbeit ist es herauszufinden, ob es möglich ist, die Vibration von Strukturen mit Schallschnelle-Sonden messen zu können. Die für die Untersuchungen verwendete dreidimensionale Sonde kann sowohl den Schalldruck als auch die Schallschnelle in allen drei Raumrichtungen (x,y,z) messen.

Ein großer Vorteil der kontaktfreien Vibrationsmessung ist die Genauigkeit der Messergebnisse gegenüber konventioneller Verfahren, da das System nicht durch zusätzliche Massen (Beschleunigungssensoren etc.) verstimmt wird. Für Kohlefaserstrukturen kommt zusätzlich hinzu, dass deren Oberfläche nicht verletzt wird. Heutzutage ist es notwendig, Messtechnik zu verwenden, die unter allen Umständen eingesetzt werden kann – ob am Boden oder während eines Flugversuchs.

Die Untersuchungen wurden an der Hochschule für Angewandte Wissenschaften in Hamburg am Lehrstuhl von Herrn Prof. Dr.-Ing. (habil) Thomas Kletschkowski und in Kooperation mit Microflown Technologies aus Arnhem, Holland, durchgeführt.

Im ersten Teil der Arbeit wird der verwendete vibroakustische Prüfstand beschrieben. Die akustischen und strukturellen Resonanzen wurden sowohl theoretisch als auch experimentell bestimmt. Um einen guten Signal-Rauschabstand während der Messung zu garantieren, wurden einige Untersuchungen zum Eigenrauschen der verwendeten Sensoren durchgeführt.

Im zweiten Teil der Arbeit wird die Messung von Strukturschwingungen mit Schallschnelle-Sonden beschrieben. Es wird ein Ansatz für ein kohärenzbasiertes Verfahren vorgestellt, der zeigt, dass es nicht nötig ist, Sensoren auf der Struktur zu verwenden.
Um diesen Ansatz zu verifizieren, wurden Parametervariationen durchgeführt. Begleitend dazu wurde der Einfluss von Hintergrundrauschen untersucht. Für die Qualifizierung des Signal-Rauschabstandes wird eine Methode, die auf den Transferfunktionen und den autospektralen Leistungsdichten beruht, vorgestellt.

Abschließend wurden Richtlinien für die korrekte Handhabung der akustischen Sonde formuliert und die Ergebnisse zusammengefasst.

Acknowledgement

It would not have been possible to write this master's thesis without the help and support of some people to whom I would like to give particular mention here.

Above all, I would like to express my deep gratitude to Professor Dr.-Ing. (habil.) Thomas Kletschkowski for his patient guidance, enthusiastic encouragement and useful critiques throughout my master's thesis. Especially his fundamental knowledge in the fields of vibro-acoustics and structural dynamics and the sharing of knowledge made this final thesis such a great experience for me.

I would also like to thank Microflown Technologies, the partner in the Netherlands, who agreed to do this master's thesis in cooperation with the chair of Prof. Kletschkowski. Primarily Mr. Emiel Tijs, PhD, for his expertise in handling the Microflown probe, helping during difficult questions and the approval to be the second reviewer.

Furthermore I would like to thank the Helmut Schmidt University Hamburg, especially the Labor of Mechatronics under the direction of Prof. Dr.-Ing. Delf Sachau for lending some parts of the measurement technique.

My grateful thanks are also extended to Mr. Dipl.-Ing. Bernd Troschitz, technical assistant of the Lightweight Laboratory of the Department of Automotive and Aeronautical Engineering of the University of Applied Science Hamburg for his help in offering me resources and helping to manufacture some mechanical parts contributing my thesis.

Finally, I wish to thank my parents for their support and encouragement throughout my study.

Table of Contents

List of Figures

List of Tables

List of Formula Symbols

Greek letters

Symbol	Unit	Marking
χ	$[N/m^2]$	Bulk modulus
λ_b	$[m]$	Wavelength of the bending wave
λ_n	$[m]$	Wavelength
μ	$[kg/m]$	Mass distribution
ν	$[Hz]$	Frequency (NASA Paper, [1])
ω_0	$[Hz]$	Eigen angular frequency
ω_n	$[Hz]$	Eigen angular frequency for certain order
φ_A	$[-]$	Test modal vector
φ_X	$[-]$	Analytical modal vector
ρ	$[kg/m^3]$	Density

Latin letters

Symbol	Unit	Marking
$(\ )_{rms}$	$[-]$	Root mean square of the value
$\{\ \}_q$	$[-]$	Mode q (MAC analysis)
$\{\ \}_r$	$[-]$	Mode r (MAC analysis)
$\{\ \}^T$	$[-]$	Transpose of the vector
A	$[m^2]$	Cross section area
b	$[m]$	Width
D	$[\%]$	Damping ratio
D_s	$[kg/s]$	Viscous damping
E	$[N/m^2]$	Young's modulus
f	$[Hz]$	Frequency
f_{cip}	$[Hz]$	Corner frequencies of the Microflown
f_n	$[Hz]$	Resonance frequency
F_s	$[N]$	External load

h	$[m]$	Height
I	$\left[mm^4\right]$	Moment of inertia
K_s	$[N/m]$	Spring stiffness
l	$[m]$	Length
L	$[dB]$	Sound level
$\overline{L}_p$	$[dB]$	Equivalent sound level
M_s	$[kg]$	Mass of piston
m_{beam}	$[kg]$	Mass of the beam structure
n	$[-]$	Order of the mode
p	$[Pa]$	Sound pressure
S_0	$[mV/g]$	Measured sensitivity
S_f	$[mV/g]$	Sensitivity for a certain frequency
t	$[s]$	Time
T_{30}	$[s]$	Reverberation time for 30dB drop-off
T_{60}	$[s]$	Reverberation time for 60dB drop-off
U	$[V]$	Voltage
V	$[m^3]$	Volume
v	$[m/s]$	Particle velocity
$\hat{x}$	$[-]$	Amplitude
Z	$[kg/m^2s]$	Acoustic resistance

Constants

Symbol	Value	Unit	Marking
a_0	$1 \cdot 10^{-6}$	$[m/s^2]$	Reference value for acceleration
a_s	$5 \cdot 10^{-8}$	$[m/s]$	Reference value for particle velocity
c	340	$[m/s]$	Speed of sound at 20°C
c_f	344	$[m/s]$	Speed of sound (NASA Paper, [1])
p_0	$2 \cdot 10^{-5}$	$[Pa]$	Threshold of audibility

List of Abbreviations

AC	Alternating Current
B&K	Bruel & Kjaer
BC	Boundary Condition
BNC	Bayonet Neill Concelman (Connerctor)
BGN	Background Noise
1-D	One dimensional
DIN	Deutsches Institut für Normung (German Institute for engineering standards)
ELAC	Manufacturer of acoustic components
EXC	Exciter
FEM	Finite Element Method
FFT	Fast Fourier Transformation
FSI	Fluid Structure Interaction
HAW	Hochschule für Angewandte Wissenschaften (Hamburg University of Applied Sciences)
HSU	Helmut Schmidt University, Hamburg
LDS	Product line of Bruel&Kjaer for vibration and controller products
LMS	Test set of the LMS International Company
LS	Loudspeaker
MAC	Modal Assurance Criterion
MATLAB	MATlab LABoratory (Software for the calculation of complex mathematical problems)
NASA	National Aeronautics and Space Administration
MDF	Medium Density Fiberboard
SC	Signal Conditioner
SH	Shaker
SNR	Signal-to-noise ratio
SPL	Sound Pressure Level
USP	Ultimate Sound Probe

1 Scope of work

Contact-free Vibration Measurements with Particle Velocity Probes

Student: Daniel Sadra, B.Eng., Master-Studiengang: Flugzeugbau, Matrikelnummer: 1925073
1st reviewer: Prof. Dr.-Ing. (habil.) Thomas Kletschkowski, Hamburg University of Applied Sciences, Faculty of Engineering & Computer Science, Department of Automotive and Aeronautical Engineering, Berliner Tor 9, 20099 Hamburg, Tel.: 040-428-75-7863, Email: thomas.kletschkowski@haw-hamburg.de
2nd reviewer[1]: Prof. M.Sc. Alexander Piskun, Hamburg University of Applied Sciences, Faculty of Engineering & Computer Science, Department of Automotive and Aeronautical Engineering, Berliner Tor 9, 20099 Hamburg, Tel.: 040-428-75-7888, Email: alexander.piskun@haw-hamburg.de

Scope of Work

The development of high performance – and nowadays lightweight – structural elements for aircraft systems or automotive applications, requires experimental investigations in order to characterize the response of existing or upcoming products to dynamic loads.

In order to detect structural vibrations, it is possible to attach conventional sensors (such as accelerometers) to the vibrating structure. Unfortunately, the latter is therefore detuned because of a change in mass, stiffness and/or dynamic absorption. These effects of sensors on the dynamic behavior can be avoided, if contact-free vibrations measurements are performed using non-contact inductive sensors or laser-scanning systems. However, the application of inductive sensors is limited to experimental investigations of metallic structures, and the use of laser scanning systems is at least impractical under working conditions (such as flight tests).

As shown in [Kletsch13], an alternative approach is based on contact-free vibration measurements with particle velocity probes that have to be used in the acoustic near field of a vibrating structure. However, to obtain reliable data, the signal-to-noise-ratio (SNR) between the self-noise of the sensor and the vibration level of the structure as well as the SNR between the investigated quantity and the acoustic background noise has to be acceptable. Furthermore, it is necessary to operate within an appropriate dynamic range. To evaluate the potential of a special acoustic sensor, it is necessary to:

1. Design a simplified test rig with defined boundary conditions,
2. Compare the self-noise of conventional sensors with the self-noise of the applied acoustic sensor,
3. Analyze the structural response of an integrated test structure using conventional sensors,
4. Analyze the structural response of the test structure with contact-free vibration measurements,
5. Study the influence of background noise and sensor location on the results,
6. Formulate guidelines for an appropriate use of the acoustic sensor.

References:

[Kletsch13] Kletschkowski T.: Identification of structural parameters based on acoustic measurements. To appear in Proc. of AIA-DAGA 2013 Conference on Acoustics, 18-21 March 2013, Merano, Italy

[1] Change in the position of the second reviewer. Emiel Tijs, PhD is allowed to be the 2nd reviewer according to the successful defeat of his PhD Thesis. He works for Microflown Technologies as a scientist and was the industrial advisor for this Master-Thesis. Tel: +31 880 010 841. Email: tijs@microflown.com

2 Theoretical background

2.1 Microflown‘s pu-probe

The Microflown is an acoustic sensor manufactured by Microflown Technologies in Arnhem, the Netherlands, which can measure the sound pressure and the particle velocity [2].

For this master’s thesis an ultimate sound probe (USP probe) has been used (figure 2-1). This probe represents the most advanced product of Microflown Technologies and consists of one pressure microphone and three orthogonal arranged particle velocity elements. It enables 3-dimensional broad-band sound (intensity) measurements [2]. Each direction is marked using a different color (blue for the x-direction, red for the y-direction and green for the z-direction).

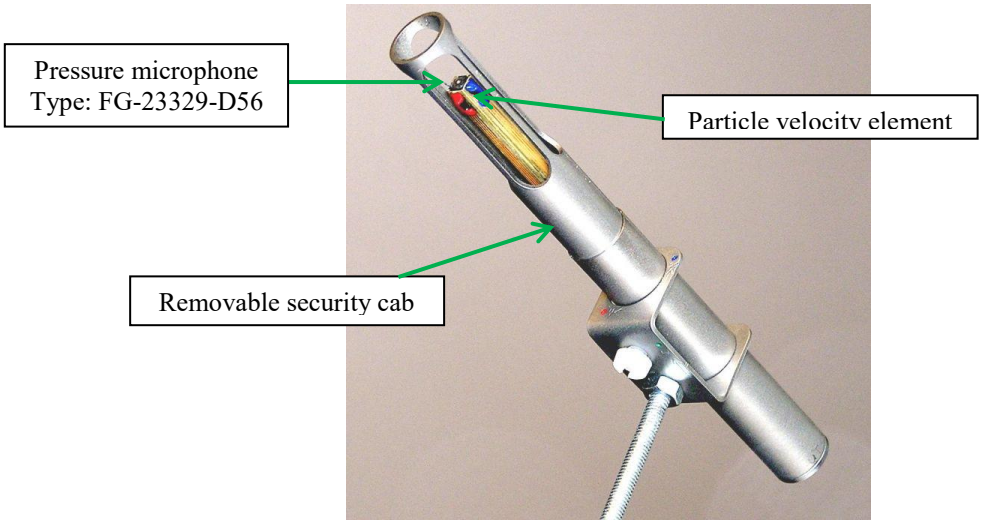

Figure 2-1 The Microflown USP probe, [3]

The particle velocity elements consists of closely arranged wires which are kept constantly heated to 200 degrees [4]. The length of the wires is 1mm, the width is 5mm and the thickness is 200nm platinum [2], (figure 2-2 left). Basically the sensor is a hot wire anemometer [5]. The airflow causes a temperature difference in the upstream and downstream wire of the particle velocity element. This temperature difference is proportional to the wires resistance providing a linear signal which is proportional to the particle velocity [4], (figure 2-2 right).

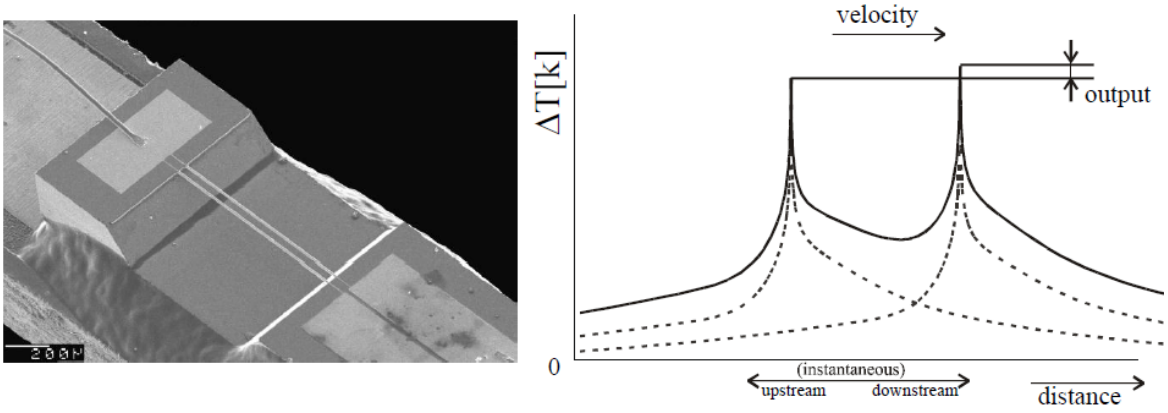

Figure 2-2 Sensor principle of the Microflown, [4]

2.1.1 The four channel signal conditioner

The measurement equipment that comes with the Microflown provides several additional possibilities to influence the data output.

The Microflown in sensitive to velocity (m/s) but not to sound pressure (Pa) [2]. That is the reason why the sensitivity cannot be given in mV/Pa. Microflown expresses the sensitivity in mV/Pa*. Pa* (velocity-Pascal) is the actual value of Pa referred to the impedance (equation [2-1]).

$$1Pa^* = \frac{1Pa}{\rho c} \qquad [2\text{-}1]$$

To enable measurements, the Microflown has to be connected to a signal conditioner. The schematic display is given in figure 2-3. Looking at the SC-Front, three switches can be seen. The first one is for the power supply on top, followed by one for the *Gain* settings (high/low) and one for the *Correction* (on/off). SC-Rear provides the connections for the Microflown probe (Lemo) as well as four BNC connectors for the pressure microphone and the particle velocity elements.

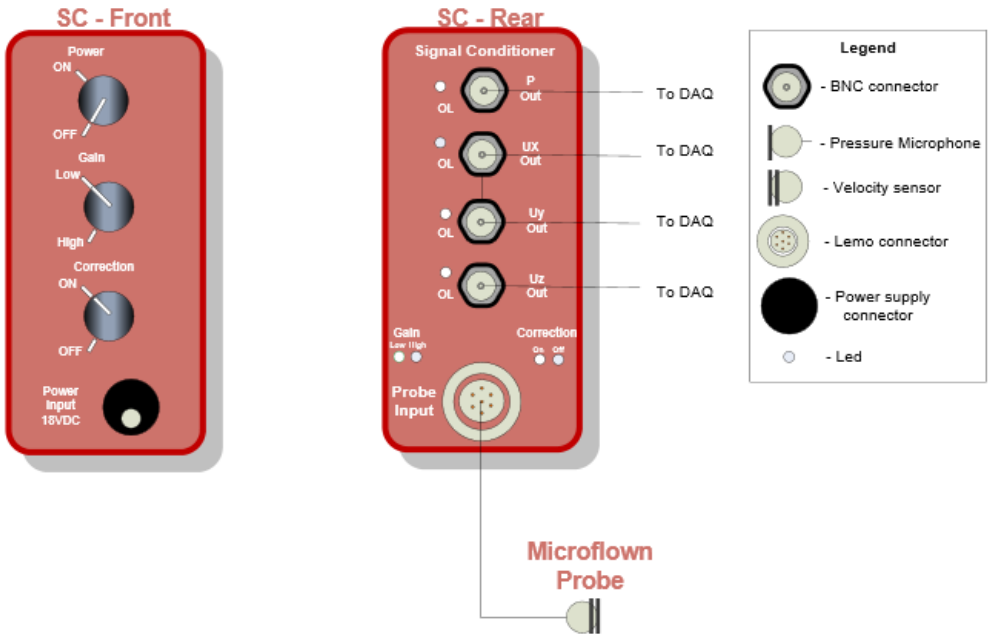

Figure 2-3 Schematic display of the signal conditioner, [6]

If the gain switch is set to high, the signal gets amplified by 40dB or in other words the sensitivity used in low gain settings is multiplied by a value of 100 (figure 2-4). Due to the fact that the sensitivity is frequency dependent, a correction can be applied. If the switch is set to on, the sensitivity will kept constant from around 100Hz onwards figure 2-4. The sensitivity can be calculated for each frequency. This is especially important for the post processing after the measurement (e.g. the implementation in MATLAB). The correction formulas are described in the following section 2.1.2.

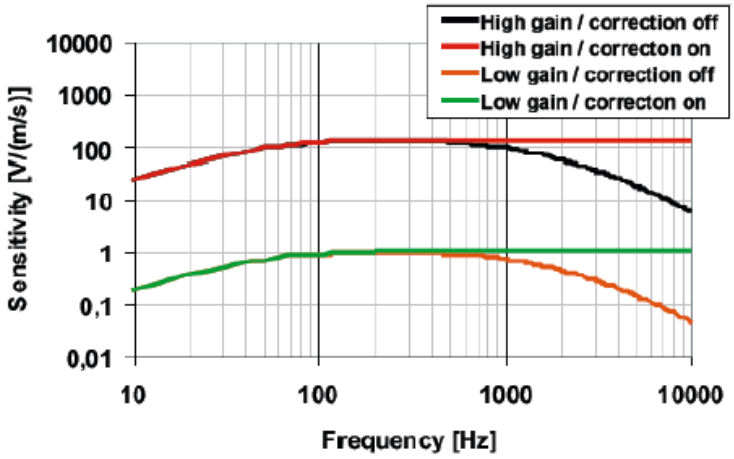

Figure 2-4 High/Low gain amplification, [6]

2.1.2 Correction formulas for the sensitivity

The high/low gain and correction on/off switches only affect the particle velocity output of the signal conditioner. The pressure output of the signal conditioner is unaffected [6].
The sensitivity correction for sound pressure microphone (where $S_p @ 1kHz$ is the nominal sensitivity given in the calibration report, f is the actual frequency given in Hz and f_{cip}^2 are the corner frequencies (table 2-1)) can be calculated using equation [2-2]. To calculate the sensitivity correction for the particle velocity elements, the nominal sensitivity $S_u @ 250Hz$ differs for high/low gain. The belonging corner frequencies stay the same.

$$S_p\left[mV/Pa\right] = S_p @ 1kHz \cdot \frac{\sqrt{1+\frac{f^2}{f_{c3p}^2}}}{\sqrt{1+\frac{f_{c1p}^2}{f^2}} \cdot \sqrt{1+\frac{f_{c2p}^2}{f^2}}} \qquad [2\text{-}2]$$

The corner frequencies for the microphone are:

Table 2-1 Corner frequencies Microflown microphone

corner frequency	microphone
fc1p	3 Hz
fc2p	182 Hz
fc3p	7531 Hz

For the particle velocity sensitivity two different filter-functions for the *uncorrected mode* (equation [2-3]) and for the *corrected mode* (equation [2-4]) have to be taken into account.

$$S_u\left[mV/Pa\right] = \frac{S_u @ 250Hz}{\sqrt{1+\frac{f_{c1u}^2}{f^2}} \cdot \sqrt{1+\frac{f^2}{f_{c2u}^2}} \cdot \sqrt{1+\frac{f^2}{f_{c3u}^2}} \cdot \sqrt{1+\frac{f_{c4u}^2}{f^2}}} \qquad [2\text{-}3]$$

$$S_u\left[mV/Pa\right] = \frac{S_u @ 250Hz}{\sqrt{1+\frac{f_{c1u}^2}{f^2}} \cdot \sqrt{1+\frac{f_{c4u}^2}{f^2}}} \qquad [2\text{-}4]$$

Each of the velocity sensor elements has different corner frequencies as shown in table 2-2.

Table 2-2 Corner frequencies Microflown particle velocity sensors

corner frequency	X-BLUE	Y-RED	Z-GREEN
fc1u	187 Hz	176 Hz	75 Hz
fc2u	746 Hz	649 Hz	675 Hz
fc3u	8687 Hz	9979 Hz	11692 Hz
fc4u	77 Hz	77 Hz	77 Hz

It can be noticed, that the corner frequencies for each particle velocity sensor in the corrected mode (equation [2-4]) act a low-pass filter, whereas for the uncorrected mode (equation [2-3]), two low-pass as well as two high-pass filter are applied. If the uncorrected mode is set for measurements, equation [2-3] has to be used, for the corrected mode equation [2-4].

2.2 Structural dynamics

2.2.1 Natural frequencies of simple beam structure

The simplified beam structure should symbolize the beam inside the vibro-acoustic test rig which is assumed to be simply supported at both ends (figure 2-5).

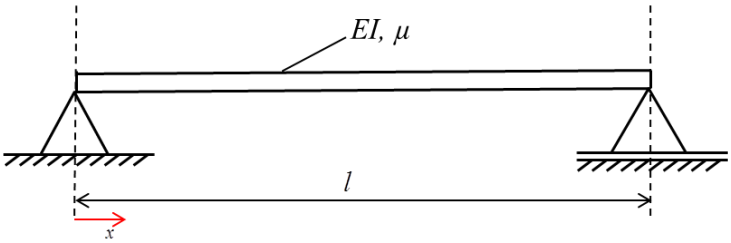

Figure 2-5 Simplified beam structure

For this case, [7] (page 228, eq. 14.38), it is possible to use equation [2-5] to calculate the eigen angular frequencies.

$$\omega_n = \frac{\pi^2 \cdot n^2}{l^2}\sqrt{\frac{EI}{\mu}} \qquad [2\text{-}5]$$

(n is the order of mode, l the length of the beam, E the Young's modulus, I the moment of inertia and μ the mass distribution)

The moment of inertia is calculated for the cross-section shown in figure 2-6 by using equation [2-6]:

$$I = \frac{b \cdot h^3}{12}. \qquad [2\text{-}6]$$

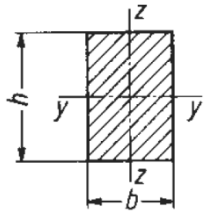

Figure 2-6 Cross section, [8] (2.4 Biegebeanspruchung, C11)

The beam mass (equation [2-7]) and the mass distribution (equation [2-8]) can be calculated:

$$m_{beam} = V \cdot \rho_{Alu} \qquad [2\text{-}7]$$

(V is the volume calculated $b \cdot h \cdot l$ and ρ the density)

$$\mu = \frac{m_{beam}}{l} \qquad [2\text{-}8]$$

2.2.2 Structural Vibration

For the modal analysis of an oscillating linear elastic system containing n degrees of freedom, the dynamic behavior can be described using n oscillators with a single degree of freedom. Performing the experimental modal analysis n is the amount of measurement points.

In the time domain, the dynamic behavior of an oscillator with a single degree of freedom can be described with a second order differential equation:

$$m\ddot{x}(t)+d\dot{x}(t)+kx(t)=f(t) \qquad [2\text{-}9]$$

(m is the mass, d the damping ratio of the system, k the stiffness of the system, $f(t)$ the excitation force as a function of time and x the displacement ($\dot{x}$ means fist derivation of x))

For a discrete system consisting of N oscillators with a single degree of freedom, the matrix representation looks like:

$$M\ddot{x}+D\dot{x}+Kx=F \qquad [2\text{-}10]$$

With the following parameters:

$M=[NxN]$ *Mass matrix*

$D=[NxN]$ *Damping matrix*

$K=[NxN]$ *Stiffness matrix*

$x=[Nx1]$ *Columnmatrix of the displacement* $(as\ a\ function\ of\ time)$

$F=[NxN]$ *Matrix of excitating forces*

An eigenvalue problem has to be solved for the solution of equation [2-10]. For the solution it is necessary to use a complex trial function:

$$x(t)=\hat{x}e^{\lambda t} \qquad [2\text{-}11]$$

The first and second time derivate of the trial function has to be substituted into equation [2-10]:

$$\ddot{x}(t)=\lambda^2\hat{x}e^{\lambda t} \qquad [2\text{-}12]$$

The result is an eigenvalue problem (equation [2-13]) and the corresponding characteristic equation [2-14].

$$\left(\lambda^2M+\lambda D+K\right)\hat{x}=0 \qquad [2\text{-}13]$$

$$\det(\lambda^2M+\lambda D+K)=0 \qquad [2\text{-}14]$$

The eigenvalues λ can be calculated, solving the characteristic equation [2-14]. If those are known, the mode shapes can be calculated too.

2.3 Engineering acoustics

2.3.1 Decibel scale for acoustic quantities

The decibel scale (dB) is a measure of different kind of signals to make them comparable. For this master's thesis sound pressure, accelerometer and particle velocity signals are essential. The equivalent level for each of these signals can be calculated using equation [2-15] to [2-17].

By looking at the named equations, it can be noticed that every equation has the same structure. The values a and p are the values measured whereas a_s and p_0 are reference values which can be taken out of table 2-3. The equivalent sound level for the sound pressure gets referred to the threshold of auditability. The accelerometer and the particle velocity signals get referred to a_s.

Table 2-3 Reference values for the calculation of the decibel scale

Symbol	value	
p_0	$2 \cdot 10^{-5}\ Pa$	threshold of auditability
v_0	$5 \cdot 10^{-8}\ m/s$	

Equivalent sound pressure level for microphones:

$$L_p = 20 \cdot \log\left(\frac{\tilde{p}_{rms}}{p_0}\right) \qquad [2\text{-}15]$$

Equivalent acceleration level for accelerometer:

$$L_a = 20 \cdot \log\left(\frac{\tilde{a}_{rms}}{\frac{\omega}{\rho \cdot c} \cdot p_0}\right) = 20 \cdot \log\left(\frac{\tilde{a}_{rms}}{\omega \cdot v_0}\right) \qquad [2\text{-}16]$$

Equivalent particle velocity level for velocity-sensor:

$$L_v = 20 \cdot \log\left(\frac{\tilde{v}_{rms}}{v_0}\right) \qquad [2\text{-}17]$$

An energetic averaging is necessary for the averaging of a various number of levels. If the variation between the levels is not bigger than 6dB, equation [2-18] is not applied.

The equivalent noise level is calculated using the following equation:

$$\bar{L}_p = 20 \cdot \log \sqrt{\frac{1}{N} \cdot \sum_{f=1}^{N} \left(\frac{p_{rms}(f)}{p_o} \right)^2} \,, \qquad [2\text{-}18]$$

(Similar formulas can be derived for $\bar{L}_a$ and $\bar{L}_v$)

2.3.2 Acoustic resonances of a rectangular enclosure

Inside a rectangular enclosure, acoustic waves can spread in all three directions (length, width and height). Axial (1D), tangential (2D) and oblique modes (3D) can occur. Axial modes occur between two opposite surfaces. Tangential modes between four surfaces and oblique modes need all six surfaces (figure 2-7). Axial modes are the most dominant modes, followed by tangential and oblique modes [9].

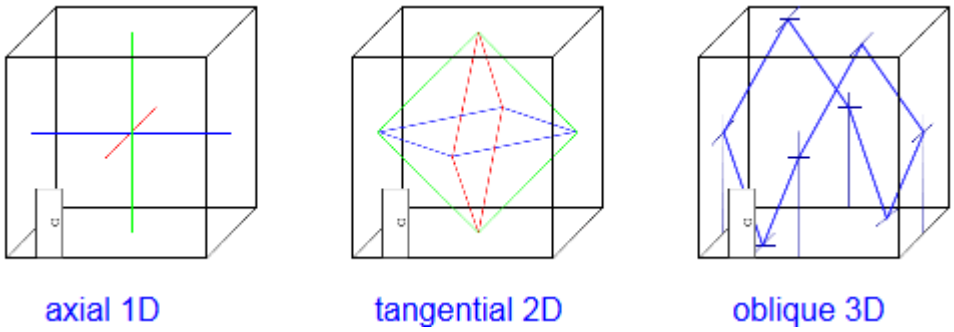

Figure 2-7 Acoustic modes inside enclosure, [9]

The resonant frequencies f_n and the according wavelength λ_n for the 1D case can be calculated using equations [2-19] and [2-20]. These equations assume a plane wave motion (axial mode) in the analyzed direction (as clarified in the simplified rectangular enclosure (figure 2-8).

$$f_n = \frac{nc}{2l} \qquad [2\text{-}19]$$

$$\lambda_n = \frac{c}{f_n} = \frac{2l}{n} \qquad [2\text{-}20]$$

(n is mode order, c the speed of sound at 20°C and l the belonging length of the enclosure)

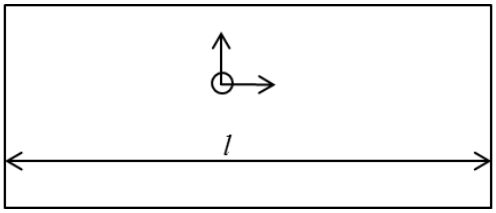

Figure 2-8 Simplified rectangular enclosure

2.3.3 Relation between acoustic pressure and particle velocity

The sound pressure level (SPL) is a measure for the acoustic potential which appears due to a chance in the pressure of the air. The SPL is commonly known as the volume which can be heard of human beings. Normally the sound pressure is given in Pascal $\left(1Pa = 1N/m^2\right)$ and bounded by the threshold of auditability which is defined at $2 \cdot 10^{-5} Pa$.

The particle velocity describes the speed of a medium particle performing small oscillations around its rest position. Usually the particle velocity is given as the amplitude per time.

$$v = \frac{d\xi}{dt} \qquad [2\text{-}21]$$

The relation between the acoustic pressure and the particle velocity can be developed from the law of inertia of the acoustics [10] (p.42, eq. 2.55a-2.55c):

$$\rho \frac{\partial v}{\partial t} + \frac{\partial p}{\partial x} = 0. \qquad [2\text{-}22]$$

Assuming time-harmonic fluctuations, such as $p(x,t) = p(x)e^{j\omega t}$ and $v(x,t) = v(x)e^{j\omega t}$, equation [2-22] results in equation [2-23] which can be used to calculate the particle velocity out of the sound pressure:

$$j\omega \cdot v = -\frac{1}{\rho}\frac{\partial p}{\partial x},$$

$$v = -\frac{1}{j\omega\rho}\frac{\partial p}{\partial x} \cdot \frac{j}{j},$$

$$v = \frac{j}{\omega\rho}\frac{\partial p}{\partial x}. \qquad [2\text{-}23]$$

Assuming a standing wave in front of an acoustically hard wall the particle velocity is theoretically zero in front of the wall, whereas the sound pressure has a maximum in amplitude (figure 2-9).

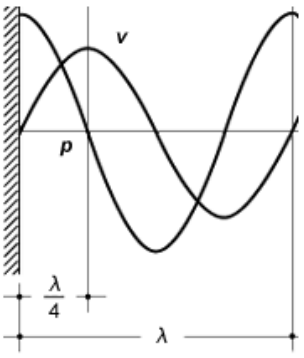

Figure 2-9 Sound pressure and particle velocity, [11]

2.3.4 Determination of damping parameters

The *damping ratio* D is a non-dimensional characteristic number for the qualification of the damping in a mechanical system. Moreover it describes how an oscillation of the system decays after a certain period of time.
After the acoustic measurement has been performed and the time signal has been recorded, the damping ratio can be determined by using equation [2-24]. The damping ratio is developed from the approach of a harmonic function:

$$x(t) = \hat{x} \cdot e^{-D\omega_0 t} \cos(\omega t + \varphi_0)$$

Looking at two different instances of time gives the ration:

$$\frac{x(t_1)}{x(t_1 + n \cdot T)} = \frac{e^{-D\omega_0 t_1}}{e^{-D\omega_0 (t_1 + n \cdot T)}} = e^{-D\omega_0 t_1} \cdot e^{D\omega_0 t_1} \cdot e^{D\omega_0 nT} = e^{D\omega_0 nT},$$

and the damping ratio (equation [2-24]) can be defined:

$$D = \frac{1}{n\omega_0 T} \cdot \ln\left(\frac{x(t_1)}{x(t_1 + nT)}\right) \qquad [2\text{-}24]$$

The *reverberation time* T_{60} is determined as the time where the noise level is decreased by a value of 60dB. During the post processing of the measurement data, the damping ratio can be derived from the linear decrease of the noise level.

$$-60dB = L\left(\frac{x(t_1 + T_{60})}{x(t_1)}\right) \text{ with } T_{60} = nT,$$

$$-60dB = 10\log_{10}\left\{\left(\frac{e^{-D\omega_0 (t_1 + n \cdot T)}}{e^{-D\omega_0 t_1}}\right)^2\right\}$$

After some mathematical conversions the damping ratio (equation [2-25]) can be defined as:

$$D = \frac{6.91}{T_{60} \cdot \omega_0}. \qquad [2\text{-}25]$$

In some cases, for a shorter reverberation, the linear decrease does not reach a value of 60dB, so that another value for the reverberation time (e.g. for 30dB→ T_{30}) has to be taken into account (equation [2-26]).

$$D = \frac{3.45}{T_{30} \cdot \omega_0} \qquad [2\text{-}26]$$

2.4 Modal assurance criterion

MAC is the abbreviation for ***M**odal **A**ssurance **C**riterion* and is a static indicator like the ordinary coherence [12]. The MAC is one of the most popular quantitative comparisons of modal vectors [13]. A MAC value of "1" means fully consistent mode shapes, whereas "0" means that the mode shapes are fully inconstant. Furthermore the MAC value is commonly used to compare mode shapes measured experimentally with those derived from analytical models [12], [13]. This is name "mode pairing".

The MAC is calculated using equation [2-27], [12], and is the normalized scalar product of two modal vectors.

$$MAC(r,q) = \frac{|\{\varphi_A\}_r^T \cdot \{\varphi_X\}_q|^2}{\left(\{\varphi_A\}_r^T \cdot \{\varphi_A\}_r\right) \cdot \left(\{\varphi_X\}_q^T \cdot \{\varphi_X\}_q\right)}, \qquad [2\text{-}27]$$

where $\{\varphi_X\}_q$ is the modal test vector for mode q and $\{\varphi_A\}_r$ is the compatible analytical modal vector for mode r.

The results can be organized in the MAC matrix, like the example given in figure 2-10. For the best case and fully consistent mode shapes, just the main diagonal have a MAC value of "1" and all off-diagonal elements are "0".

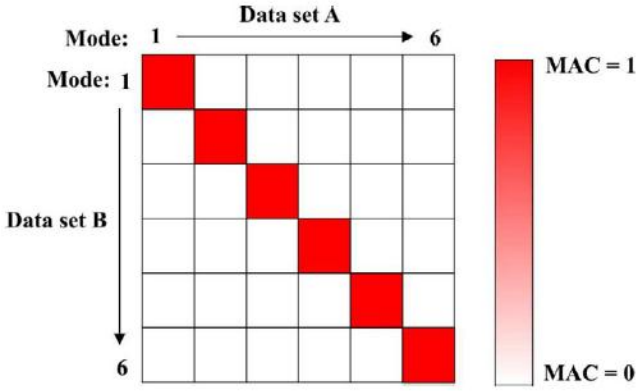

Figure 2-10 MAC matrix, [12]

2.5 Analysis of a one dimensional analytical model

It is very difficult to obtain a theoretical solution for practical fluid-structure interaction. However [1] (p.62 ff.) provides such an analytical model for a one dimensional sound tube with a length of $l = 1.25m$ (figure 2-11). After some simplifications the vibro-acoustic test rig gets represented the in a good way. The spring-damper-piston system can be compared to the beam structure inside cavity. Although the test rig is a two dimensional sound tube and the analytical model just allows a one dimensional observation, it can be used to obtain general ideas about how the vibro-acoustic test rig behaves under certain conditions. The parameters of this analytical model can be found in the MATLAB Code in appendix F and G.

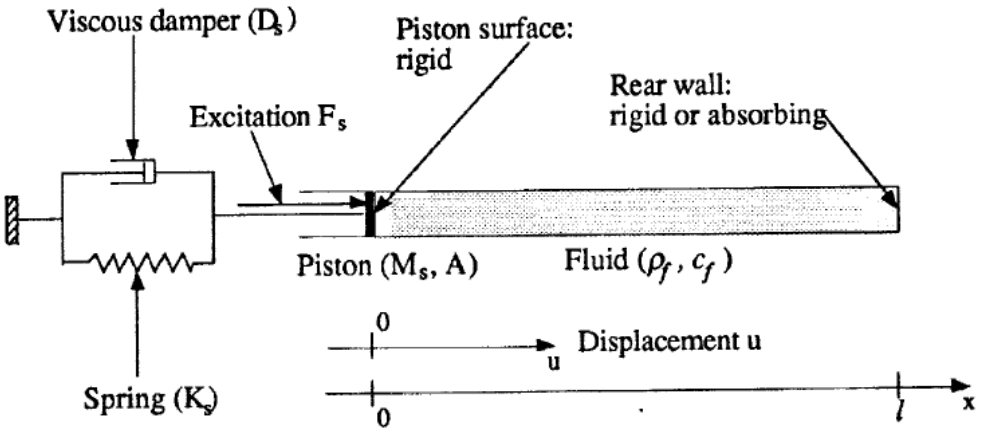

Figure 2-11 Spring-damper-piston-tube system, [1]

After some mathematical conversions ([1], p. 62-64) and the combination of the structural part of the equations combined with the acoustic part, a transcendental equation [2-28] for the frequencies $\nu = \nu_i \left(j = 1,2,3,... \right)$ of the coupled system is obtained:

$$\tan \frac{2\pi l}{c_f} \nu = \frac{Z_0 A}{2\pi M_s} \cdot \frac{\nu}{\nu^2 - \nu_s^2} \cdot \qquad [2\text{-}28]$$

(ν is the frequency, l the length of the tube, A the cross section Area, M_s the mass of the piston and Z_0 the impedance)

The natural frequencies of both the coupled and uncoupled system can be seen in table 2-4. (Parameters of the model extracted from [1] p.63 or seen in MATLAB Code – appendix F or G):

Table 2-4 Coupled and uncoupled natural frequencies of the analytical model

Spring-Piston-System	Tube (air-filled)	Coupled System
137.7 Hz	137.7 Hz	128.33 Hz
		147.18 Hz
	275.5 Hz	
	412.8 Hz	
	550.4 Hz	

The natural frequencies for the tube have been calculated using equation [2-19]. For the spring-piston system the natural frequencies can be calculated using equation [2-29]:

$$\nu_s = \frac{1}{2\pi}\sqrt{\frac{K_s}{M_s}}\,. \qquad [2\text{-}29]$$

To be able to calculate the frequency response of the piston displacement u (equation [2-30]) and the pressure p (equation [2-31]) of the coupled system, the boundary value problem has to be solved. The closed form solution, worked out in [1] is given by:

$$u(\nu) = \frac{f_{M_s}}{\left(\xi_1^2 + \xi_2^2\right)}\left(\xi_1 - i\xi_2\right) \qquad [2\text{-}30]$$

$$p(x,\nu) = 2\pi Z_0 \frac{f_{M_s}}{\xi_1^2+\xi_2^2}\left\{\begin{aligned}&\left[\xi_1\left(\Gamma_1\cos\frac{2\pi\nu}{c_f}x + \sin\frac{2\pi\nu}{c_f}x\right) + \xi_2\Gamma_2\cos\frac{2\pi\nu}{c_f}x\right] \\ &+i\left[\xi_1\Gamma_2\cos\frac{2\pi\nu}{c_f}x - \xi_2\left(\Gamma_1\cos\frac{2\pi\nu}{c_f}x + \sin\frac{2\pi\nu}{c_f}x\right)\right]\end{aligned}\right\} \qquad [2\text{-}31]$$

Respectively, where

$$\begin{aligned}\xi_1 &= \left(\nu_s^2 - \nu^2\right) + \frac{AZ_0}{2\pi M_s}\Gamma_1\nu \\ \xi_2 &= \frac{D_s + AZ_0\Gamma_2}{2\pi M_s}\nu \\ f_{M_s} &= \frac{F_s}{4\pi M_s}\end{aligned} \qquad [2\text{-}32]$$

$$\Gamma_1 = \frac{\frac{1}{2}\left[1-\alpha^2\left(\sigma^2-\gamma^2\right)\right]\sin\frac{4\pi l}{c_f}\nu + \alpha\sigma\cos\frac{4\pi l}{c_f}\nu}{\left(\sin\frac{2\pi l}{c_f}\nu + \alpha\sigma\cos\frac{2\pi l}{c_f}\nu\right)^2 + \alpha^2\gamma^2\left(\cos\frac{2\pi l}{c_f}\nu\right)^2} \qquad [2\text{-}33]$$

$$\Gamma_2 = \frac{\alpha\gamma}{\left(\sin\frac{2\pi l}{c_f}\nu + \alpha\sigma\cos\frac{2\pi l}{c_f}\nu\right)^2 + \alpha^2\gamma^2\left(\cos\frac{2\pi l}{c_f}\nu\right)^2}$$

$$\alpha = \begin{cases}0: \text{ boundary at x=l is rigid} \\ 1: \text{ boundary at x=l is absorbing}\end{cases}$$

$$\gamma = \frac{Z_0 + Z_1}{Z_1^2 + Z_2^2}, \qquad \sigma = -\frac{Z_0 + Z_2}{Z_1^2 + Z_2^2} \qquad [2\text{-}34]$$

$$Z_0 = \rho_f c_f, \quad Z_1 = \mathrm{Re}\{Z_n\}, \quad Z_2 = \mathrm{Im}\{Z_n\}$$

[1] provides two small typographical errors. At first the frequency in equation [2-33] is missing. Furthermore in the calculation of gamma and sigma, the nomenclature of the impedances is incorrect (equation [2-34]).

For the 1-D case, the complex particle velocity is the first derivation of the sound pressure (equation [2-31]). The second derivation of the sound pressure results in complex particle velocity gradient. Due to the fact that equation [2-31] is a combination of sine and cosine functions, the equation reproduces itself after two derivations.

A high sound pressure means a high gradient in particle velocity which means that the allowable distance for measurements decreases significantly. The allowable distance means the distance where the structural oscillation can be measured sufficiently well in the air. In the following this analytical model is used to get generate an idea about the influence of the distance for acoustic measurements.

The equations [2-30] till [2-34] have been implemented in the MATLAB Code given in appendix F and G.

To be sure that the implementation has been completed successfully, the results of the fully absorbing boundary condition (BC) (no reflections) will be shown first.

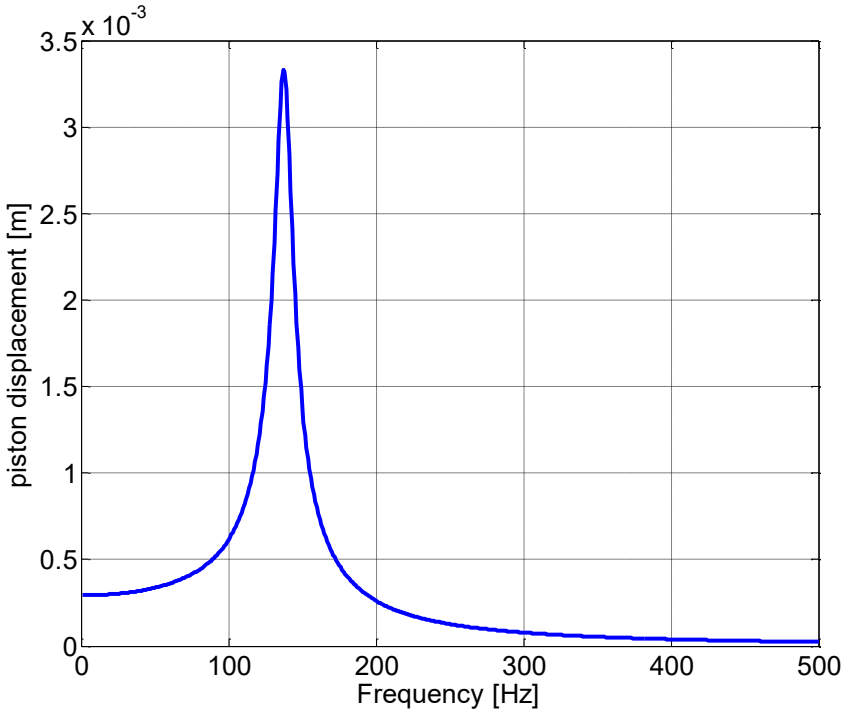

Figure 2-12 FRF of the analytical model for the fully absorbing boundary condition

The ***F**requency **R**esponse **F**unction* (FRF) has been calculated for the particle velocity of the piston. In the FRF for the fully absorbing boundary condition ($Z_1 = \rho c$, $Z_2 = 0$ at $x = l$) (figure 2-12) just one resonance can be found. This belongs to the fact that there are no reflections which may cause additional resonance peaks. The frequency belonging to the resonance can be found in table 2-4 as well.

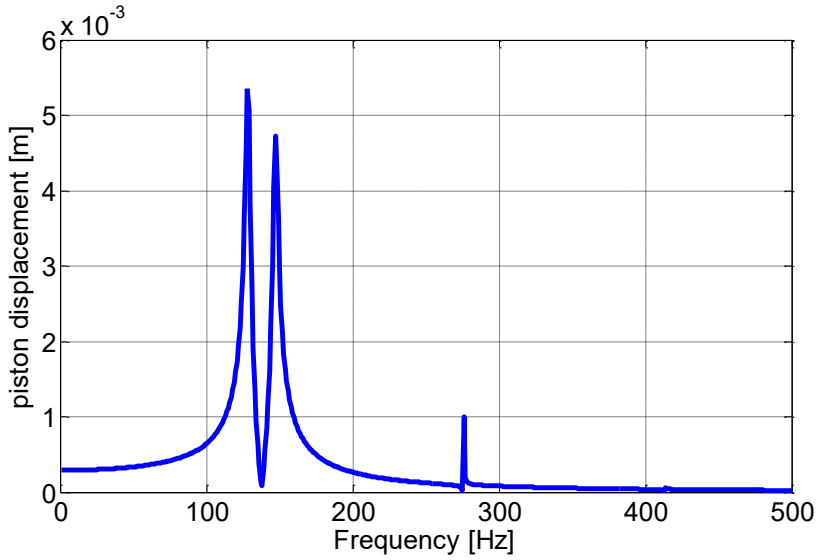

Figure 2-13 FRF for analytical model and acoustically hard boundary condition

The FRF for the acoustically hard boundary condition (Z_1 and Z_2 at $x = l$ given in [1]) shows two more resonances. This belongs to the reflections of the walls which are now sound hard. The resonances can also be found in table 2-4.

The failure in the magnitude has been calculated for four different distances (1.25mm, 6.25mm, 12,50mm and 62.50mm) by calculating the ratio between the complex particle velocity of the piston and the air (equation [2-35]):

$$failure = 1 - \frac{abs(v)}{abs(v_s)}. \qquad [2\text{-}35]$$

Distance means the difference between measurement point and piston surface. For the free field conditions there is as expected absolutely no failure in magnitude (figure 2-14). The y-axis has a scale of ten to the power of minus sixteen.

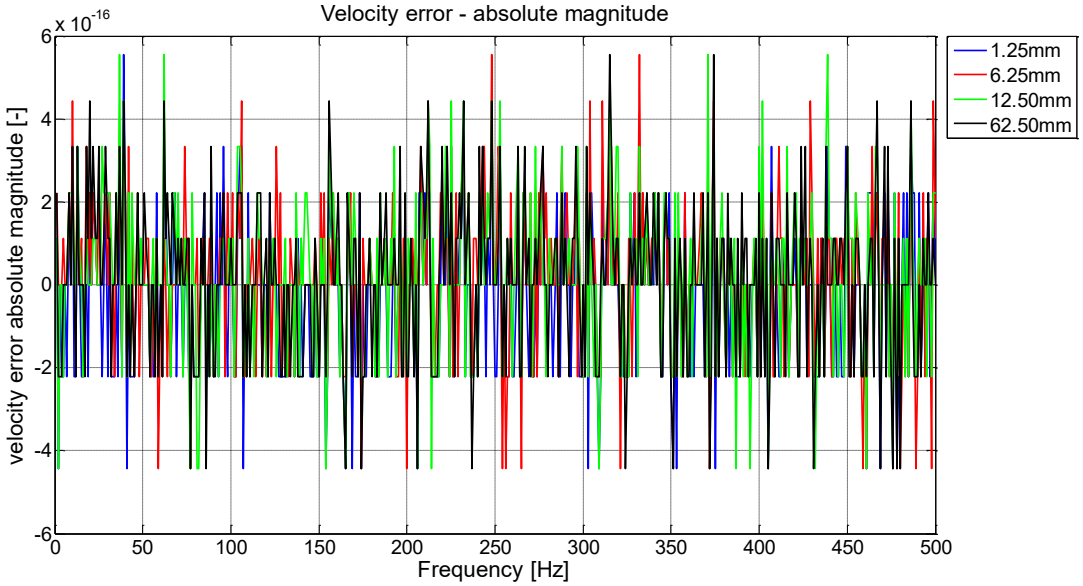

Figure 2-14 Velocity failure - absolute magnitude, absorbing BC

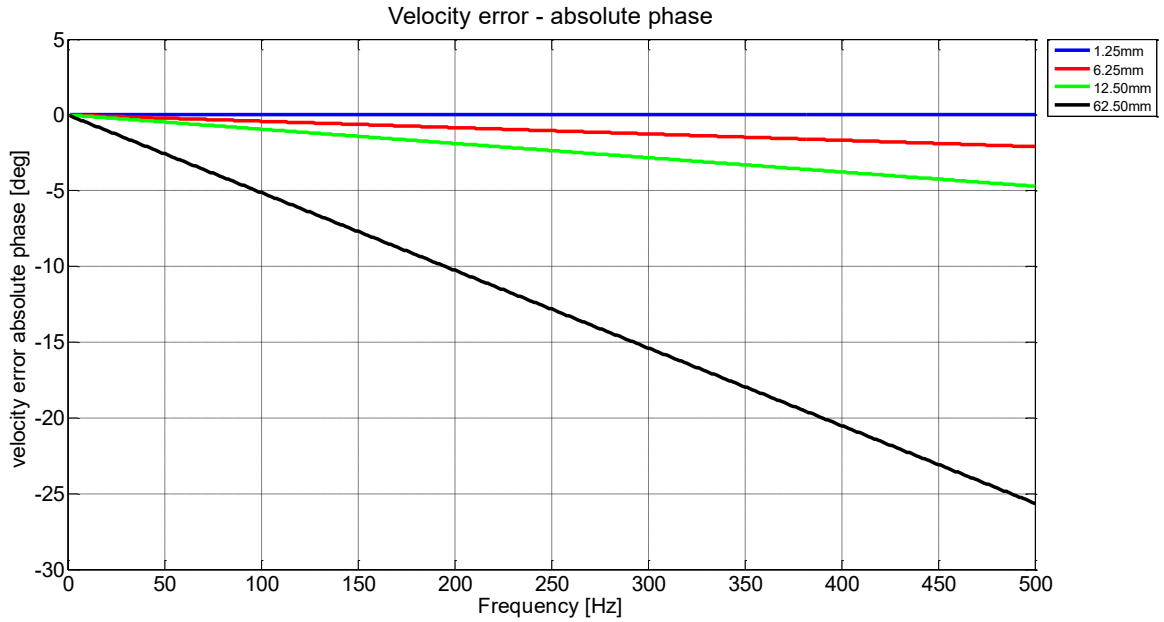

Figure 2-15 Velocity failure - absolute phase, absorbing BC

Figure 2-15 verifies that under free field conditions, the failure in the phase increases to higher frequencies in form of a linear function. The gradient rises with the measurement distance.

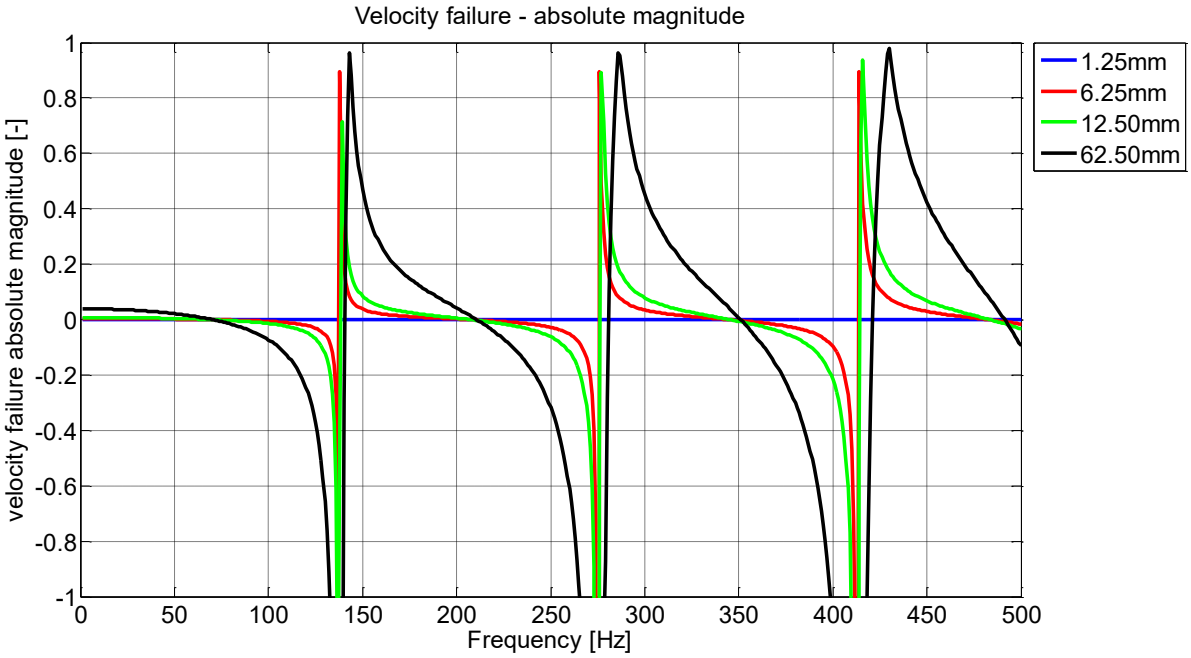

Figure 2-16 Velocity failure - absolute magnitude, acoustically hard BC

Figure 2-16 shows the velocity failure of the absolute magnitude according to the acoustically hard boundary condition in the frequency range up to 500 Hz. First of all it can be recognized, that the same pattern returns at certain frequencies and has a discontinuity where a division through zero takes place and the function switches from maximum negative to maximum positive (see also figure 2-17). These points are exactly the anti-resonances of the FRF given in figure 2-13. If the measurement will be performed right in front of the piston (blue line) the

failure is close to zero. By exceeding the distance to the piston, the failure rises. The effect is even bigger, if one gets closer to the anti-resonances.

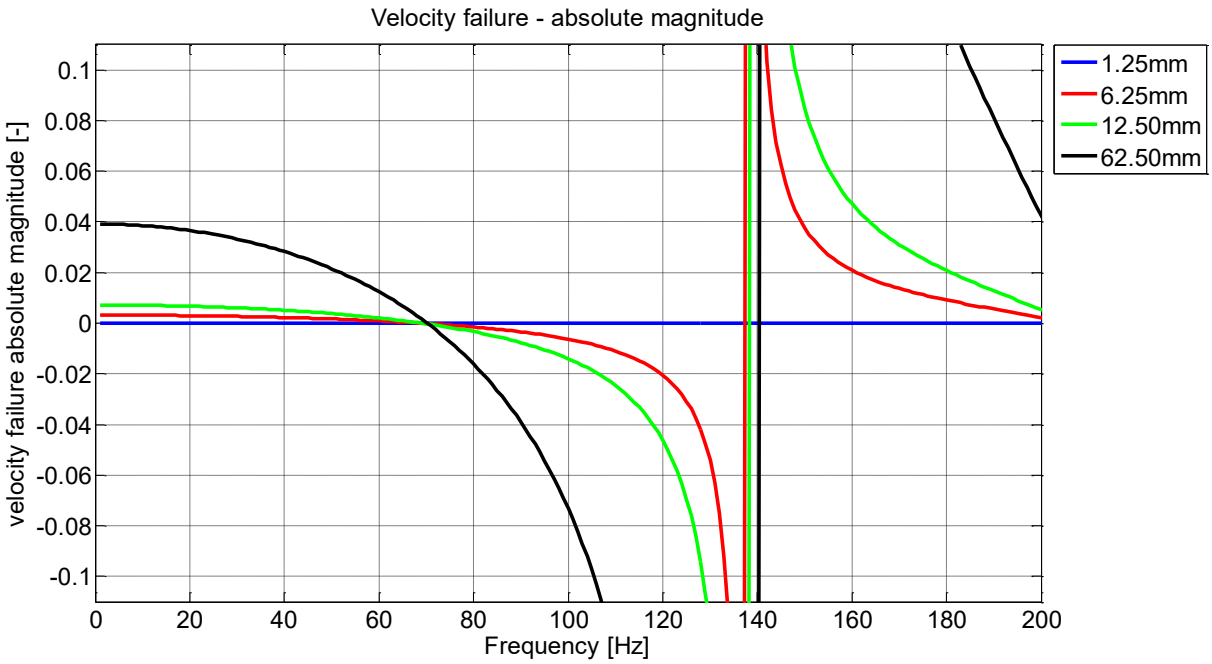

Figure 2-17 Velocity failure - absolute magnitude, acoustically hard BC zoomed in

Figure 2-17 is a zoomed in version of Figure 2-16 to have an idea what the failure even at the beginning is. It can be noticed that the failure is relatively small (first three distances) 0-1% failure in absolute magnitude, whereas the failure at a distance of 62.50mm is four times bigger. Moreover the gradient is the biggest.

The maximum allowable distance for a constant measurement error of one, five and ten percent (figure 2-19) has been calculated using an optimization algorithm in MATLAB which results in a numerical convergence if the objective function [2-36] is fulfilled. This algorithm iterates to the results. The criterion for the iteration can be seen in Nassi-Shneiderman diagram (figure 2-18).

$$abs\_feh(i) = 1 - abs\left(\frac{v(i)}{v_s(i)}\right) \qquad [2\text{-}36]$$

The acoustically hard BC has been taken into account. The MATLAB Code can be seen in appendix G. The maximum allowable distance rises with the measurement error. For one percent constant error (figure 2-19, blue curve) the smallest distances are allowed. The linear drop-off in figure 2-19 belongs to the chance in the sign of the error (see also figure 2-17). Those frequencies where all the curves drop to zero can clearly be identified as the anti-resonances (see figure 2-13).

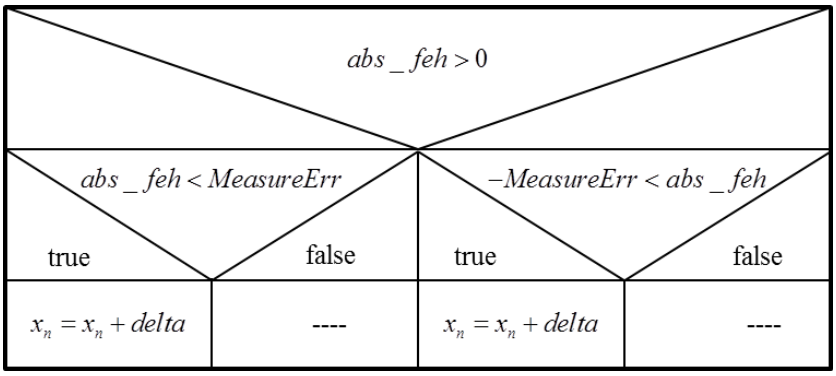

Figure 2-18 Nassi-Shneiderman diagram for iteration criterion

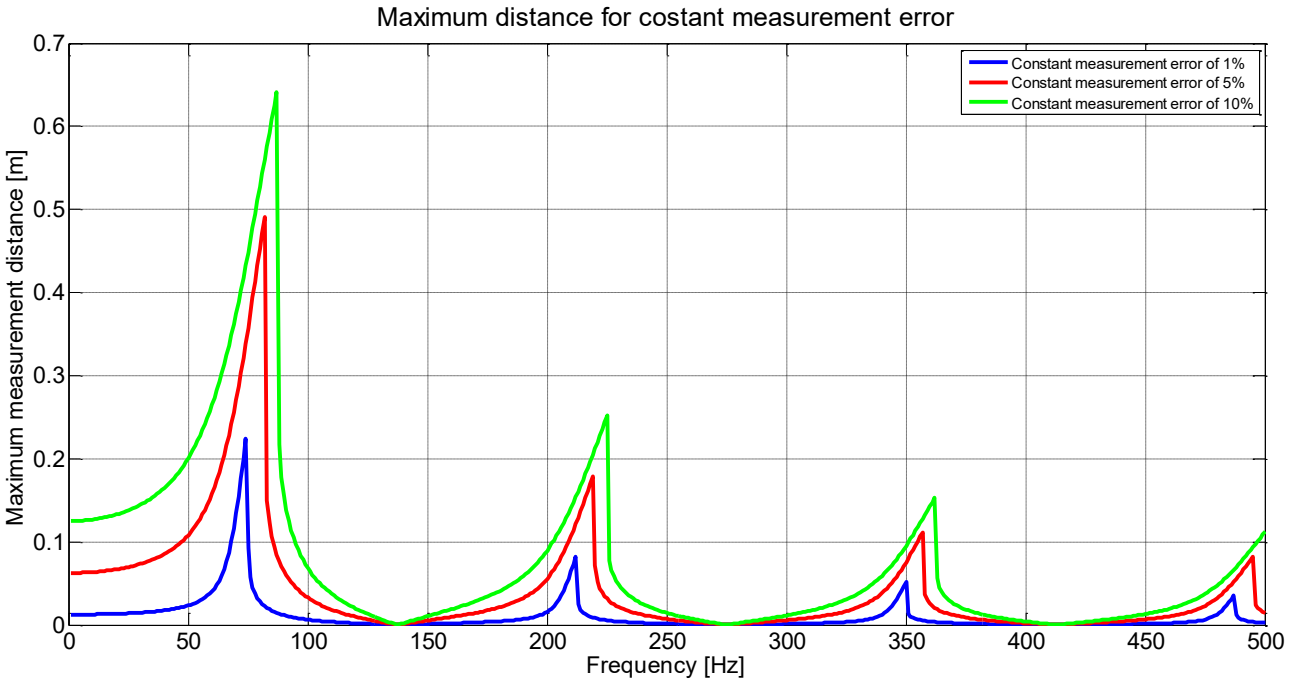

Figure 2-19 Maximum measurement distance of certain measurement errors

The FRF for the piston and the cavity as well as measurement error in dB have been plotted for those three cases of measurement errors to clarify the gained insights (figure 2-20 to figure 2-22). The distance is related to the wavelength.

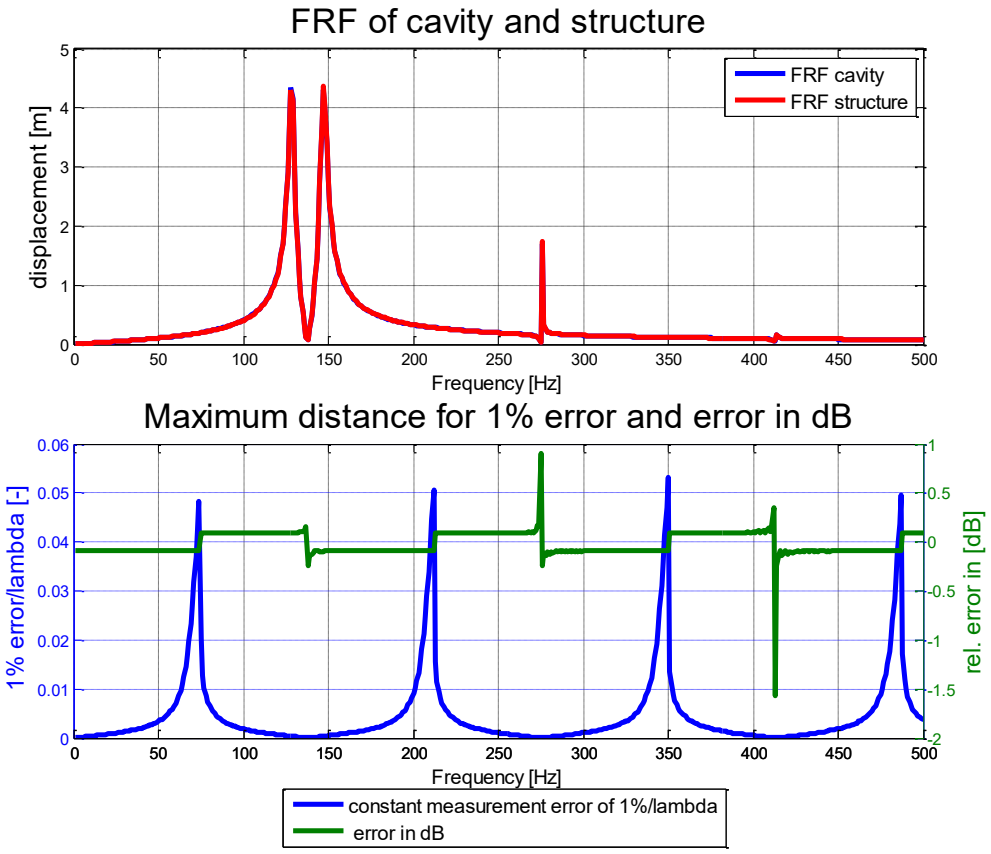

Figure 2-20 FRF of cavity and structure, 1% error and dB wise error

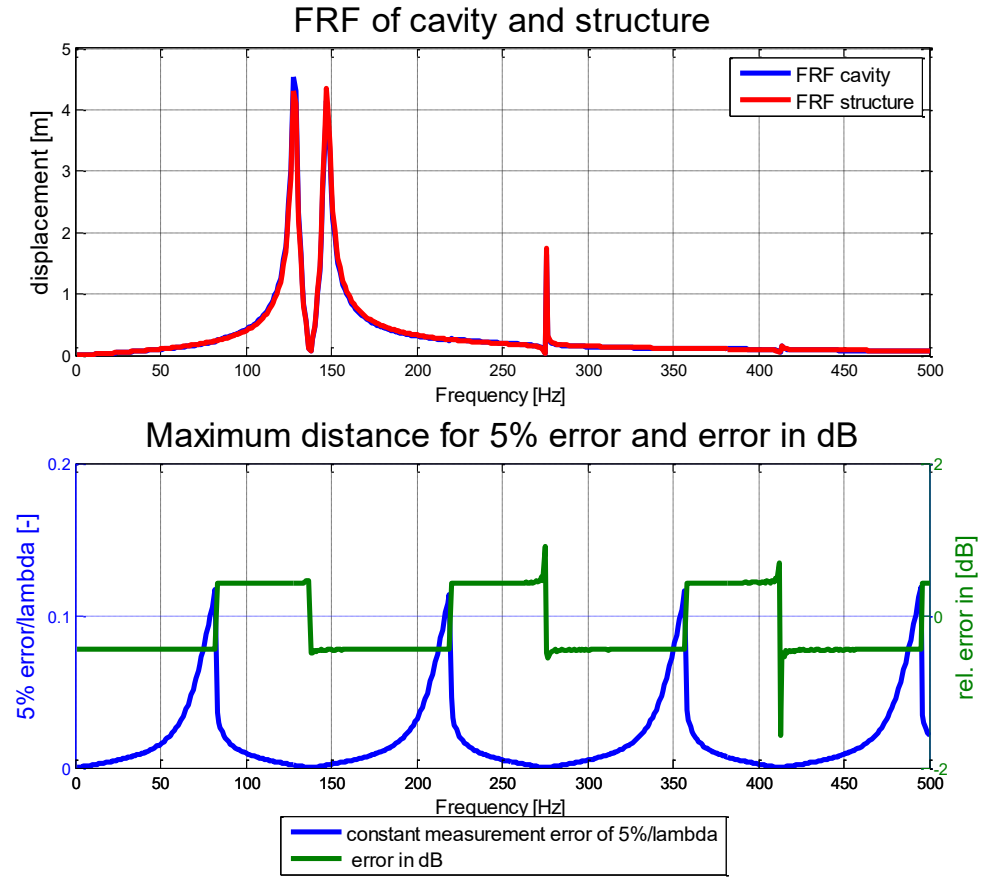

Figure 2-21 FRF of cavity and structure, 5% error and dB wise error

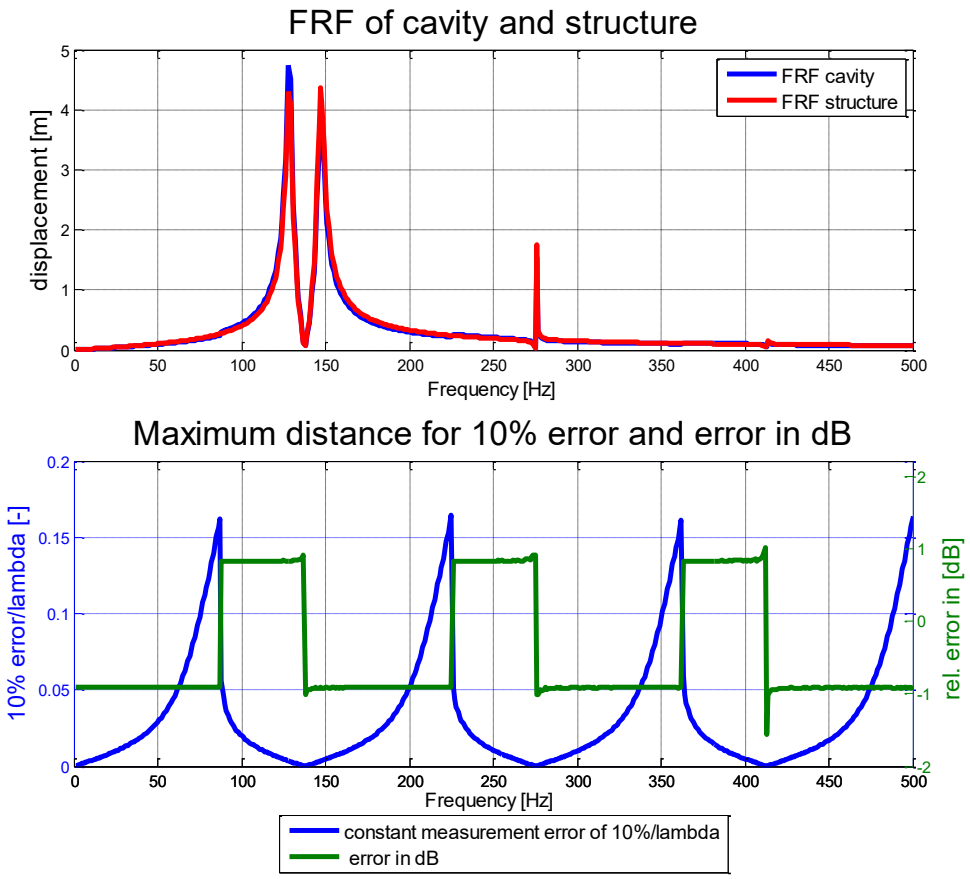

Figure 2-22 FRF of cavity and structure, 10% error and dB wise error

The FRF's fit perfectly together for the one percent measurement error and show some deviation for the five and ten percent case. Furthermore it can be noticed, that the maximum distance rises with an increasing error. Moreover the dB wise error rises from 0.1 dB for the one percent case to almost 1dB for the ten percent case. The maximum distance for 1% constant measurement error is 23cm, for 5% constant measurement error 45cm and 63cm for 10% constant measurement error. This is the maximum distance to be sure that the error in the amplitude will not be higher than the given percentage. The lower frequency range defines the maximum allowable distance for the positioning of the Microflown. For higher frequencies, the distance gets even smaller.

3 Vibro-acoustic test environment

3.1 Vibro-acoustic test rig

The test rig is a rectangular box made out medium density fiberboard (MDF) (figure 3-1). The inner dimensions are given in table 3-1.

Figure 3-1 Vibro-acoustic test rig

Each wall and the floor plate is 22mm thick. To top plate is an acrylic glass plate which is 4mm thick. A loudspeaker (eighteen sound, type 6ND430) has been installed in one of the walls to be able to excite the cavity acoustically. The loudspeaker has been placed eccentrically in order to excite axial, tangential and oblique modes.

Table 3-1 Dimensions of the vibro-acoustic test rig

Dimensions of the test rig		
length	[m]	1.495
width	[m]	0.950
height	[m]	0.200

A beam structure has been installed at half of the length and height and has been attached to the walls using some Aluminum brackets. The beam structure has been manufactured out of Aluminum sheet metal. The parameters are given in table 3-2:

Table 3-2 Parameters of the beam structure

Parameters of the beam structure		
length	[m]	0.895
width	[m]	0.030
height	[m]	2.035e-3
E-module	[N/m²]	7.000e+10
ρ_{Alu}	[kg/m^3]	2.700e+3

To ensure that the vibration of the beam structure is decoupled from the vibrations of the walls, some small patches of foam rubber have been put between the foot of the beam and the bracket (figure 3-2).

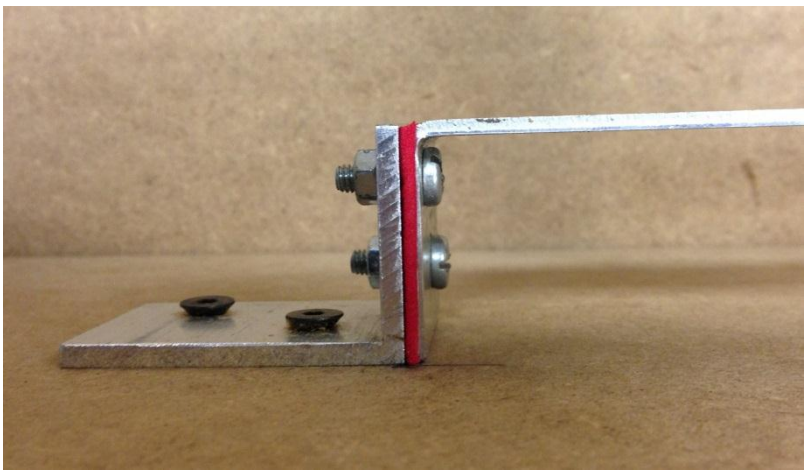

Figure 3-2 Foam rubber between beam structure and bracket

Some foam rubber has been bonded on top the walls to ensure that the cavity does not let through any of acoustic noise if the acrylic plate is put on top of it (figure 3-1). The acrylic plate is clamped using two Aluminum sheet metal brackets at both short sides (figure 3-3).

Figure 3-3 Clamping of the acrylic plate and foam rubber

3.1.1 Sensor placement device

The sensor check rail has been realized using a quadratic aluminum profile (30mmx30mm) which has been attached to the acrylic plate with two screws within a distance of 565mm from the side, where the loudspeaker has been placed.

The holding for the sensor has been realized using a wagon (build out of LEGO® Technik) which is running inside the aluminum profile (figure 3-4). A slot of 14mm has been milled into the aluminum profile to be able to move the wagon inside the check rail.

A guide bar has been clamped to the sensor holding as well to move the wagon inside the profile and along different positions in front of the structure while the cavity is closed for measurements. The guide bar can be controlled from outside the cavity.

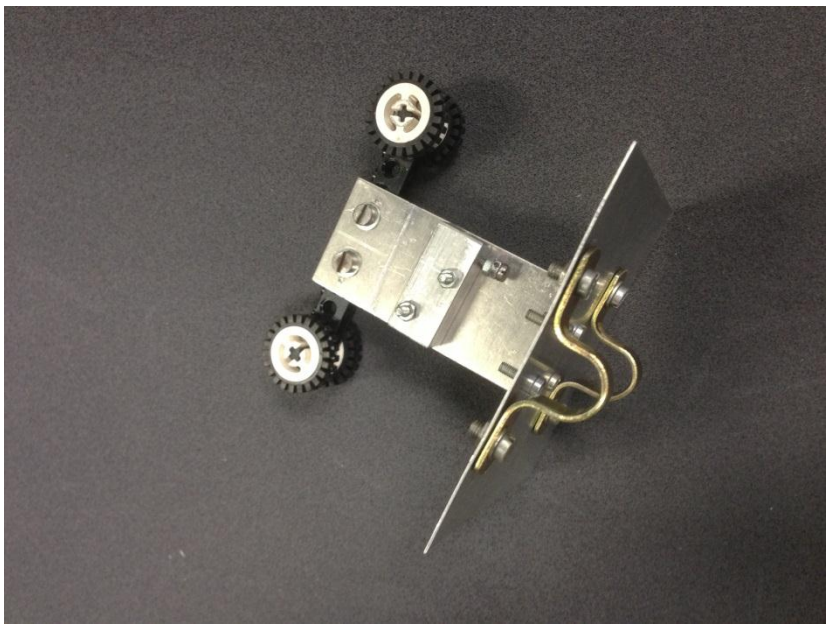

Figure 3-4 Sensor placement device

3.2 Measurement technique and - chain

The measurement chain is shown in figure 3-5. Both, the acoustic- and structural part is illustrated (dotted boxes). The frequency generator and the power amplifier have been involved in both parts. The red paths show a broadband excitation (acoustic noise), whereas the blue paths demonstrate a tonal excitation (sine wave). The recording of the measurement data has been realized using a measurement system from SoundTec (Live Pad 4 channel measurement with Touch PC). The classical experimental modal analysis including an impact hammer test is also shown in figure 3-5.

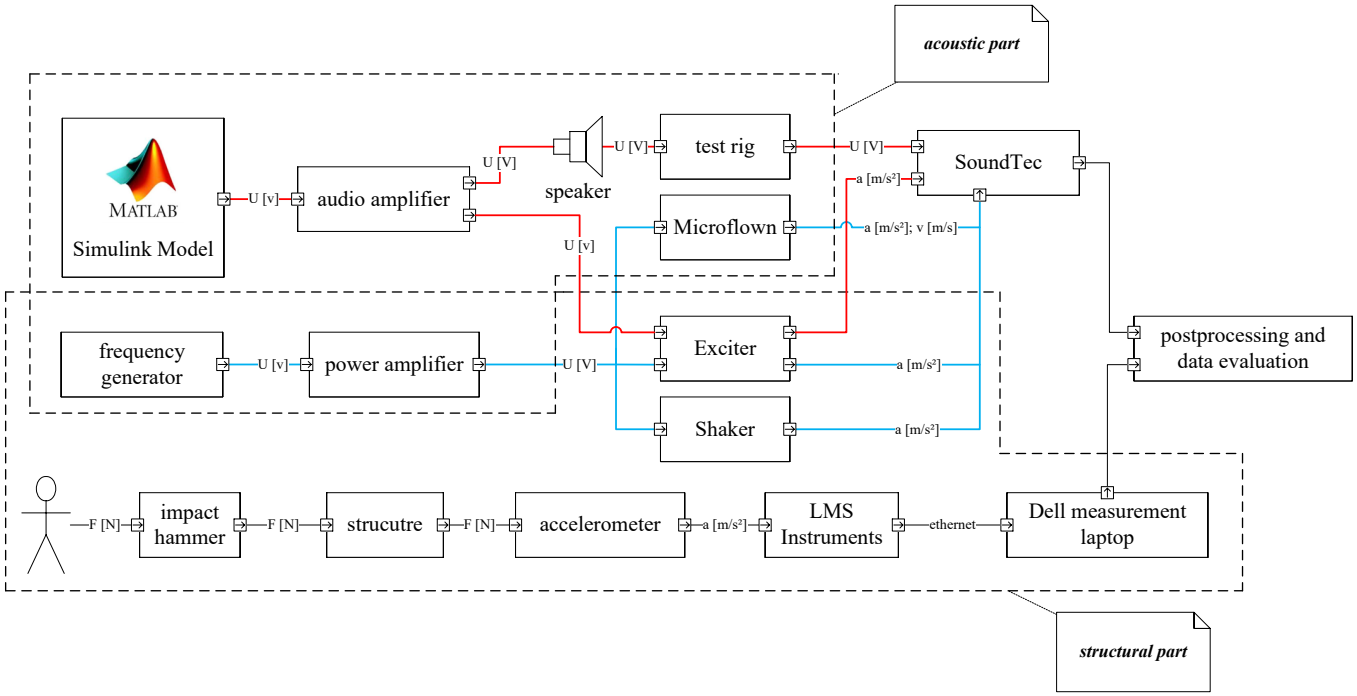

Figure 3-5 Measurement chain

The MATLAB model for signal generation (figure 3-6) has been programmed using the MATLAB Simulink toolbox and release 7.14.0.739 (R2012.a).

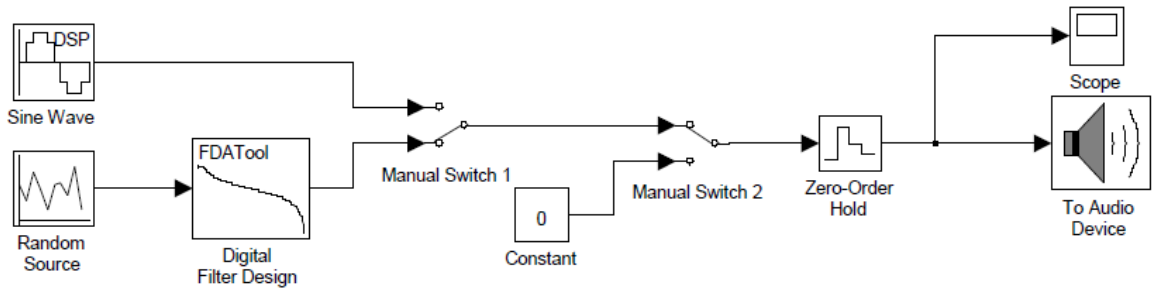

Figure 3-6 MATLAB Simulink model

The model has the ability to generate either a tonal sine wave or a random source (noise) which will be filtered inside the software afterwards with a high sample rate before the signal will be sent to the audio device (soundcard of the laptop). The output to the soundcard can be stopped by flipping *Manual Switch 2* to the constant position. To be able to control what kind

of signal is sent to the audio device, a scope has been applied as well. *The Zero-Order-Hold* controls the sample rate of the signal which is sent to the loudspeaker.
An overview over the measurement technique that has been used is given in table 3-3.

Table 3-3 Overview of the measurement technique

Component of the measurement technique	Type
Microflown	PU-Regular
function generator	FLUKE PM 5136
reference accelerometer	Bruel&Kjaer Type 4517
power amplifier	Bruel&Kjaer Type 2706
audio amplifier	Kenwood KRF-V7020
exciter	ELAC Standart, Autotune II KST
minishaker	LDS ltd. V101/2
three-dimensional accelerometers	Dytran Instruments. Type 3273-M2

The datasheets of the components listed in table 3-3 can be found on the data disc in appendix L for detailed information.

The data recording has been realized using a combination of a touchpad and a computer from *SOUNDTEC* (figure 3-7), especially developed for acoustic measurements. The device can handle up to four measurement channels at once.

Figure 3-7 SOUNDTEC

A measurement system of LMS International (figure 3-8) as well as an impulse hammer of Kistler (figure 3-9) and three dimensional accelerometers -Type 3273 M2- from Dytran Instruments Inc. have been used to perform the experimental modal analysis. Those belong to the inventory of the University of Applied Science Hamburg.

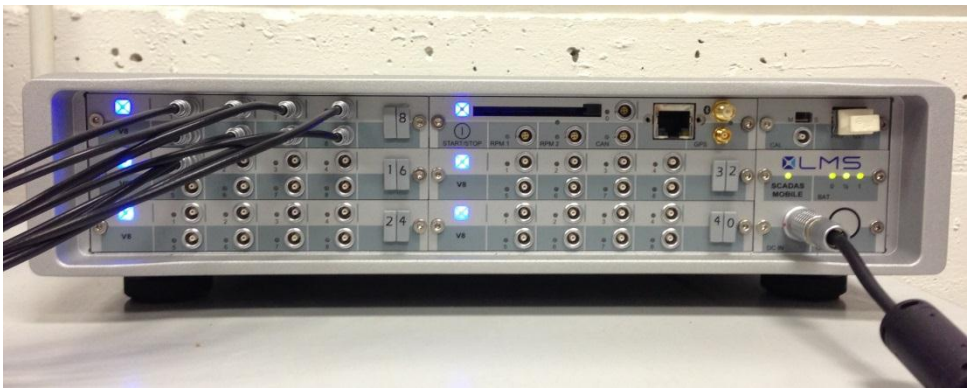

Figure 3-8 LMS measurement system

Figure 3-9 Kistler impulse hammer

3.3 Self-noise measurement of different sensors and microphones

For further measurements which are part of this master's thesis, it is important to compare the self-noise level of the different sensor types. The Bruel & Kjaer microphone and accelerometer belong to the inventory of the HSU.

The used sensors and microphones are:

- Bruel & Kjaer Type 4188 (microphone),
- Bruel & Kjaer Type 4175 (accelerometer),
- Microflown PU-probe.

Table 3-4 Comparison between different B&K accelerometers

Bruel&Kjear Type	Sensitivity [mV/g]	Weight [g]	Frequency range [Hz]	Special features
4517	10.12	0.65	1-20000	- low weight - wide frequency range
4514	100	8.7	1-10000	- low-impedance output - high resolution
4507-B-002	1000	4.8	0.1-6000	- low-impedance output - used for rough environments
4513--002	500	8.6	1-10000	- low-impedance output - high resolution

The accelerometer used is a regular type accelerometer. Especially the lowest weight and the widest frequency range met our demands.
The self-noise measurement has been performed at the Helmut-Schmidt-University Hamburg using a noise-isolated container which is vibration decoupled (figure 3-10). The container itself has been built regarding the DIN 60268-4.

Figure 3-10 Noise isolated container

3.3.1 Test setup for the self-noise measurement

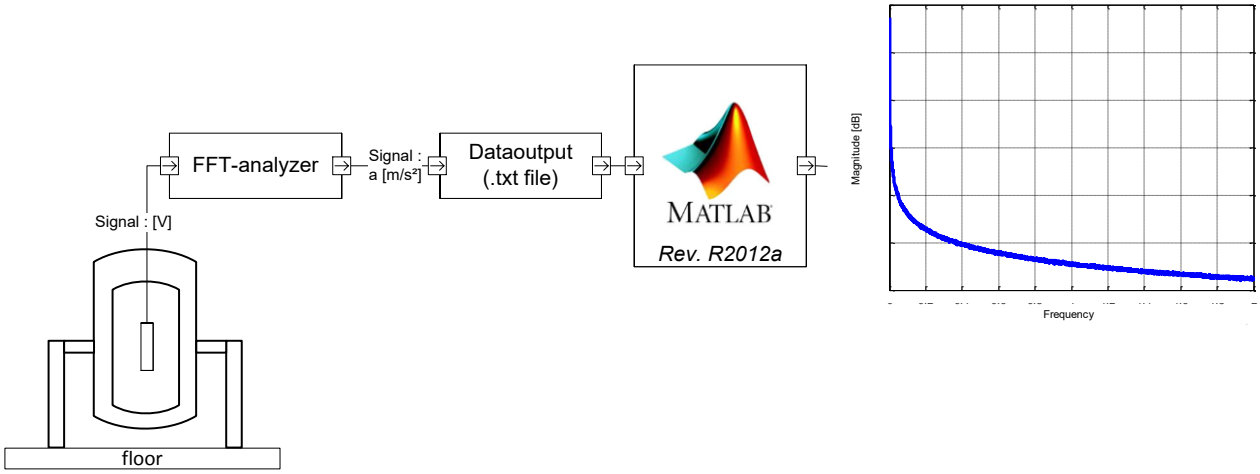

Figure 3-11 Schematic measurement chain for self-noise

As shown in figure 3-11 the sensors have been placed inside the noise isolated container. Via BNC-cable all sensors have been connected to a FFT-analyzer (type *OnoSokki DS-2000*).
The OnoSokki itself is connected via input card to a laptop. The detailed information about specific settings is given in chapter 3.3.2.

Output files in the form of a .txt file have been chosen, because this format is easy to handle in MATLAB for further interpretations.

3.3.2 Test procedure for the self-noise measurement

The measurements have been performed for the fullband (0-20KHz) and a more detailed resolution called the lowband (0-1,6KHz). 16384 lines have been used for FFT-analysis. This results in a frequency resolution of 3.125Hz for the fullband and 0.25Hz for the lowband. The two input channels (AC-coupling, used for the microphones and the accelerometer) were preamplified with 4.0mA.

Before starting the actual self-noise measurement, the B&K and the Microflown microphone and the B&K accelerometer have been calibrated.
For the calibration of both of the microphones a class one sound calibrator (Type 4231 from Bruel&Kjaer) has been used. The calibration has been done for 1kHz and 1Pa (rms). The resulting sensitivities were 0.032 V/Pa for the B&K micro, 0.03193 V/ Pa for the Microflown micro and 0.00039 V/Pa for the B&K accelerometer.

To be able to use the calibrator of the B&K Microphone, some layers of paper have been wrapped around the whole housing which was consisting of the metal mesh, to ensure that there are no sound leakages. The calibration value has not exactly been the same, but with 0.0319 V/Pa in the same order of Magnitude, compared to a value of 0.0489 V/Pa taken out the calibration sheet of Microflown.

The sound pressure p in the equation for the equivalent sound pressure level [2-15] has been calculated by multiplying the sensitivity S_0 with the voltage U :

$$p = S_0 \cdot U \,. \qquad [3\text{-}1]$$

An estimation of the deviation can be calculated using the ratio of both sensitivities. S_0^{HSU} means the sensitivity measured at the Helmut Schmidt University and $S_0^{Microflown}$ the sensitivity taken out of the calibration sheet of Microflown.

$$S_0^{HSU} = \frac{1}{0.0319}\frac{Pa}{V} \qquad S_0^{Microflown} = \frac{1}{0.0489}\frac{Pa}{V}$$

Building the ratio of both sensitivities delivers:

$$\frac{S_0^{HSU}}{S_0^{Microflown}} = \frac{0.0489}{0.0319} = 1.53 \,.$$

Inserting the ration into the equation for the equivalent sound pressure level and use the logarithmic laws:

$$L_p = 20 \cdot \log\left(\frac{1.53 \cdot p}{p_0}\right) = 20 \cdot \log(1.53) + 20 \cdot \log\left(\frac{p}{p_0}\right),$$

$$L_p = 3.69\text{dB} + 20 \cdot \log\left(\frac{p}{p_0}\right).$$

To assume the same calibration, 3.69dB have to be added to each value plotted.

The sensitivities (low and high gain) for each element (blue, red, green) out of the calibration sheet delivered from Microflown technologies have been used. These are:

Low gain: Blue 0.2622 V/Pa, Red 0.2307 V/Pa, Green 0.1277 V/Pa

High gain: Blue 33.01 V/Pa, Red 16.08 V/Pa, Green 29.04 V/Pa

For the identification of the self-noise level the B&K microphone, the B&K accelerometer and the Microflown PU-probe have been placed (one after another) inside the noise-isolated container. The measurement has been performed for both frequency ranges.

Consecutively the test series are shown:

- B&K microphone
- B&K accelerometer
- Microflown microphone
- Microflown particle velocity sensors
    - low gain – correction off
    - low gain – correction on
    - high gain – correction off
    - high gain – correction on

For the statistic safety every configuration has been measured three times, whereas each test series itself contained of an average of 128 datasets.

3.3.3 Results of the self-noise measurement

The post-processing has been done with MATLAB (release R2012a). To compare each of the self-noise levels (microphones in [Pa], accelerometer in [m/s²] and the velocity in [m/s]) the signals have been converted into dB, using equations [2-15] to [2-17]. For each of the three measurement runs the root mean square has been calculated. In section 3.3.3.1 the self-noise plots are shown assuming a constant sensitivity for the Microflown. In reality, the Microflown has a frequency dependent sensitivity. The curves have been calculated using equations [2-2] to [2-4]. These are taken out of the Microflown calibration report. The scatter plots of each measurement run are shown in section 3.3.3.3.

3.3.3.1 Results assuming a constant sensitivity of the Microflown

Figure 3-12 shows the comparison between the Bruel&Kjaer microphone (blue) and the Microflown microphone (black). A logarithmic scale has been used to have a closer look at the lower frequencies. Till 100Hz, the Microflown micro has a lower self-noise level than the B&K micro. From around 100Hz onwards, the B&K microphone has a self-noise level which is about 5dB to 10dB lower that the Microflown microphone.

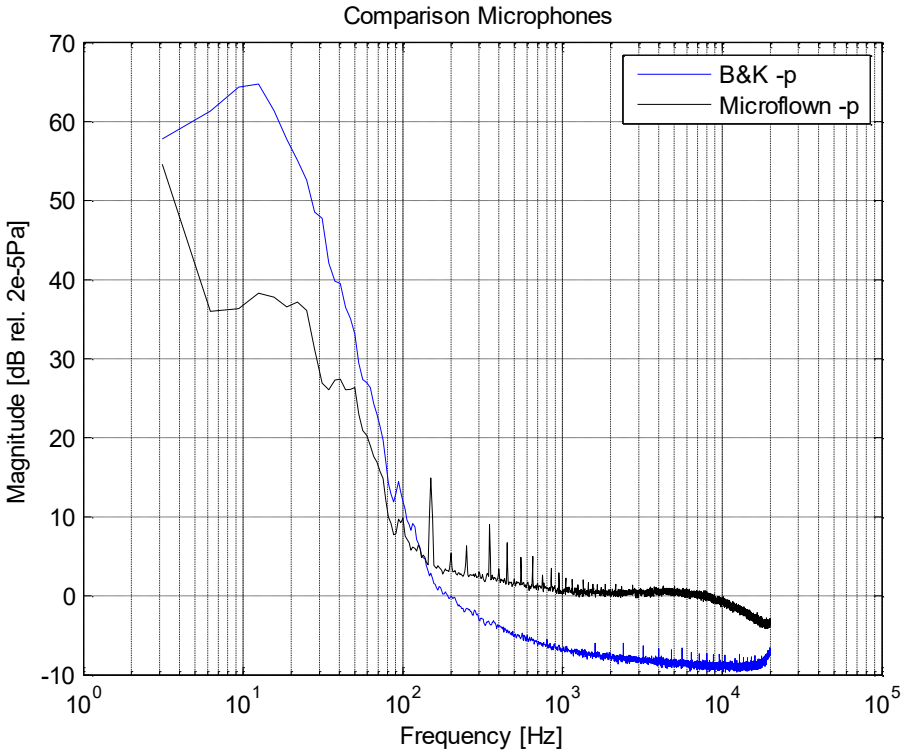

Figure 3-12 Comparison of microphones

Figure 3-13 shows the comparison between the B&K accelerometer and die Microflown X-Blue Element. Due to the fact that the other two elements (Y-Red, Z-Green) have the same trend, these plots can be found in appendix A.

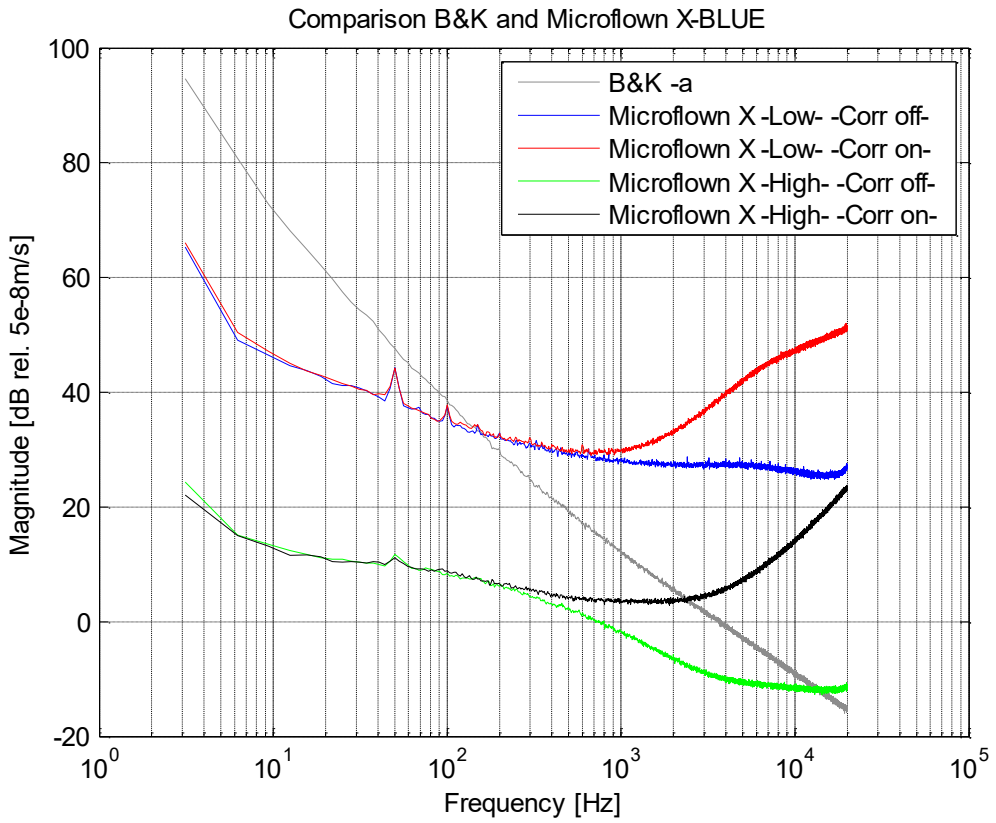

Figure 3-13 Comparison B&K and Microflown X-BLUE fullband

The blue and red curve represents the low gain configuration with the correction on and off. They have a self-noise level which is nearly 30dB higher than the high gain configuration (black and green). It can also be noticed that both of the curves: *correction on* and *correction off* have the same trend till 300Hz. The *correction on* curves almost have the same trend till 300Hz. From this point onwards, the high gain magnitude rises exponential whereas the low gain magnitude is almost linear.
The accelerometer (grey curve) has as linear decreasing slope of approximately 10dB per octave.

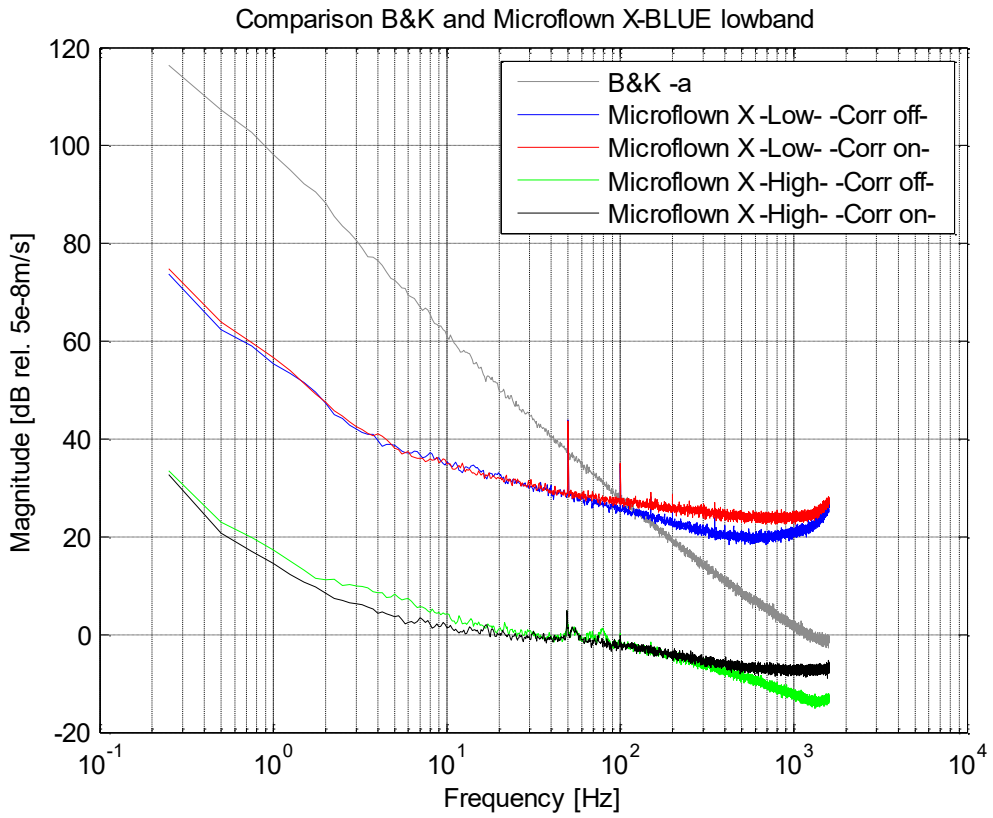

Figure 3-14 Comparison B&K and Microflown X-BLUE lowband

It is important to know that figure 3-14 does not result from the fullband measurement. It's a complete new data set (freq. resolution 0.25Hz). However, the trends known from figure 3-13 can be found.

3.3.3.2 Results assuming a frequency dependent sensitivity of the Microflown

From around 100Hz on the Microflown microphone has an almost constant self-noise around 0Hz (figure 3-15). The self-noise of the B&K microphone is around 10dB lower from 100Hz onwards. In the lower frequency range the B&K microphone has a self-noise between 30dB to 60dB. The Microflown microphone is out of range.

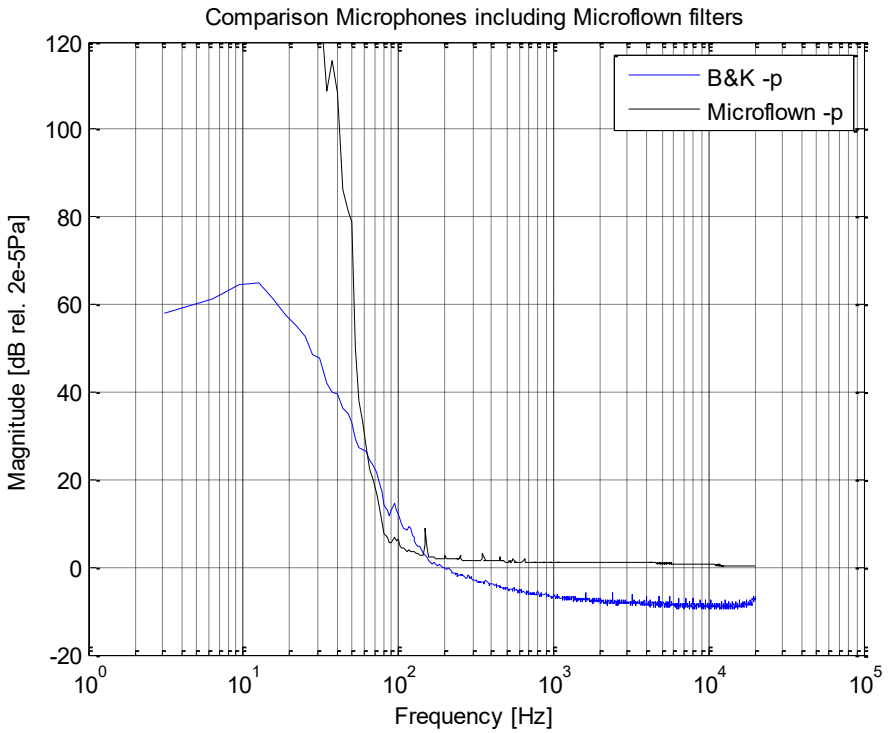

Figure 3-15 Comparison of microphones (Microflown with filter)

For the comparison of the B&K accelerometer and the Microflown particle velocity sensor the color schemes are the same like in figure 3-13 and figure 3-14. It can be noticed that if the filter are applied, all of the four curves of the Microflown show the same trend independent of *high* or *low gain* settings or the *correction on/off* settings. Still there is a shift of about 30dB between the high and low gain settings. The *correction on/off curves are* almost congruent (figure 3-16 and figure 3-17).
However the trends known from figure 3-13 can be found in figure 3-14 as well.

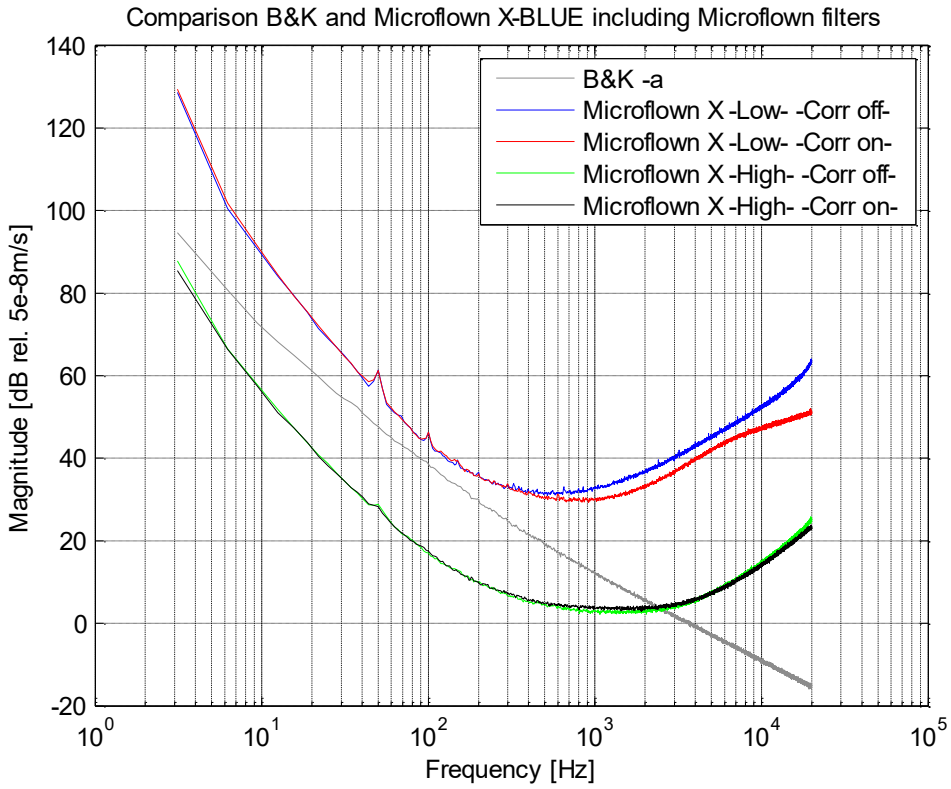

Figure 3-16 Comparison B&K and Microflown X-BLUE including Filter

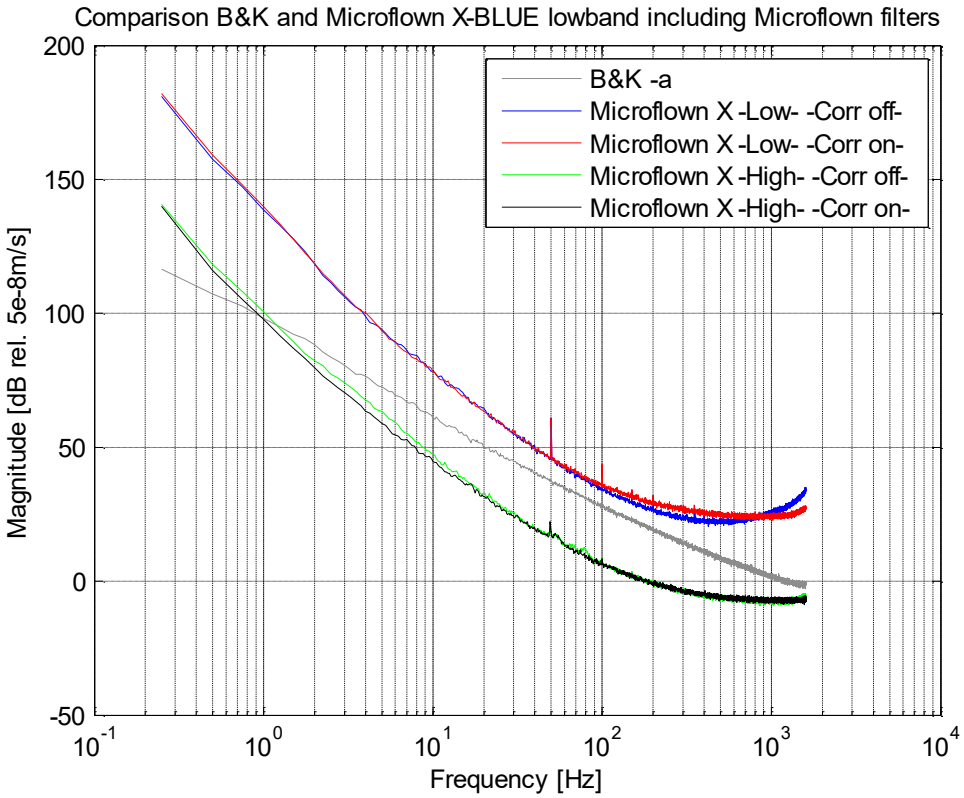

Figure 3-17 Comparison B&K and Microflown X-BLUE lowband including filter

3.3.3.3 Scatter of test series

All of the curves shown before have been calculated by building the root mean square of the three measurement runs.

It is also important to have an idea about the scatter of these three measurement runs for each configuration. For the particle velocity plots only the X-Blue direction will be shown. All the other plots can be found in appendix C.

The plots on the left hand side show the measurement consisting the fullband (0-20KHz), the plots on the right hand side belong to the measurement for the lowband (0-1,6KHz).

B&K type 4188 microphone:

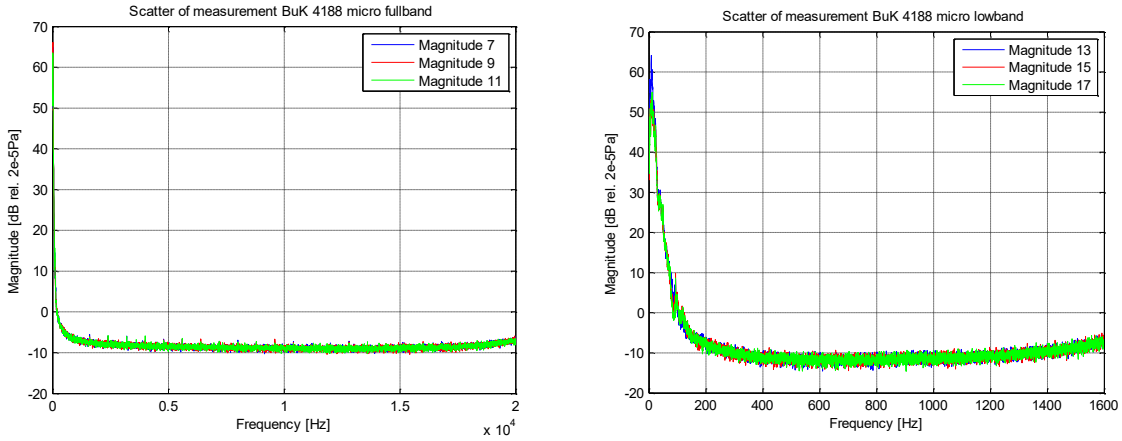

B&K type 4517 accelerometer:

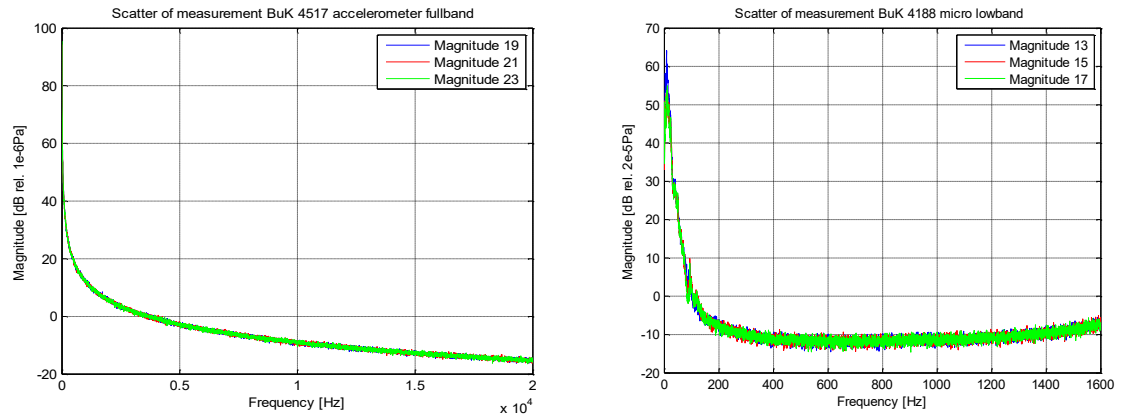

Figure 3-18 Scatter plots of B&K microphone (top) and B&K accelerometer (bottom). Labeling is for internal use.

Microflown microphone:

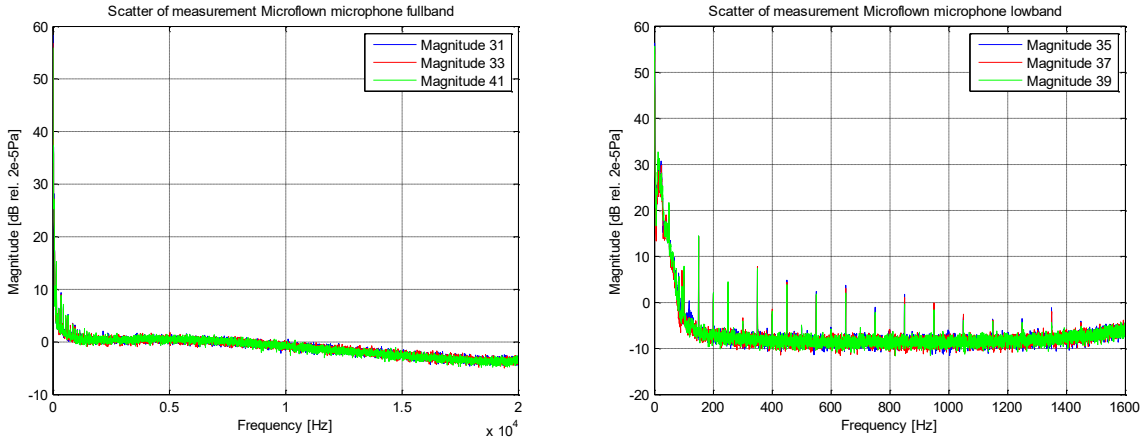

Microflown particle velocity – low gain- correction off (X-Blue)

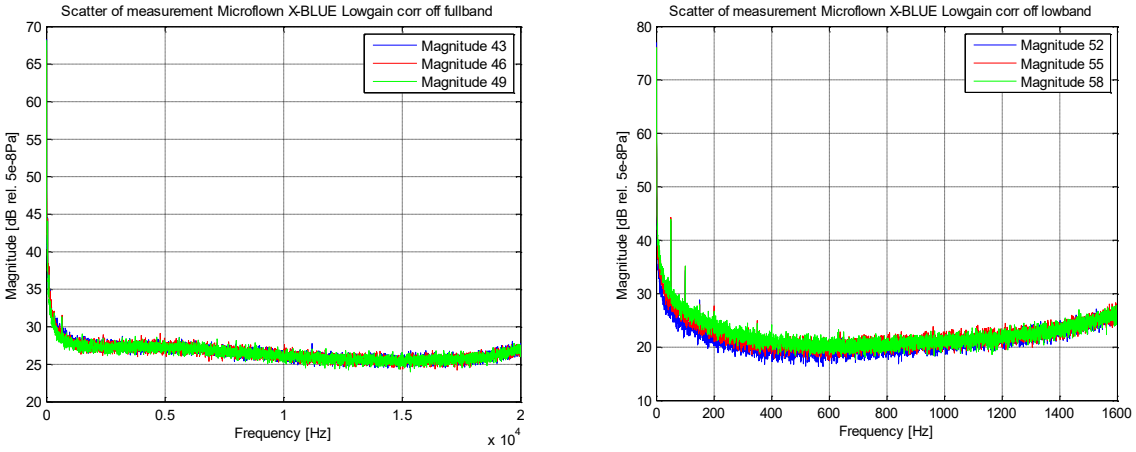

Microflown particle velocity – low gain- correction on (X-Blue):

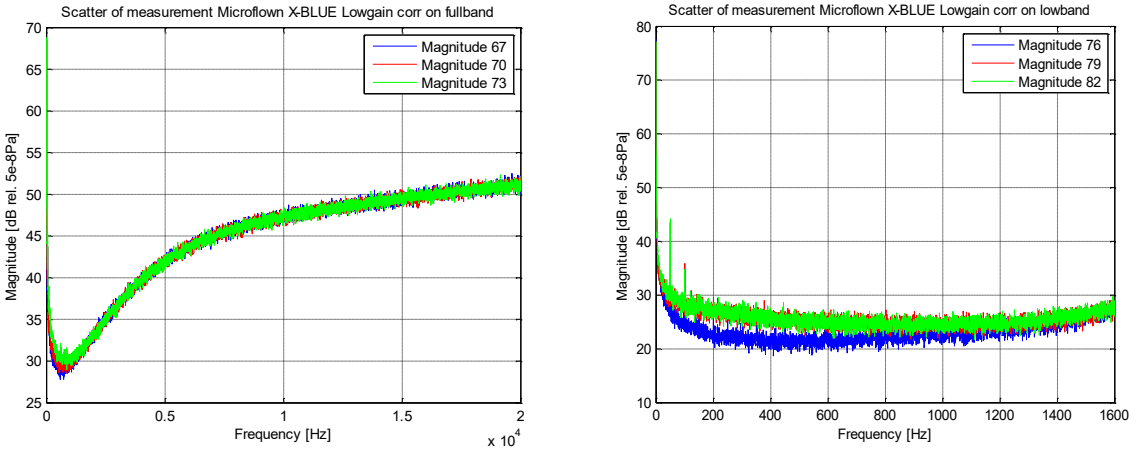

Figure 3-19 Scatter plots of Microflown microphone (top), Microflown particle velocity low gain correction off (X-Blue) (middle) and Microflown particle velocity low gain correction on (X-Blue) (bottom)

Microflown particle velocity –high gain- correction off (X-Blue):

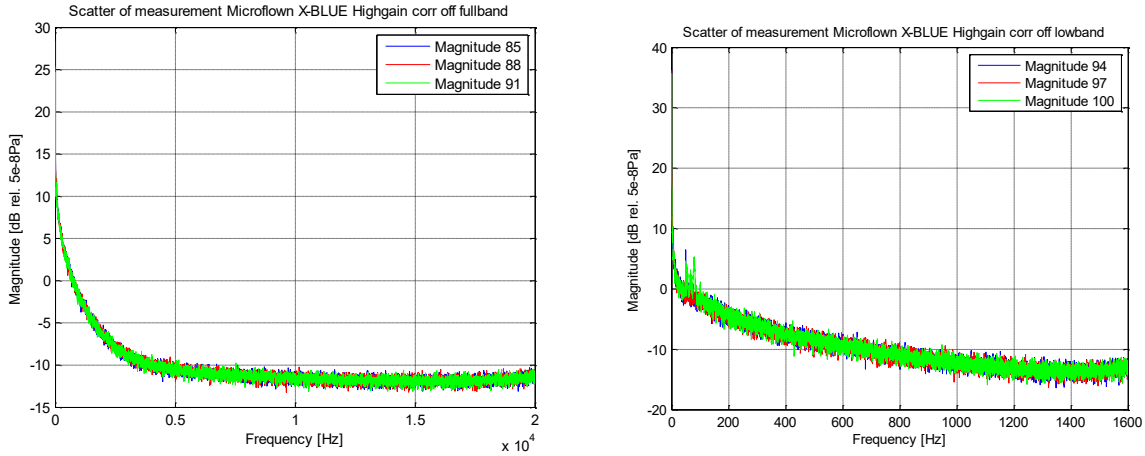

Microflown particle velocity – high gain- correction on (X-Blue):

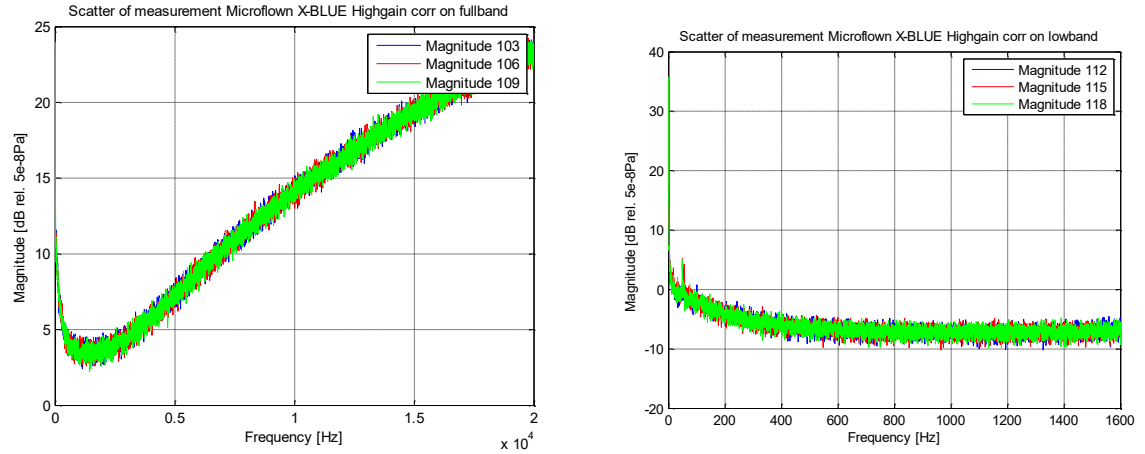

Figure 3-20 Scatter plots of Microflown particle velocity high gain correction off (X-Blue) (top) and Microflown particle velocity high gain correction on (X-Blue) (bottom)

It has been found that the influence of the averaging by using the root mean square is insignificantly small. Just in some cases (e.g. low gain correction on X-Blue) there might be a small influence (gap between two curves approximately 5dB in the range up to 600Hz).

For the B&K microphone and accelerometer all of the three plotted curves fit perfectly together.

3.3.3.4 Equivalent self-noise level

If one calculates the equivalent noise level out of measurement data, it follows that around the first 15Hz the self-noise level can reach values of about 80dB (e.g. the B&K accelerometer). Therefore, the equivalent noise level has been calculated for the fullband as well as for the lowband using equation [2-18], section 2.3.1.

The result can be seen in the following table 3-5:

Table 3-5 Equivalent self-noise of different types of sensors and microphones

			0-20 KHz [dB rel.]	15 Hz-20 KHz [dB rel.]	0-1,6 KHz [dB rel.]	15Hz-1,6 KHz [dB rel.]
B&K	micro	B&K Typ 4188	32	26	34	22
	accelerometer	B&K Typ 4517	64	61	63	54
Microflown	micro	Micro	21	7	22	7
	Lowgain *Correction off*	X_Blue	33	27	41	23
		Y_RED	55	27	55	23
		Z_Green	66	33	68	29
	Lowgain *Correction on*	X_Blue	48	47	42	25
		Y_RED	54	47	54	24
		Z_Green	64	52	65	30
	Highgain *Correction off*	X_Blue	-5	-6	1	-8
		Y_RED	14	-3	14	-4
		Z_Green	18	-8	17	-9
	Highgain *Correction on*	X_Blue	17	17	1	-6
		Y_RED	23	22	13	-3
		Z_Green	20	17	18	-8

Table 3-5 indicates the influence of noise measured between 0-15Hz. Due to the fact that the equation [2-18] contains a summation it is not allowed to simply subtract the results for both bands. However, there is a reduction in the equivalent noise level if the first 15Hz are neglected.

Table 3-6 Equivalent self-noise of the Microflown velocity sensors including filters

			0-20 KHz [dB rel.]	15 Hz-20 KHz [dB rel.]	0-1,6 KHz [dB rel.]	15Hz-1,6 KHz [dB rel.]
Microflown	Lowgain *Correction off filterd*	X_Blue	91	56	143	44
		Y_RED	76	57	144	42
		Z_Green	85	62	151	48
	Lowgain *Correction on filtered*	X_Blue	51	49	103	44
		Y_RED	76	48	143	41
		Z_Green	85	54	147	45
	Highgain *Correction off filterd*	X_Blue	50	19	103	13
		Y_RED	39	23	102	15
		Z_Green	39	17	100	9
	Highgain *Correction on filterd*	X_Blue	47	19	102	12
		Y_RED	39	23	102	14
		Z_Green	39	18	100	9

Table 3-6 indicates the influence of noise measured between 0-15Hz too but compared to table 3-5 the filters have been taken into account as well. It can also be recognized that there is an influence of the first 15Hz, although the overall self-noise level of the whole bandwidth is even higher than in table 3-5 without the applied filters.

3.4 Mechanical resonances of the beam structure

3.4.1 Theoretical calculation of the beam structure

By using the parameters of the beam structure given in table 3-7, the theoretical eigenfrequencies have been calculated (table 3-8).

Table 3-7 Parameters theoretical mechanical resonances

Parameters		
length	[m]	0.895
width	[m]	0.030
height	[m]	2.035e-3
Young's modulus	[N/m²]	7.000e+10
ρ_{Alu}	[kg/m^3]	2.700e+3
I	[m^4]	2.100e-11
Beam mass	[kg]	1.475e-1
μ	[kg]	0.165

Due to the fact that the height is in the third power (equation [2-6]), the solution is very sensitive to this parameter and has been measured using a micrometer screw.

The wavelength of the bending wave has been calculated using equation [3-2] ([10], p.130, eq. 4.14). The analytical formulas for the mass distribution and the moment of inertia which are needed for the solution of equation [3-2] can be found in section 2.2.1.

$$\lambda_b = 2\pi \cdot \sqrt[4]{\frac{EI}{\omega^2 \mu}} \qquad [3\text{-}2]$$

Table 3-8 shows the theoretical eigenfrequencies and the associated wavelengths of the beam structure.

Table 3-8 Theoretical eigenfrequencies of the beam structure

mode	ω_n [Hz]	f_n [Hz]	λ_n [m]
1	36.9	5.9	1.76
2	147.4	23.5	0.90
3	331.7	52.8	0.60
4	589.7	93.9	0.45
5	921.4	146.6	0.36
6	1326.8	211.2	0.30
7	1805.9	287.4	0.26
8	2358.7	375.4	0.22
9	2985.2	475.1	0.20
10	3685.5	586.6	0.18
11	4459.4	709.7	0.16

To proof the calculated eigenfrequencies of the beam structure, the FEM Model described in [14] has been used. The MATLAB code for this FEM Model provided by Prof. Kletschkowski can be found in appendix D. The results are shown in table 3-9 and it can be recognized, that the results verify the theoretical eigenfrequencies. Only the third eigenfrequency has a small variation of 0.95Hz (1.8%).

Table 3-9 Eigenfrequencies of the beam FEM model

mode	f_n [Hz]
1	5.86
2	23.55
3	53.75

3.4.2 Experimental determination of the mechanical resonances

While performing the measurement or in- or uninstalling measurement technique, it is important not to unscrew the beam from its mounting to guarantee that there will be no change in the values of the stiffness. For the measurement of the mechanical resonances three different methods have been used:

(1) Experimental modal analysis using the LMS measurement system,
(2) Excitation caused by an exciter of ELAC,
(3) Excitation caused by a minishaker of LDS.

To perform the experimental modal analysis, eight accelerometers of Dytran Type 32739M2 have been applied to the structure in equivalent distances of 100mm using adhesion wax (figure 3-21). All of those have been connected to the LMS front end (e.g. figure 3-8).

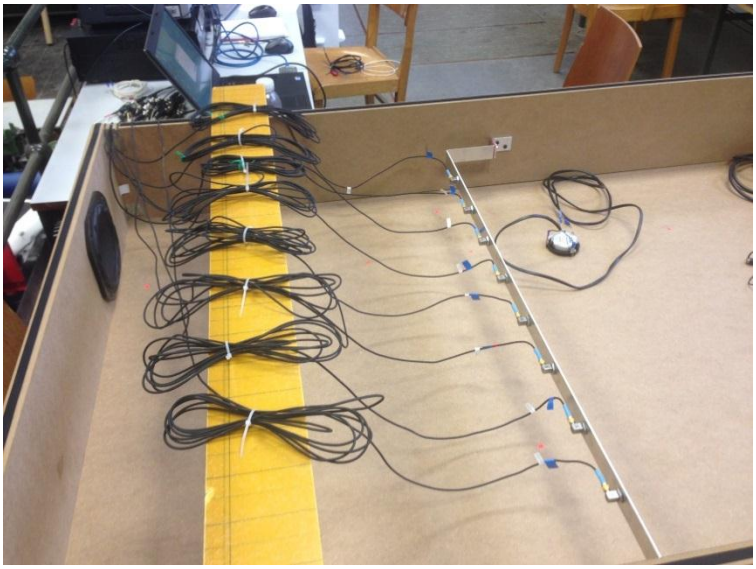

Figure 3-21 Test set-up for the experimental modal analysis

The excitation of the structure has been applied by hitting the beam structure from the opposite direction of the accelerometers. To ensure that all of the mode shapes have been excited, the impact position of the impulse hammer has been varied during the recording of the measurement data (averaged over 20hits). The LMS software *TestLab 10B*, which belongs to the measurement system, provides the proper tools to calculate the eigenfrequencies and the damping ratios.
The results are given in (table 3-10). Considering the animated mode shapes of every resonance, the first seven belong directly to the ones expected of the theory. For resonances in higher frequencies it has been difficult to make an assignation of the mode shapes animated.

Table 3-10 Resonant frequencies and damping ratio of the LMS measurement

resonance	f_n [Hz]	D [%]
1	10.4	2.29
2	21.5	2.22
3	55.2	1.8
4	94.1	1.55
5	138.4	1.5
6	193.2	1.21
7	253.5	1.01
8	313.5	1.35
9	402.7	2.8
10	462.9	0.43
11	630.2	0.45

Another way to determine the eigenfrequencies of the beam structure is to use the ELAC exciter or the LDS minishaker to excite the structure. By plotting the first ten modes (sin(x), sin(2x), etc.) the position of the exciter and the minishaker has been defined (150mm from the mounting). For this position it has been essential not to be in a nodal point, because otherwise this mode would not have been excited in further measurements. To be able to record the movement of the beam structure, a reference accelerometer (Bruel&Kjear Type 4517) has been placed eccentric on the structure.

The test set-up using the ELAC exciter is shown in figure 3-22.

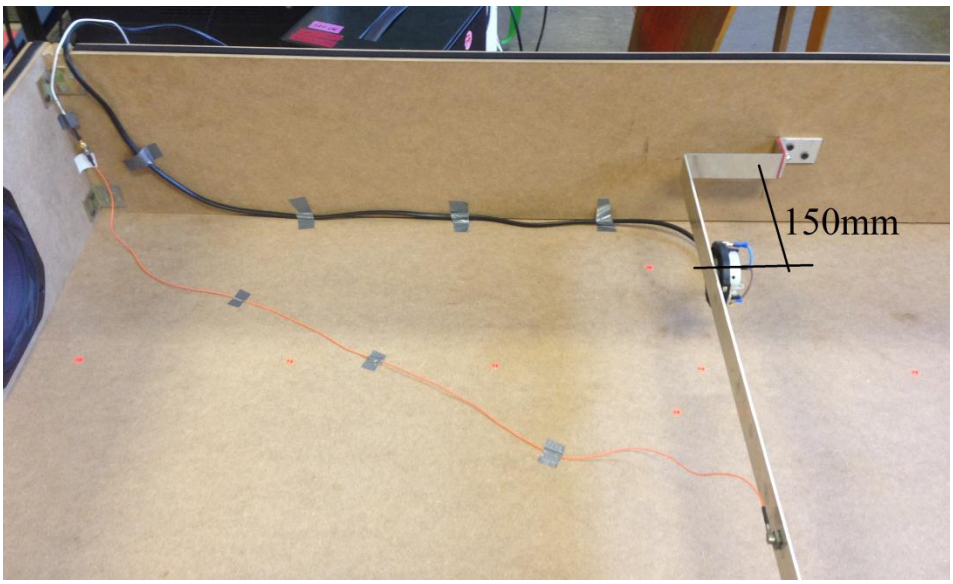

Figure 3-22 Test set-up ELAC exciter

Before applying an acoustic noise signal (MATLAB Simulink model) to the exciter, the test rig has been closed by putting the acrylic plate on it. The accelerometer has been connected to the SoundTec. The exciter has been connected to the power amplifier. The signal of the soundcard has been connected to both the SoundTec and the power amplifier. Two signals have been measured. The signal of exciter and the response of the beam structure measured with the reference accelerometer.

The coherence is a measure for the correlation between two signals. If the coherence is one the signals are fully correlated. It is the regular case that the coherence has some quality drop-offs but especially in the resonances the coherence should be close to one [15], p.156 ff.

Figure 3-23 shows the coherence of the broadband excitation of the beam structure using the ELAC exciter. It can be noticed, that the coherence is not good enough in below 50Hz and has some wide quality fall-offs in the higher frequency range. Therefore the modes and the belonging eigenfrequencies have been determined visually using tonal excitation.

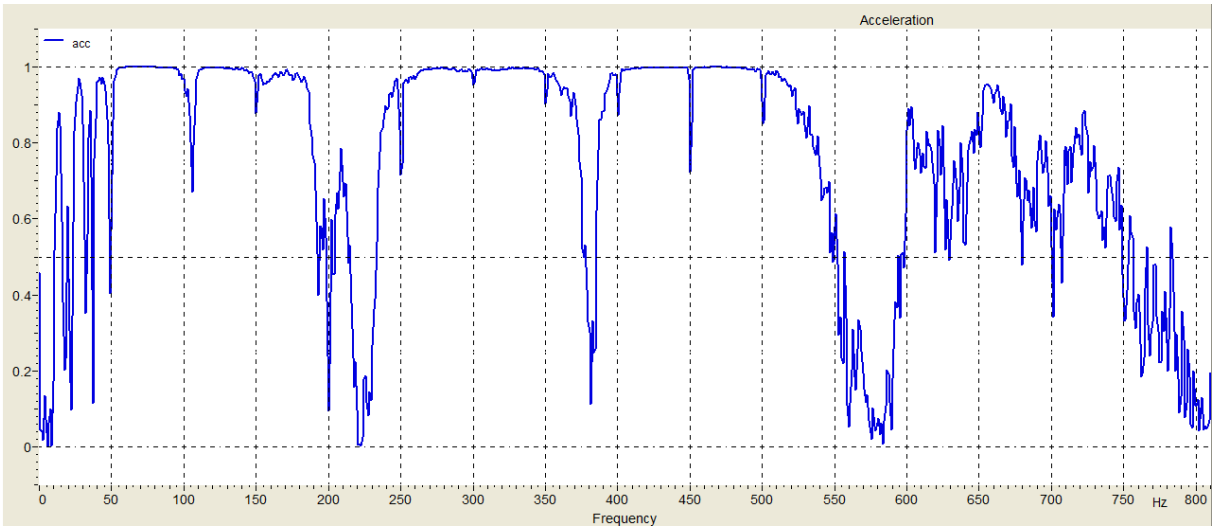

Figure 3-23 Coherence broadband excitation using ELAC exciter

The results are given in table 3-11. By looking at the beam structure, the first five bending modes have been determined and belong directly to the ones expected of the theory. For the higher frequencies it has been difficult to say what kind of mode it has been due to the small structural movements. It's just a presentation of the detected resonances.

Table 3-11 Resonant frequencies of the ELAC exciter measurement

resonance	f_n [Hz]
1	9.8
2	17.8
3	47.5
4	94.8
5	148.5
6	241.0
7	314.0
8	403.0
9	491.0

To use the minishaker to excite the beam structure, a mounting for the ram had to be developed. An eyebolt on the centerline of the beam has been used to realize this mounting. For the application of a pre-load to the structure, the ram and the beam have been decoupled using a spring (figure 3-24).

Figure 3-24 Mounting and installation of the minishaker

The connection of the cables and the measuring process have been the like the ELAC exciter measurement. The coherence shown in figure 3-25 is worse compared to the coherence of the ELAC exciter. This belongs to the shaker which has excited the structure insufficiently. Another problem has been that the spring has its own resonances. It has just been possible to measure up to 120Hz. The results of the visual detection are given in table 3-12. For the visual detection, maxima in the amplitude as well as nodal points have been counted.

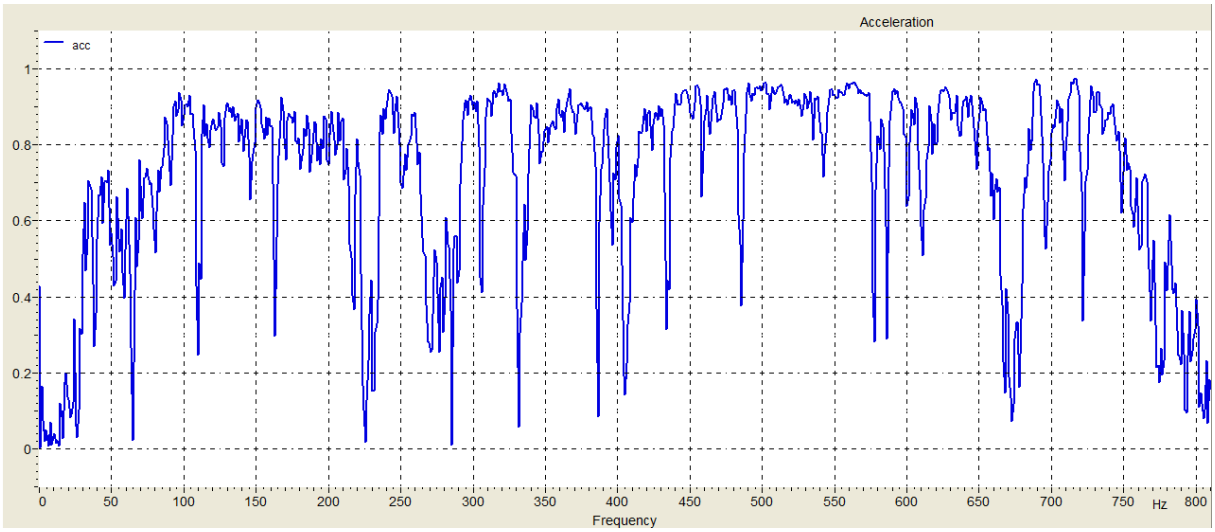

Figure 3-25 Coherence of the minishaker measurement

Table 3-12 Resonances measured with the minishaker

resonance	f_n [Hz]
1	12.1
2	26.5
3	64.8
4	110.5

To make a statement for the damping ratio of each resonance (ELAC and minishaker measurement) the decay curve of each resonance has been recorded by starting the measurement and turning the gain of the power supply to zero (measurement time 6s). Looking at the level display of each measurement run gives the opportunity to determine the reverberation time out of the linear decrease of the level (see equation [2-26] section 2.3.4).

3.5 Acoustic resonances of the rectangular cavity

3.5.1 Theoretical calculation of the acoustic resonances

As previously described in section 2.3.2 the acoustic resonances can be calculated analytically by using equations [2-19] and [2-20].

The necessary parameters to solve these equations are given in table 3-13.

Table 3-13 Parameters for calculation of theoretical acoustic resonances

Dimensions of the test rig			**constants**		
length	[m]	1.495	**c**	[m/s]	340
width	[m]	0.950			
height	[m]	0.200			

Tangential and oblique modes have not been taken into account. The first oblique mode has been calculated with 876 Hz, using [9].

The resonant frequencies are given in table 3-14. Due to the fact that the beam structure has its first eleven eigenfrequencies below 800Hz and the first acoustic mode in the height direction is 850Hz, only this range has been taken into account.

Table 3-14 Theoretical resonant frequencies and wavelengths

mode	**direction - length**		**direction - width**		**direction - height**	
	f_n [Hz]	λ_n [m]	f_n [Hz]	λ_n [m]	f_n [Hz]	λ_n [m]
1	113.7	3.0	178.9	1.9	850.0	0.4
2	227.4	1.5	357.9	1.0		
3	341.1	1.0	536.8	0.6		
4	454.8	0.7	715.8	0.5		
5	568.6	0.6				
6	682.3	0.5				
7	796.0	0.4				

3.5.2 Measurement of the acoustic resonances

To measure the acoustic resonances inside the cavity it is important to know that the particle velocity is zero close to the walls. This is the reason why the Microflown has been placed right in front of the wall (figure 3-26).

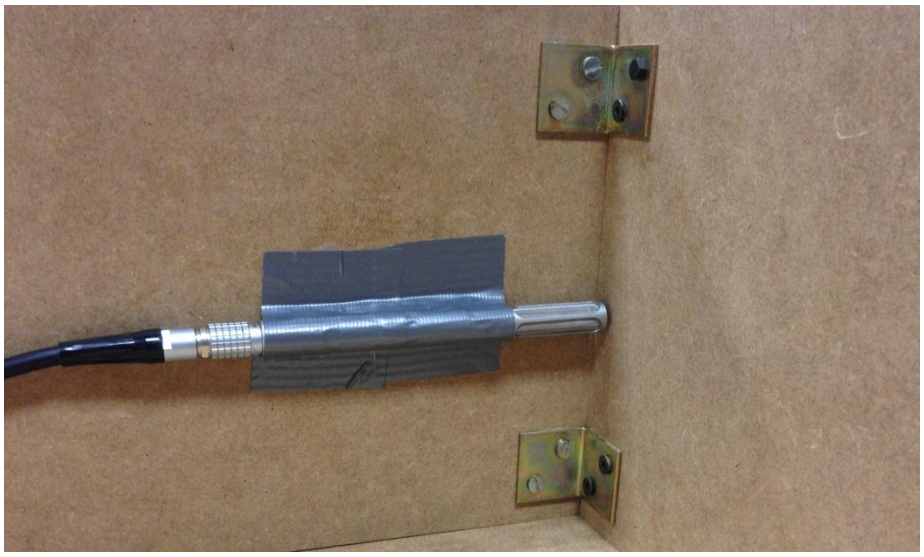

Figure 3-26 Measurement of the acoustic resonances

The MATLAB model (figure 3-6) has been used to generate the broadband signal. The laptop soundcard has been connected to the audio amplifier which itself has been connected to the loudspeaker. The data recording has been realized using the SoundTec. Two signals have been measured. The excitation generated from the MATLAB model and the response measured with the Microflown microphone.

The level range of the Microflown microphone is 110 dB [4]. It has been important to be careful that the level is not too high to prevent non-linear distortion of the microphone. This would result in an insufficient measurement.

Figure 3-27 shows the coherence of the acoustic broadband excitation. It can be noticed that the coherence is almost one at all resonances. The coherence gets worse at higher frequencies, but is still in an acceptable range.

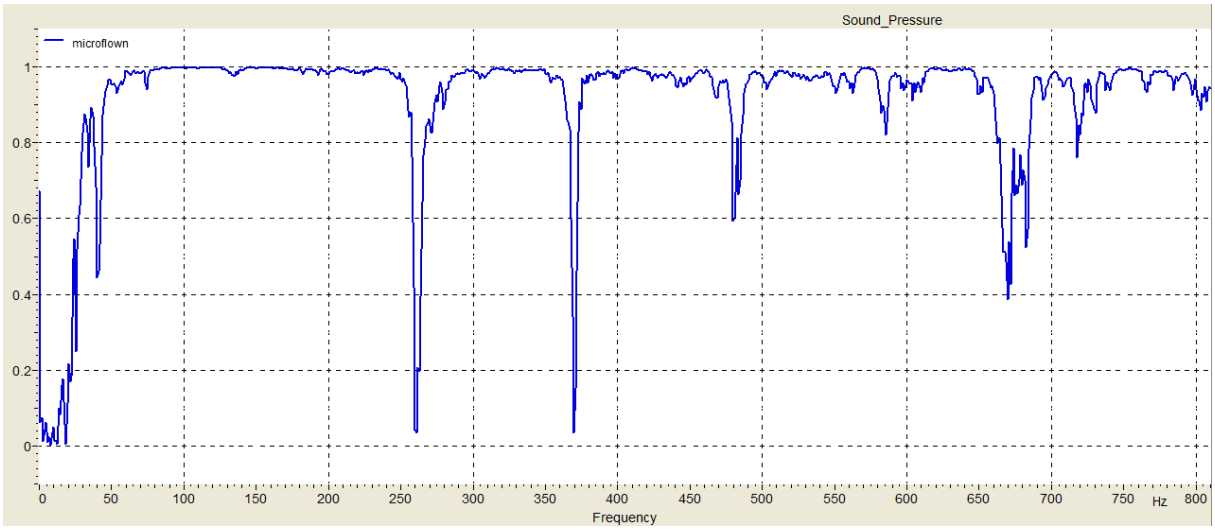

Figure 3-27 Coherence of the acoustic broadband excitation

The calculation of the transfer function (Input: signal of MATLAB model, Output: pressure signal measured with the Microflown microphone, resolution 1Hz) shows the resonant peaks in the linear diagram (figure 3-28).

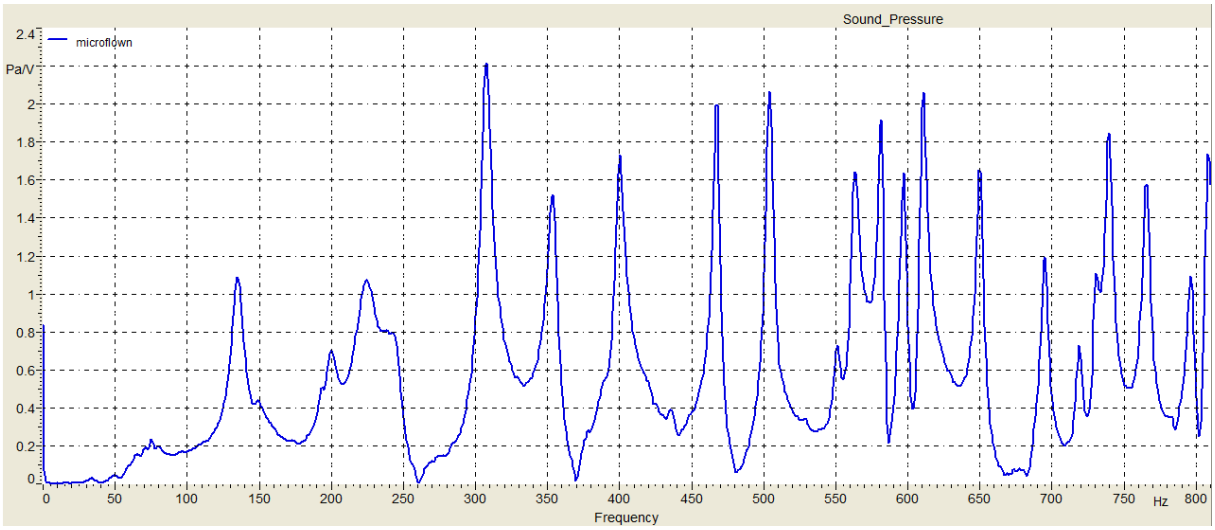

Figure 3-28 Transfer function of the acoustic broadband excitation

To be able to make a statement for the damping ratio of each resonance, the cavity has been exited tonally using the frequency generator. After the cavity has been set into the certain resonance, the decay curve for each resonance has been recorded.

The acoustic resonances have been:

Table 3-15 Measured acoustic resonances

resonance	f_n [Hz]	resonance	f_n [Hz]
1	134.2	10	598.0
2	229.0	11	609.0
3	307.0	12	648.0
4	352.0	13	693.0
5	398.0	14	717.0
6	502.0	15	738.0
7	548.0	16	763.0
8	561.0	17	794.0
9	580.0		

Looking at the level display of the measured decay curves a linear decrease of the level can be noticed. The reverberation can be read off the linear decrease afterwards (figure 3-29) and is the difference between the two time steps t1 and t2. The decay curves to determine the damping ratio have been recorded three times for each resonance which has been excited tonally to give a statistic safety.

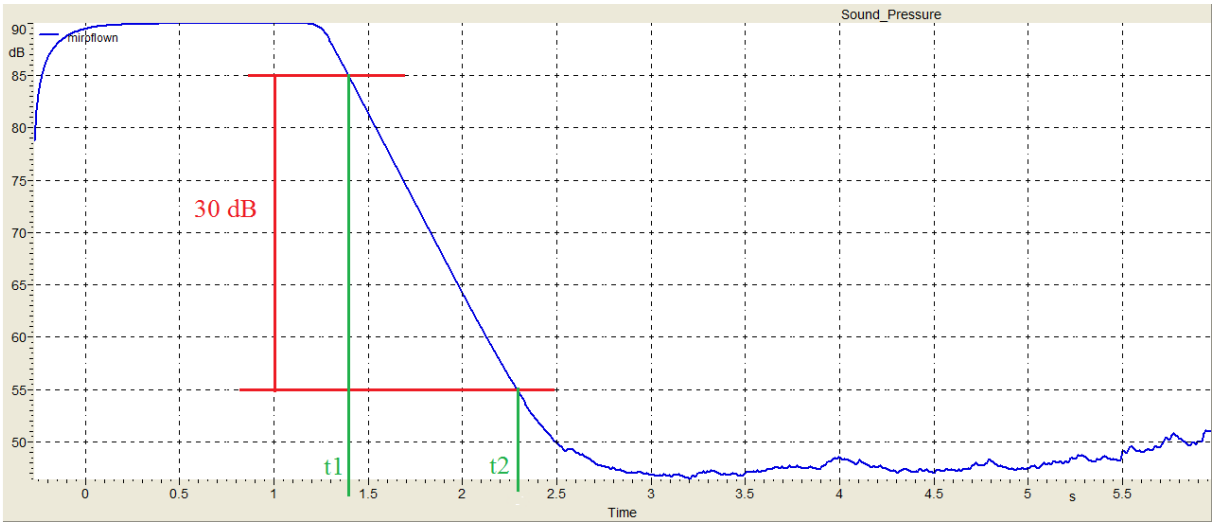

Figure 3-29 Reverberation time

Equation [2-26] to determine the damping ration can be found in section 2.3.4.

For the acoustic resonances, the calculated damping ratios are given in table 3-16:

Table 3-16 Damping ratios of the acoustic resonances

resonance	frequency [Hz]	D [%]	resonance	frequency [Hz]	D [%]
1	134.2	0.46	10	598.0	0.09
2	229.0	0.27	11	609.0	0.10
3	307.0	0.20	12	648.0	0.09
4	352.0	0.17	13	693.0	0.09
5	398.0	0.15	14	717.0	0.08
6	502.0	0.12	15	738.0	0.08
7	548.0	0.10	16	763.0	0.08
8	561.0	0.10	17	794.0	0.08
9	580.0	0.10			

The plot of the damping ratios of the acoustic measurement allows the assumption of an exponential relation between the frequency and the damping ratio (figure 3-30). The best-fit curve has been generated with *Microsoft Office Excel 2010* to verify the exponential relation.

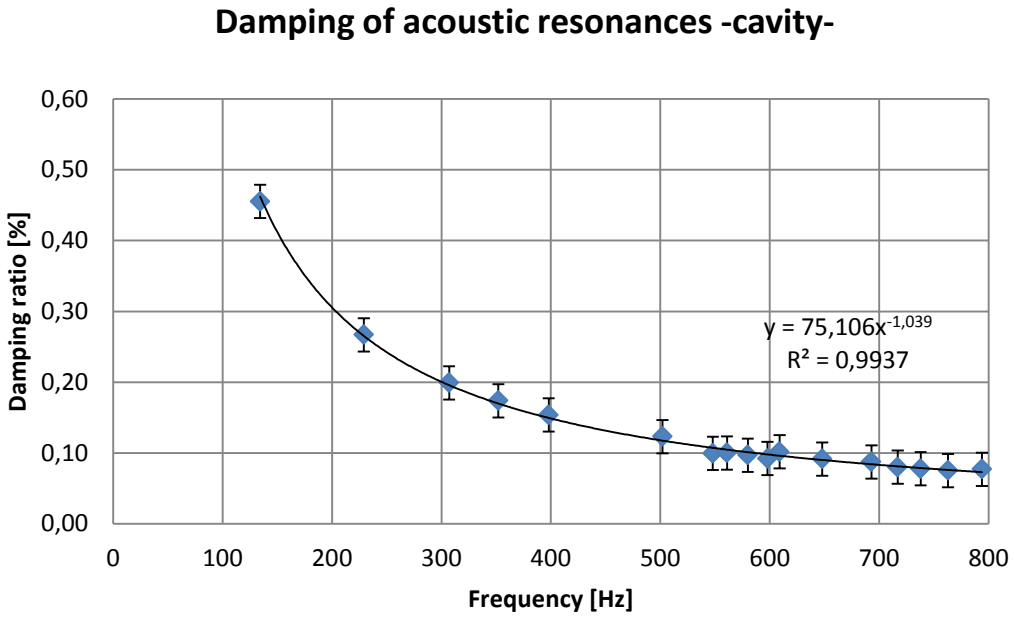

Figure 3-30 Damping of acoustic resonances –cavity-

The damping ratios for the structure excited by the exciter as well as by the shaker which have been determined out of the reverberation time are given in table 3-17 and table 3-18. An exponential relation between damping and frequency can be assumed for the structural excitation as well (figure 3-31 and figure 3-32).7

Table 3-17 Damping rations of structural resonances -exciter-

resonance	f_n [Hz]	D[%]
1	9.8	0.21
2	17.8	0.63
3	47.5	0.91
4	94.8	0.67
5	148.5	0.43
6	241.0	0.26
7	314.0	0.20
8	403.0	0.16
9	491.0	0.13

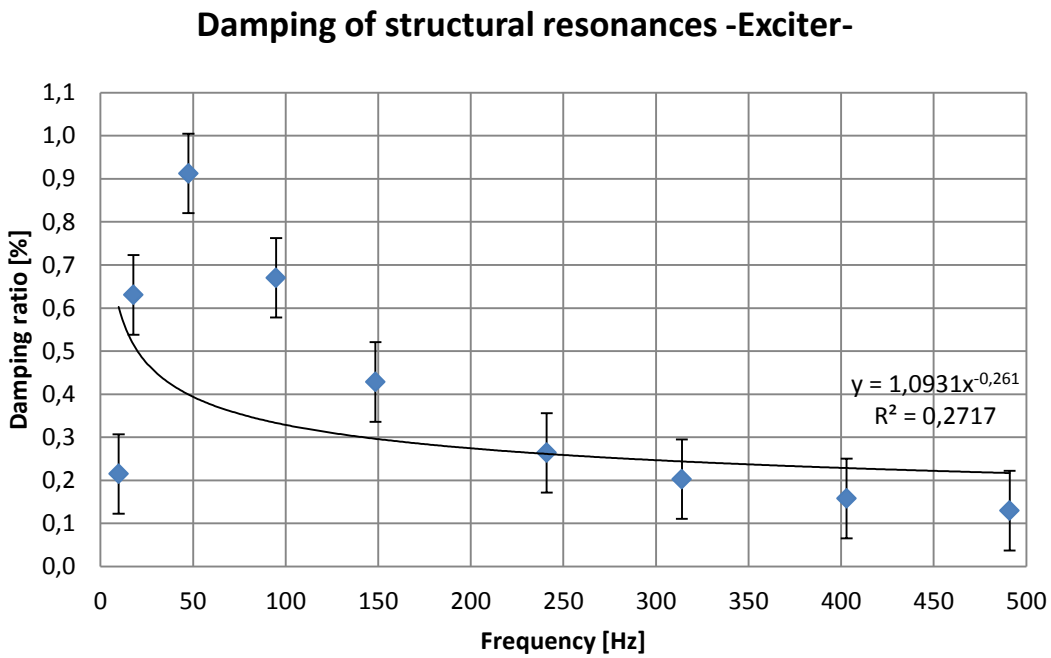

Figure 3-31 Damping of structural resonances -exciter-

Table 3-18 Damping ratio of structural resonances - shaker-

resonance	f_n [Hz]	D[%]
1	12.1	0.23
2	26.5	0.39
3	64.8	0.26
4	110.5	0.10

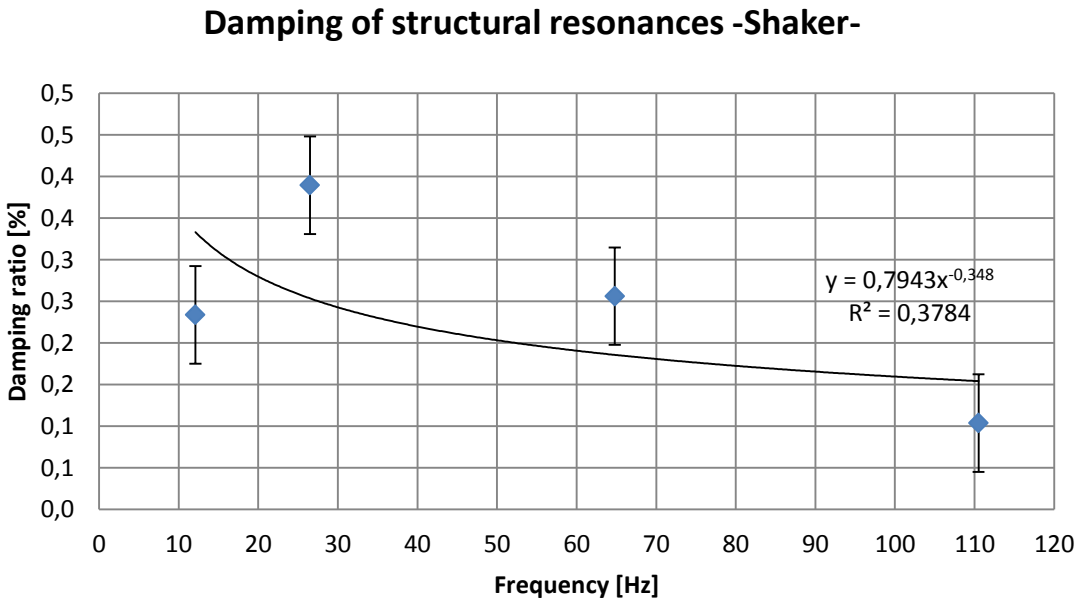

Figure 3-32 Damping of structural resonances - shaker-

3.6 Fluid-structure interaction

To be able to measure the interaction between the fluid and the structure, both, signals for the sound pressure and particle velocity as well as for the acceleration of the structure has been measured. To get an idea which frequencies couple well and worse with the structure, the Microflown has been placed in front of the structure (8-9mm) and centrally held by a placement device described in the section 3.1.1. The cavity has been excited by the loudspeaker using the broadband excitation signal coming from the MATLAB Simulink model.

Three possible sound transmission paths (table 3-19) for delivering sound have been figured out (figure 3-33). The red one is just delivering sound on the airborne sound path. The light blue line characterizes a path which is mainly delivering sound on the structure borne path. Right at its end the sound of the structure is emitting to the fluid before the particle velocity gets measured from the Microflown. The most complex path is the black one. Here the sound coming from the loudspeaker gets delivered on the airborne path first before coupling to the structure and at its end again to the fluid.

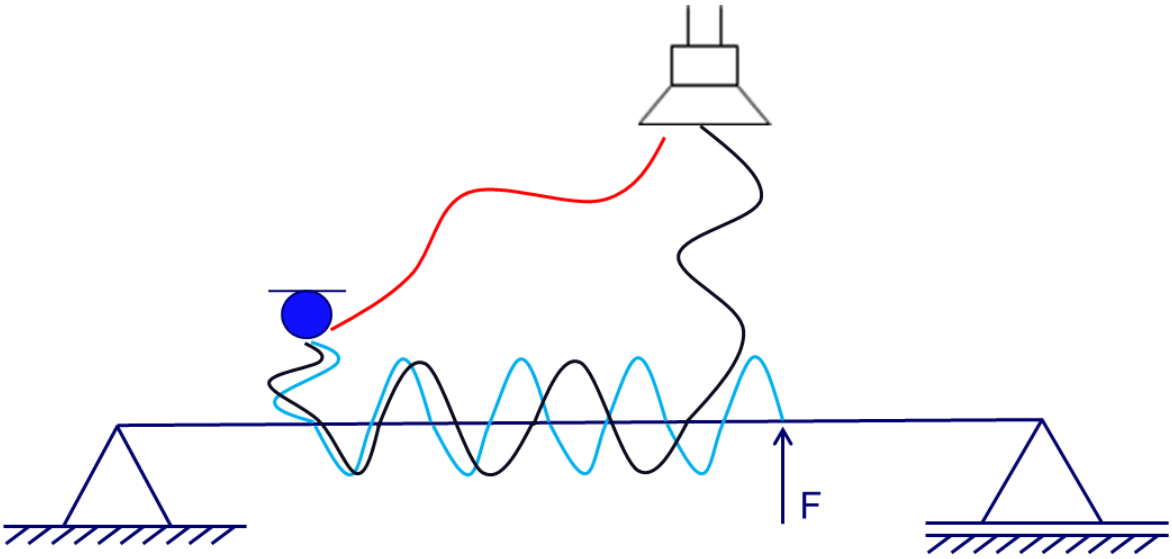

Figure 3-33 Fluid structure interaction – sound transmission paths

Table 3-19 Sound transmission paths

red line	Airborne path
blue line	Structure borne path
black line	Mixed path

3.6.1 Transfer path analysis

Figure 3-34 is building the basis for the next investigations. In this figure the coherence for the Microflown pressure (blue line), the normal particle velocity (blue element, green line) and the reference accelerometer (red line) has been plotted. All the input data is referred to the broadband excitation signal of the loudspeaker coming from the MATLAB Simulink model (figure 3-6). The Microflown itself has been placed centric in front of the beam structure during the measurement.

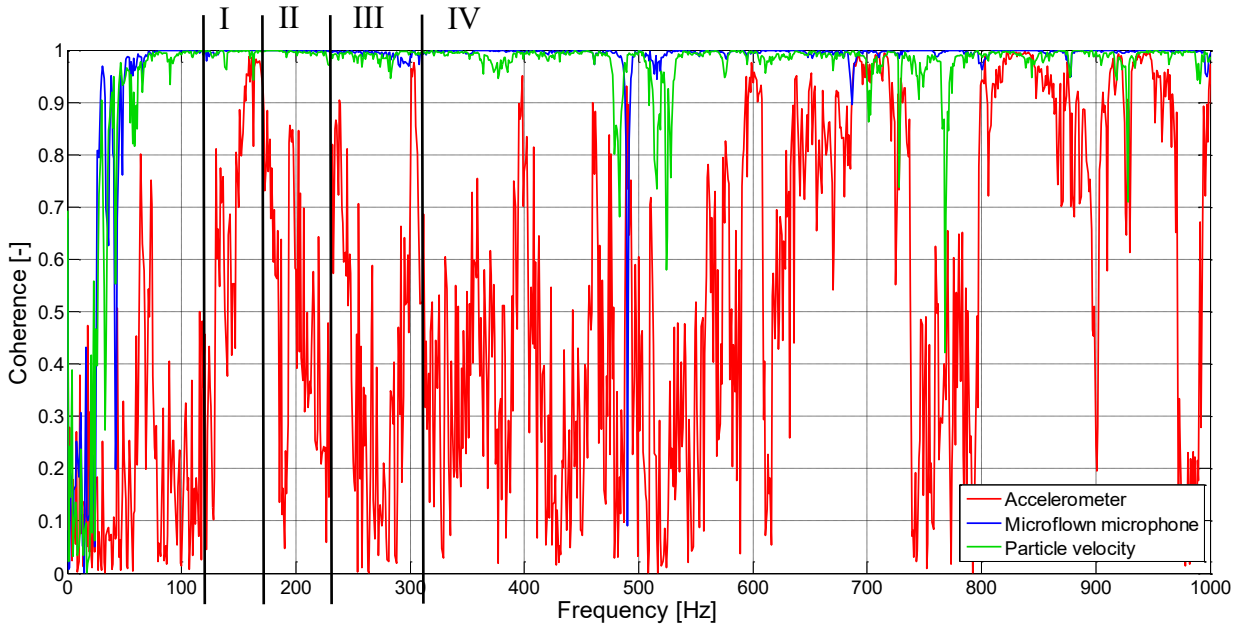

Figure 3-34 Coherence for the fluid-structure interaction

Four frequencies have been detected, depending on their coherence between the structure (given by the signal of the accelerometer) and the fluid (given by the Microflown pressure and particle velocity). The determined frequencies are given in table 3-20.

Table 3-20 Overview of the frequencies for the fluid-structure interaction

Frequency	f_n [Hz]
I	134
II	175
III	238
IV	307

Frequency I and IV show a rather bad coherence (0.6 and 0.4) compared to frequency II and III (0.7 and 0.8). Investigations about how the different mode shapes of the fluid and the structure in these certain frequencies look like have been done as well.

The four frequencies have been excited tonally for the measurement one after another using the exciter, shaker or the loudspeaker. The Microflown has been placed under the placement device and moved to each of the five measurement points which have been defined in equivalent distances of 100mm to each other (distance between structure and Microflown approximately 8-9mm). The normal velocity as well as the sound pressure has been measured using the Microflown and the acceleration of the structure has been measured using the reference accelerometer.

The measurement has been performed three times for every of the four frequencies and five measurement points to guarantee a statistic safety.

For the MAC-Analysis, described in section 2.4, the eigenvector given by the magnitude and the phase for every frequency at each measurement points needed to be defined. The Input data for the MAC-Analysis, which has been programmed in MATLAB (appendix E), can be seen in table 3-21, table 3-22 and table 3-23.

In all of the three tables the magnitudes (abs) as well as the belonging phases for each measurement point can be read off directly. These are normalized to the first component of the belonging vector (in amplitude and phase). The averaging for the statistic safety has been done previously using *Microsoft Excel 2010*.

Table 3-21 MAC input data - exciter

	Measurement point 1		**Measurement point 2**		**Measurement point 3**		**Measurement point 4**		**Measurement point5**	
	abs	phase [°]	abs	phase [°]	abs	phase [°]	abs	phase [°]	abs	phase [°]
Vector 134 Hz norm.	1.00	0.00	6.00	-77.40	4.27	-66.40	2.68	87.30	0.71	-11.40
Vector 175 Hz norm.	1.00	0.00	0.30	-90.90	1.32	10.20	1.04	-187.40	0.25	-308.0
Vector 238 Hz norm.	1.00	0.00	0.22	-59.70	0.24	1.00	0.63	22.30	0.73	-67.40
Vector 307 Hz norm.	1.00	0.00	0.05	128.70	0.25	149.10	0.31	186.60	0.08	104.50

Table 3-22 MAC input data - shaker

	Measurement point 1		**Measurement point 2**		**Measurement point 3**		**Measurement point 4**		**Measurement point5**	
	abs	phase [°]	abs	phase [°]	abs	phase [°]	abs	phase [°]	abs	phase [°]
Vector 134 Hz norm.	1.00	0.0	0.87	211.20	2.35	42.20	0.96	214.10	0.66	1.00
Vector 175 Hz norm.	1.00	0.0	1.71	-158.20	2.35	-196.40	1.26	-260.70	0.67	-127.30
Vector 238 Hz norm.	1.00	0.0	0.38	13.20	1.01	-147.30	0.52	3.80	1.40	18.60
Vector 307 Hz norm.	1.00	0.0	2.88	13.70	2.970	3.3	0.65	-159.00	1.38	104.50

Table 3-23 MAC input data - loudspeaker

	Measurement point 1		**Measurement point 2**		**Measurement point 3**		**Measurement point 4**		**Measurement point5**	
	abs	phase [°]	abs	phase [°]	abs	phase [°]	abs	phase [°]	abs	phase [°]
Vector 134 Hz norm.	1.00	0.00	1.02	-6.10	0.53	10.50	0.67	14.80	0.95	23.40
Vector 175 Hz norm.	1.00	0.00	0.72	-25.20	3.60	-32.90	2.07	-6.60	2.93	-94.10
Vector 238 Hz norm.	1.00	0.00	0.18	62.40	1.41	-168.30	2.42	-224.20	0.35	67.30
Vector 307 Hz norm.	1.00	0.00	0.81	-7.30	0.38	-104.30	0.81	-179.40	0.64	-168.50

Each component of the vector for the MATLAB Code has been calculated using equation [3-3]:

$$x = \hat{x} \cdot e^{j\varphi} \qquad [3\text{-}3]$$

The results of the MAC value calculation are given afterwards. For the nomenclature it is important to know that for the MAC matrix EXC_LS the input data of the EXC corresponds to data Set B given in figure 2-10 and the input data for the LS to data set A. A combination of three different MAC matrices is possible, EXC_LS, SH_LS and EXC_SH. To calculate the MAC matrix with the same set of data provides does not make sense, due to the fact that the result has to be an ideal matrix as described in section 2.4.

MAC Matrix EXC_LS:

$$MAC\_EXC\_LS = \begin{pmatrix} 0.2931 & 0.1679 & 0.0189 & 0.2331 \\ 0.1155 & 0.1413 & 0.1018 & 0.2049 \\ 0.5143 & 0.2752 & 0.1427 & 0.0911 \\ 0.1179 & 0.0208 & 0.3065 & 0.4300 \end{pmatrix}$$

MAC Matrix SH_LS:

$$MAC\_SH\_LS = \begin{pmatrix} 0.0587 & 0.2949 & 0.0294 & 0.0131 \\ 0.1095 & 0.1674 & 0.4329 & 0.1620 \\ 0.4059 & 0.0115 & 0.1045 & 0.0115 \\ 0.1952 & 0.2208 & 0.0538 & 0.3686 \end{pmatrix}$$

MAC Matrix EXC_SH:

$$MAC\_EXC\_SH = \begin{pmatrix} 0.0865 & 0.4314 & 0.0576 & 0.7334 \\ 0.7320 & 0.0434 & 0.0413 & 0.3212 \\ 0.0560 & 0.0380 & 0.1975 & 0.0775 \\ 0.1359 & 0.1838 & 0.1772 & 0.0187 \end{pmatrix}$$

The matrices show, that none of the various types of excitation (exciter, shaker and loudspeaker) provide the same excitation for the same frequency. In none of the matrices the values of the main diagonal elements get close to “1” and the elements on the secondary diagonal close to “0”, which means that there has been an excitation but the mode vectors for each frequency have not been the same and do not correspond to each other.

There are three main considerations. Looking at the matrix EXC_SH, the weight of the exciter de-tunes the system in a way that the resonant frequencies slip of the rail to lower frequencies. Furthermore, the deviation of the matrices which show the MAC values of either the shaker or the exciter compared to the loudspeaker can be explained with the different type of excitation. The excitation with the acoustic noise coming from the loudspeaker acts as a distributed load on the beam structure, whereas the excitation the exciter or the shaker equates to a more or less concentrated point force. By looking at figure 3-33, the third mixed path can be neglected compared to the two other ones due to the fact that the acoustic level has to be too high to achieve a level of excitation without the Microflown being in an overload for the particle velocity sensor and the pressure microphone. This means that there is only one source for structure borne sound which is controllable.

4 Measurement of the structural vibration using particle velocity probe

4.1 Coherence based measurement technique

The coherence describes the dependency of the measured signals over the frequency. It can be proofed, if all frequencies have been excited in the same way. The coherence can differ between values of zero to one. The measured signals are fully correlated if the coherence reaches a value of one [15], p.156. According to the deviation of this value, a statement about the quality of the measurement can be made. For this coherence based measurement technique, the deviation of this value is a measure for the coupling between the structure and the fluid, if the coherence is calculated between the signals of the particle velocity and the accelerometer signal.

4.1.1 Idea for the measurement technique

The idea was to test a measurement technique to fully utilize the possibilities the Microflown provides. Due to the fact that particle velocity can be measured in all three directions, the normal and the tangential elements are used to perform particle velocity measurements. The normal particle velocity is mostly the vibration coming from the structure whereas the tangential particle velocity can be used to define the distance to be able to perform good measurements. The theory predicts that the tangential particle velocity is zero if the distance is zero. The normal particle velocity can be defined as:

$$a_n = j\omega \cdot v_n ,$$

$$v_t = 0 .$$

The Microflown has been placed in front of the structure using the sensor placement device (section 3.1.1) at three different distances (figure 4-1). The color nomenclature for the plots given in the following sections 4.1.3 and 4.1.4 will be the same. The nomenclature for the distances is given in table 4-1. The measurement has been performed without the protection cab on top of the Microflown due to the high loss in distance between the particle velocity element and the structure. Please notice that the colors do NOT correspond to the coloring of the particle velocity elements of the Microflown.

Table 4-1 Color nomenclature for three distances

color	distance [mm]
green	1-2
red	3-4
blue	7

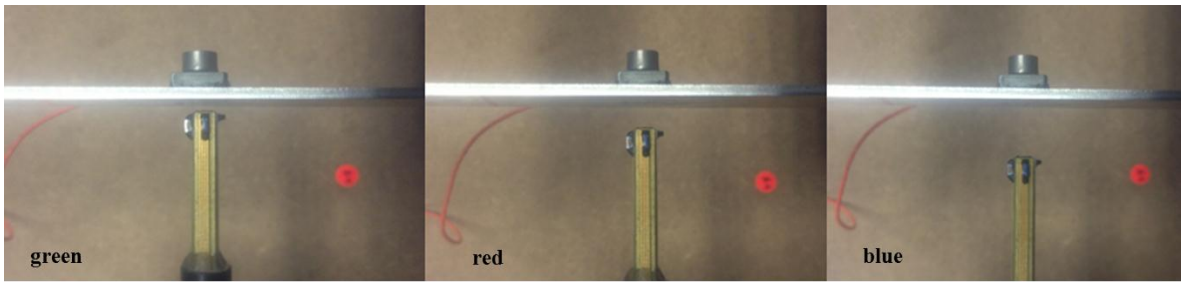

Figure 4-1 Measurement distances between Microflown and structure

The accelerometer has been placed on the opposite direction of the beam structure (figure 4-2). This has been done to have a chance to measure the coherence between the particle velocity of the Microflown and the accelerometer placed on the structure.

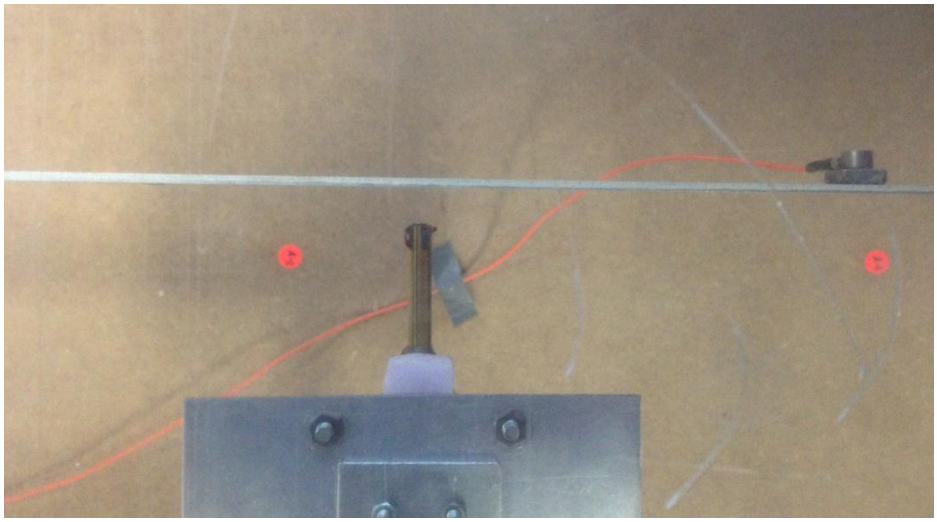

Figure 4-2 Sensor placed in front of structure for coherence measurement (case IV section 4.1.2)

For the measurement without back ground noise (BGN) the structure has been excited with a level of 98dB. Some parameter variations have been tested (section 4.1.2). Two different levels of BGN have been applied with the loudspeaker (see section 4.1.4)). The acoustic level of excitation has been measured using the Microflown microphone. All excitations have been performed with a broadband signal generated with the MATLAB Simulink model (section 3.2). For the measurements including the BGN, the same broadband signal has been used, but in an uncorrelated way by sending the signal to the loudspeaker using a second laptop. The normal particle velocity has been measured using the green element and the tangential particle velocity with the blue element.

4.1.2 Parameter variations

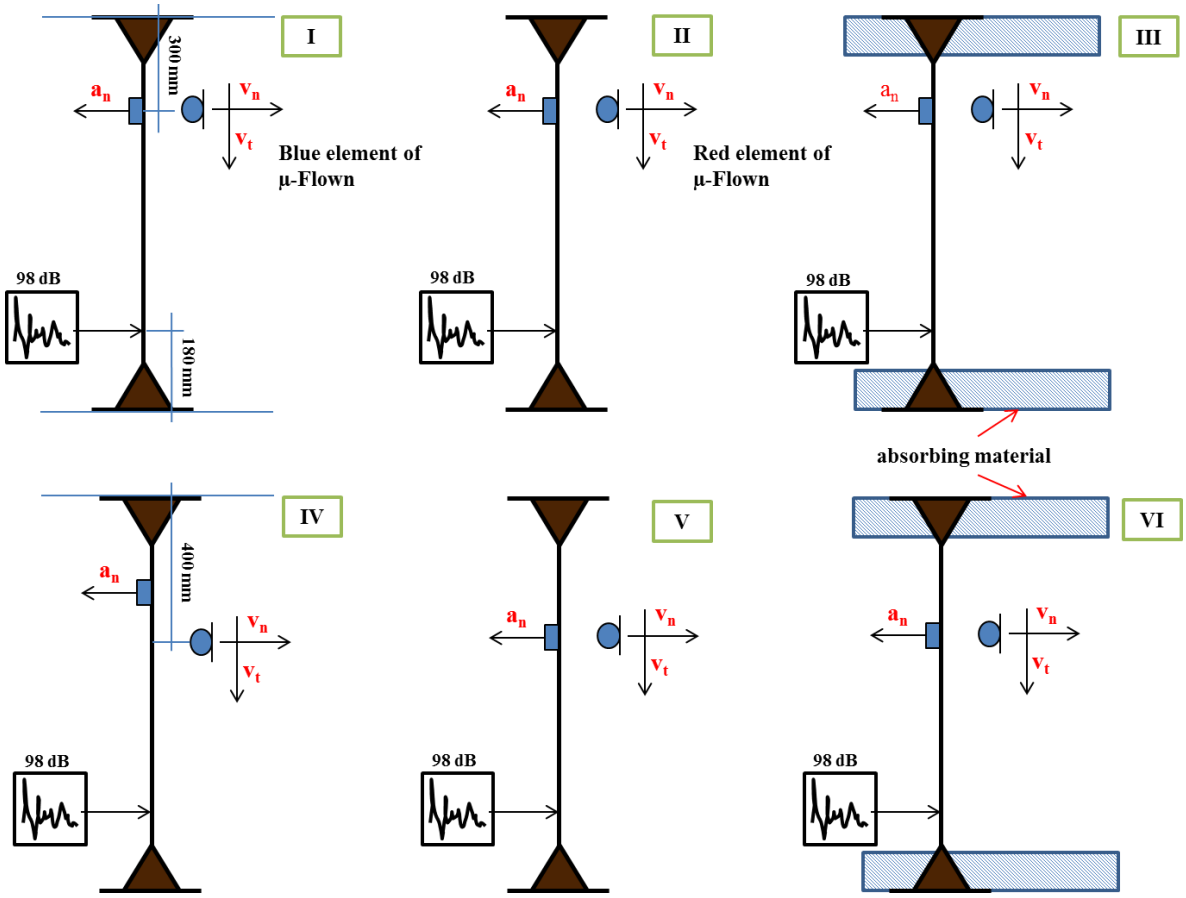

Figure 4-3 Parameter variation of the coherence measurement

Figure 4-3 gives an overview of the different parameters which have been varied. These have been:

(1) blue or red element for the tangential particle velocity (I and II)

(2) Position of the combination Microflown – accelerometer (I, II and V)

(3) Position of the accelerometer (IV)

(4) Position of the Microflown (IV)

(5) Distance Microflown – structure (all cases)

(6) Influence of absorbing material on both sides of the vibro-acoustic test rig. (III and VI)

Case I will be the nominal one for the investigations concerning the BGN. In section 4.1.3 and section 4.1.4 the results for this nominal case will be illustrated. The frequency range is 0Hz to 1kHz. All other results can be found in the appendix H due to the fact that these results show the same trends.

4.1.3 Results of the coherence measurement without background noise

At first the results for the coherence between the accelerometer signal a_n and the tangential particle velocity v_t measured with the blue element (case I, figure 4-3) will be shown in figure 4-4.

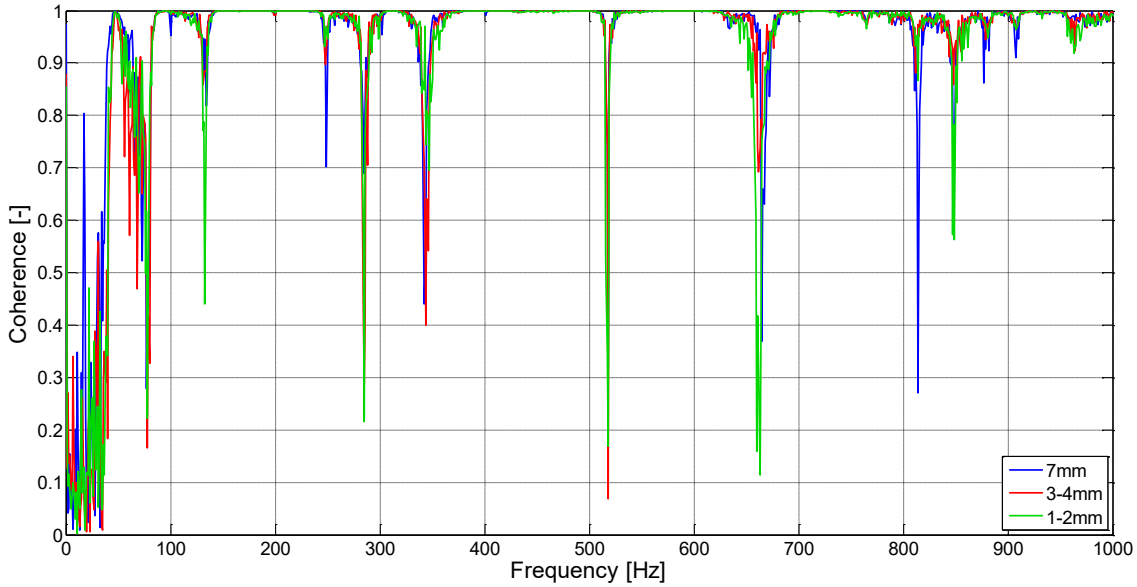

Figure 4-4 Coherence accelerometer and tangential particle velocity

The coherence is almost perfect due to the face that the coherence is one. The quality fall-offs are the anti-resonances. Furthermore, no significant influence of the distance has been figured out. Figure 4-5 shows the coherence between the accelerometer and the normal particle velocity which has been measured using the green element. In the range of 120Hz to 220Hz the coherence is close to one. In this area, the structure couples well with the fluid. The influence of the measurement distance can also be noticed.

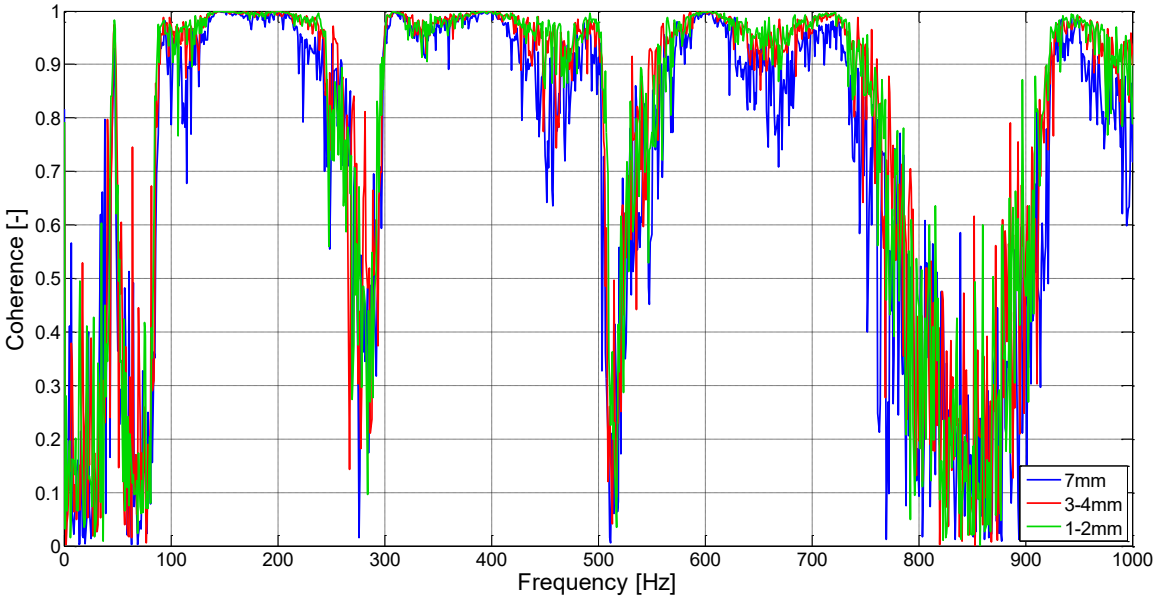

Figure 4-5 Coherence accelerometer and normal particle velocity

Taking figure 4-6 into account as well, it is interesting to see that the plot does not differ so much from figure 4-5. This belongs to the fact that if one coherence is almost perfect and another one has even more quality fall-offs, this first coherence curve will not have a big influence on the combination of those two. What is even more important is the fact that the signal of the accelerometer is not necessary to get a coherence plot, which has the same statement like the figure 4-5 with the accelerometer. Furthermore it can be noticed, that the distance for the measurement does have an influence especially in the quality fall-offs. A good example for this is the frequency range between 420Hz and 500Hz (figure 4-6).

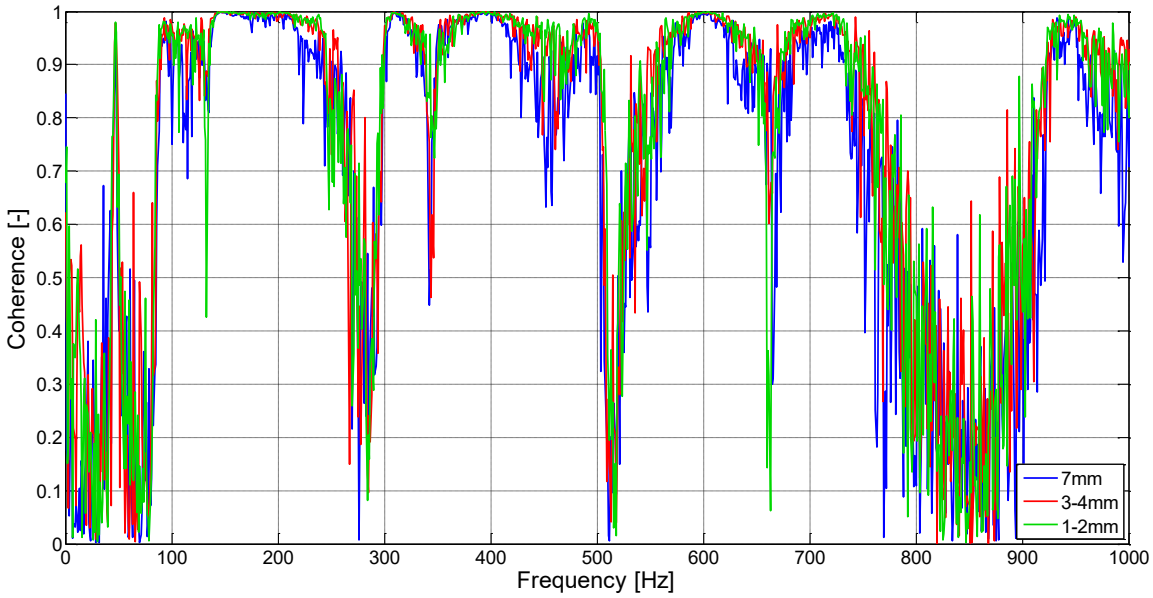

Figure 4-6 Coherence between normal and tangential particle velocity

The absorbing materials on both sides of the walls of the vibro-acoustic test rig do not have a big influence on the tangential coherence. These measurements (case III and VI) have been performed due to the fact that some quality fall-offs in the tangential coherence have been expected with some absorbing material.

4.1.4 Results of the coherence measurement with background noise

The influence of BGN has been examined according to two different cases:

(1) 68 dB BGN

(2) 82 dB BGN

The sound pressure of the loudspeaker has been measured using the Microflown microphone previously.

The test set-up for these measurements has been modified like figure 4-7.

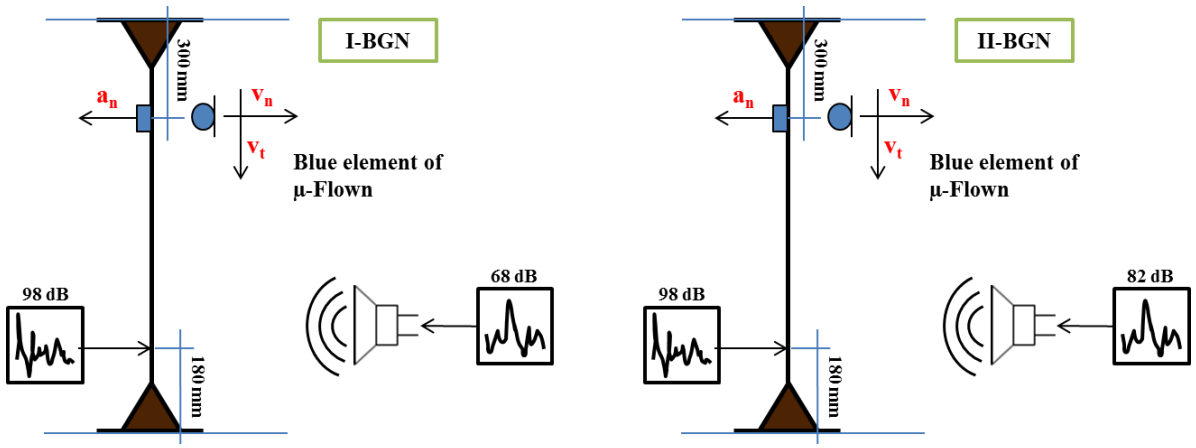

Figure 4-7 Test cases for the coherence measurement with BGN

Like previously described in section 4.1.1, a second broadband excitation signal has been applied to the loudspeaker (68dB in case I-BGN and 82dB in case II-BGN). To guarantee the same signal generation, both laptops used the same MATLAB Simulink model (figure 3-6). To guarantee that the signals are uncorrelated, the signal output has been started at a different time. As seen in the previous chapter it is sufficient to look at the coherence between the normal and the tangential particle velocity.

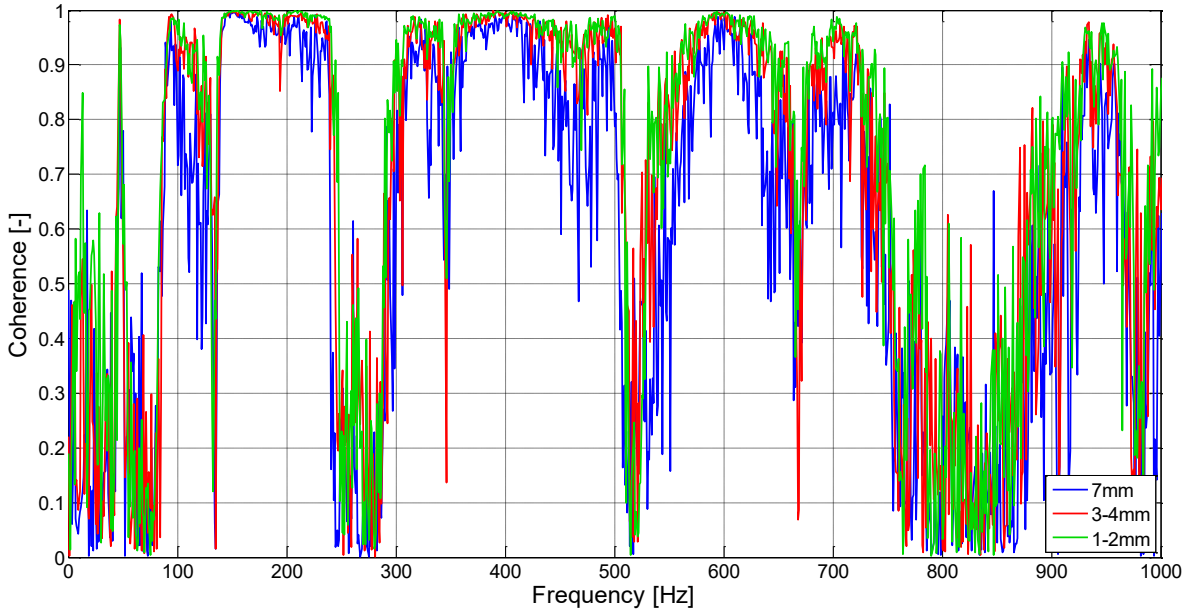

Figure 4-8 Coherence between normal and tangential particle velocity, 62dB BGN

Figure 4-8 shows the case I-BGN. An influence of the background noise can be found compared to Figure 4-6. Especially the influence of the measurement distance between the structure and the Microflown becomes particularly obvious. The blue curve representing the biggest measurement distance is below the red and green curve at the whole frequency range. The coherence rises, if the measurement distance decreases. Nevertheless the level of distortion was not big enough to have a significant influence on the measured coherence between the normal and tangential particle velocity. The same trends can be found in figure 4-9 representing the case II-BGN. The coherence does not even reach a value of one, e.g. at the frequency range between 140Hz to 240Hz due to the high level of distortion. The coherence significantly rises when the measurement is performed as close as possible to the structure compared to figure 4-8. The influence of a BGN of 82dB becomes even more clear if figure 4-9 (Coherence measurement without BGN) and figure 4-6 (Coherence measurement with 82dB BGN)

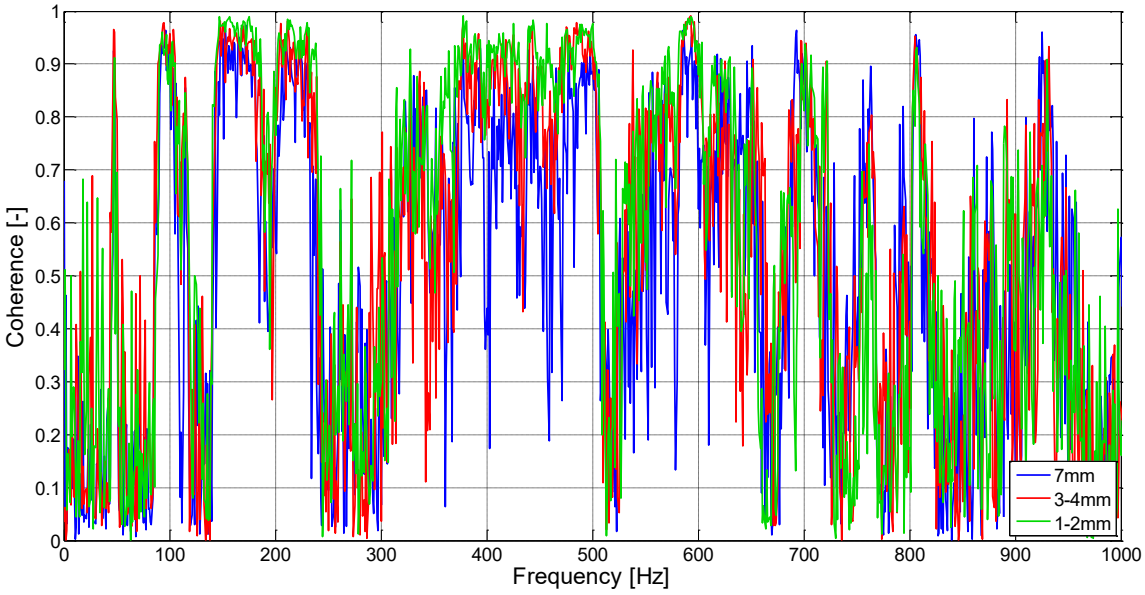

Figure 4-9 Coherence between normal and tangential particle velocity, 82 dB BGN

4.2 Quantification of the signal-to-noise ratio

4.2.1 Transfer function and auto spectral density

The transfer function and the auto spectral density can be used to quantify the signal-to-noise ratio. The transfer function is the response spectrum referred to the excitation spectrum (figure 4-10, [15], p. 362).

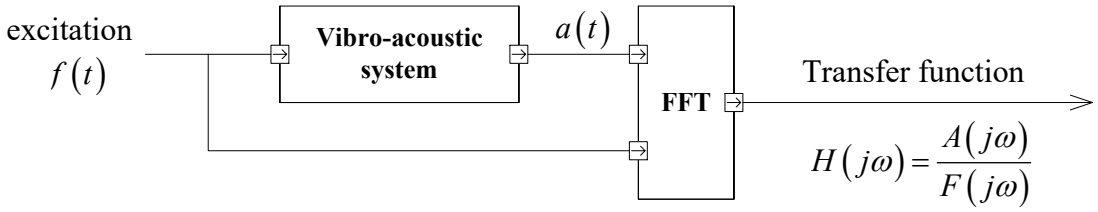

Figure 4-10 Schematic display of the transfer function, [15]

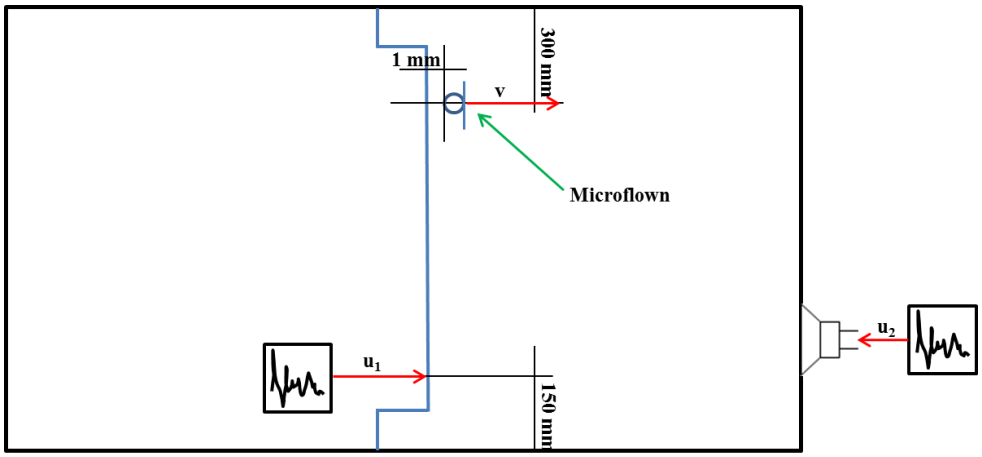

Figure 4-11 Transfer function measurement inside vibro-acoustic test rig

The Microflown has been placed 300mm (measured from the wall) in front of the structure at 1mm distance. The normal particle velocity has been measured. Two different ways of excitation have been used. The exciter has been used for the beam structure and the loudspeaker for the cavity. The broadband signal had a level of 82dB.

If two uncorrelated signals are used as an input for a system, the particle velocity can be calculated according to figure 4-12.

Figure 4-12 System input for transfer function measurement

The following two transfer functions have been measured:

(1) $H_1 = \frac{v}{u_1}$, exciter Microflown (broadband signal on exciter, loudspeaker turned off)

(2) $H_2 = \frac{v}{u_2}$, loudspeaker Microflown (broadband signal on loudspeaker, exciter turned off)

These transfer functions have been plotted together in figure 4-13. It can be noticed, that both curves show resonance peaks at certain frequencies. At around 150Hz, there is a structural resonance. The loudspeaker could not excite this resonance that's why the transfer function does not show a resonance peak. Around 240 Hz the situations is exactly vice versa. Looking at 305Hz, it can be noticed that this resonance has been excited by both, the loudspeaker and the exciter.

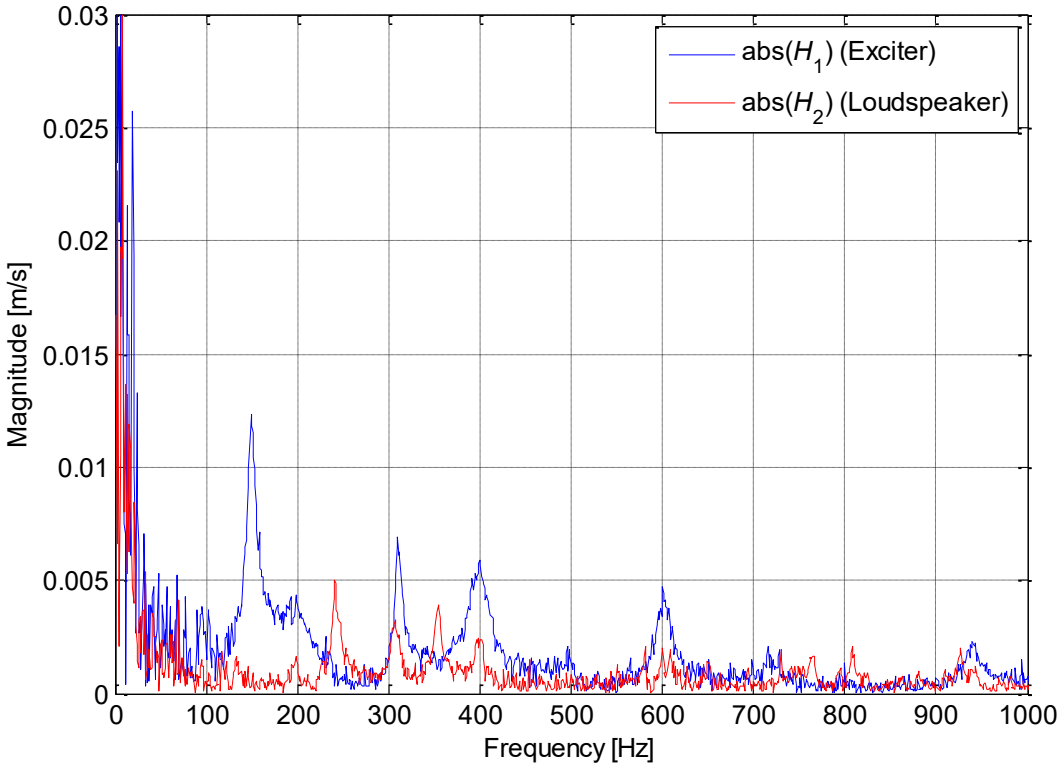

Figure 4-13 Measured transfer functions inside vibro-acoustic test rig

The auto spectral density is defined as:

$$S_{xx} = \lim_{T\to\infty} \frac{1}{2T} \left| \underline{\bar{X}}^{*}(j\omega)\, \underline{\bar{X}}(j\omega) \right| \qquad [4\text{-}1]$$

After some mathematical reformulations equation [4-1] for the analyzed system becomes:

$$S_{vv} = |H_1|^2 S_{u_1u_1} + |H_2|^2 S_{u_2u_2} \qquad [4\text{-}2]$$

The first part of equation [4-2] can be defined as the wanted signal and the second part as the disturbing signal.

The signal-to-noise ratio can be calculated as:

$$SNR = 10\log_{10}\frac{wanted\ signal}{disturbing\ signal},$$

$$SNR = 10\log_{10}\frac{|H_1|^2 S_{u_1u_1}}{|H_2|^2 S_{u_2u_2}},$$

$$SNR = 10\log_{10}\left(\frac{|H_1|}{|H_2|}\right)^2 + 10\log_{10}\left(\frac{S_{u_1u_1}}{S_{u_2u_2}}\right). \qquad [4\text{-}3]$$

In the complex formulation equation [4-3] results in:

$$SNR = 10\log_{10}\left(\frac{|H_1(j\omega)|}{|H_2(j\omega)|}\right)^2 + 10\log_{10}\left(\frac{S_{u_1u_1}(j\omega)}{S_{u_2u_2}(j\omega)}\right) \qquad [4\text{-}4]$$

The ratio of the transfer functions defines the part the structure has to the SNR (equation [4-4]). The auto spectral density the part the system inputs have to the SNR.

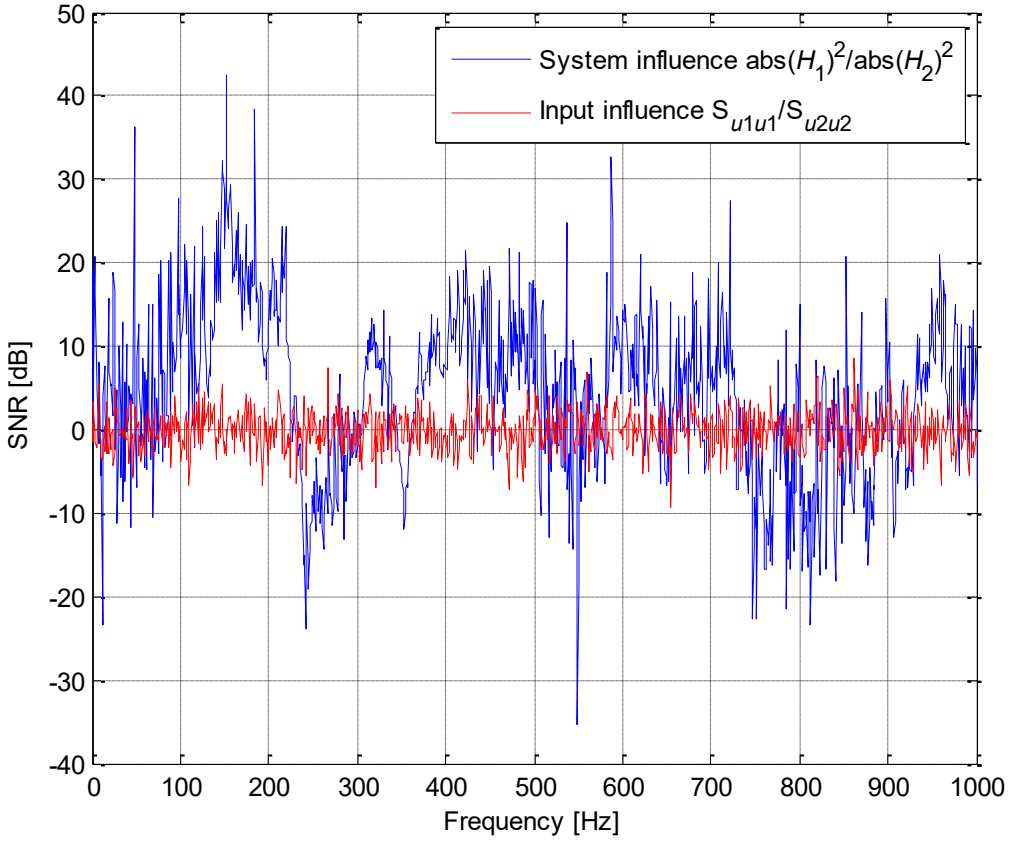

Figure 4-14 Signal-to-noise ratio

Figure 4-14 shows the signal-to noise ratio according to equation [4-4]. It can be noticed that the system influence (the ratio of the transfer functions) is not always above the influence of the inputs which results in a bad SNR. Taking figure 4-15 into account as well, the bad SNR can exactly be defined in the areas where the exciter could not measure a resonance (e.g. around 240Hz. The bad SNR means that the level of excitation should have been higher to

have a good chance to measure. Whenever the transfer function of the exciter is below one of the loudspeaker, a bad SNR can be detected.

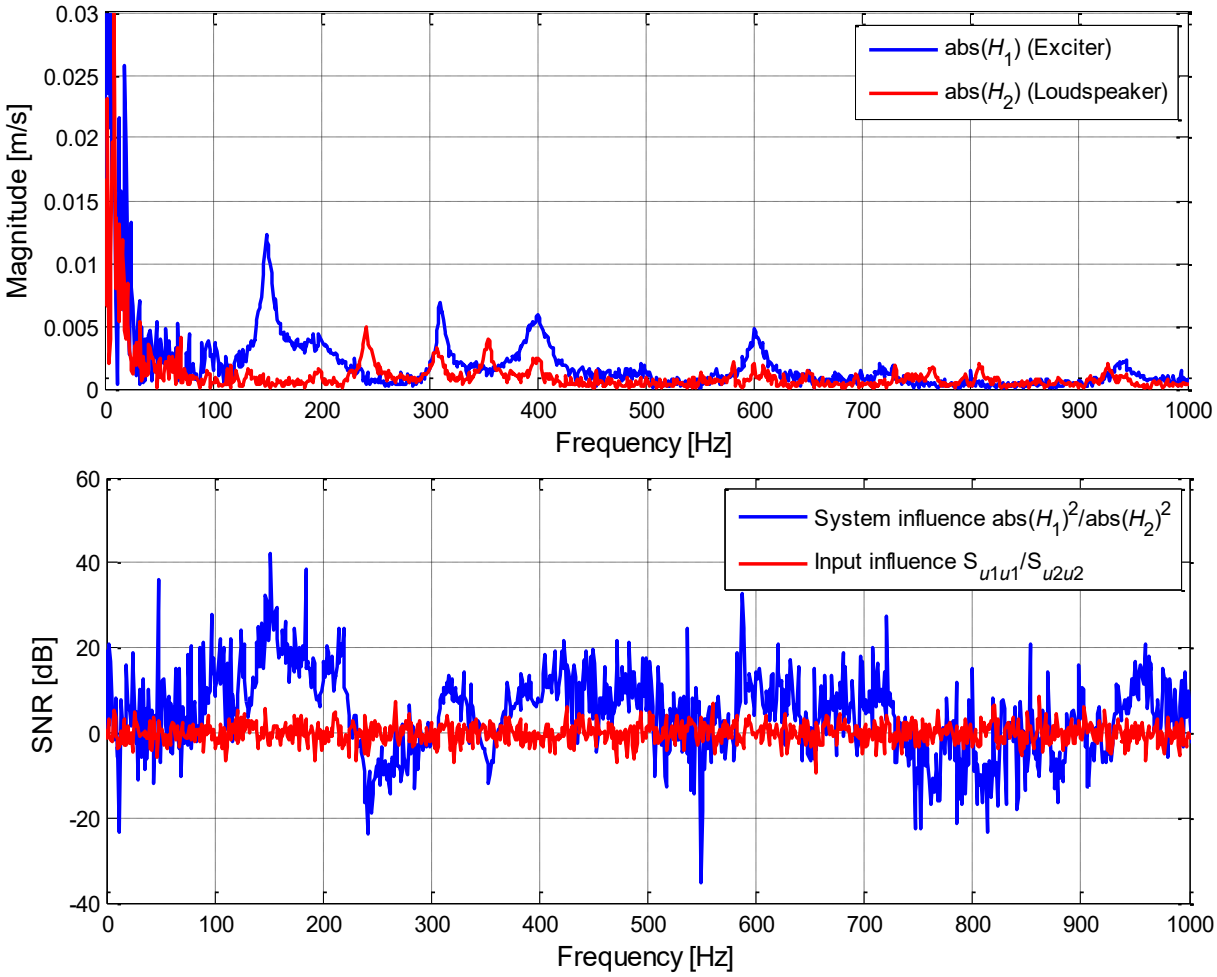

Figure 4-15 Transfer functions and SNR

Moreover it is interesting to see what the error in dB was with regards to the SNR and BGN (figure 4-16). Therefore, the signals of the accelerometer and the normal particle velocity of the Microflown have been used. The investigations have been done for three cases (no BGN, 68dB BGN and 82dB BGN). The transfer functions between the accelerometer and the normal particle velocity have been calculated using MATLAB. Due to the fact that the signals are not the same (acceleration and speed signal), the following conversion has to be taken into account (equation [4-5]):

$$T_{a_s v_s} = \frac{v_n}{a_s} = \frac{v_n}{j\omega \cdot v_s} = \frac{1}{j\omega}\frac{v_n}{v_s} = \frac{1}{j\omega} T_{v_s v_n},$$

$$T_{v_s v_n} = j\omega T_{a_s v_s}. \qquad [4\text{-}5]$$

(v_n is the measured normal particle velocity with the Microflown and a_n the signal coming from the accelerometer)

The error can be calculated using equation [4-6]:

$$error = 20\log_{10}\left(\left|T_{v_s v_n}\right| \cdot 2\pi f\right). \qquad [4\text{-}6]$$

The relative error can be calculated using equation [4-7]:

$$rel.error = 20\log_{10}\left(1-\left(\left|T_{v_s v_n}\right| \cdot 2\pi f\right)\right). \qquad [4\text{-}7]$$

Figure 4-16 shows the rel. error between the normal particle velocity and the accelerometer signal (equation [4-7]).The MATLAB code can be found in appendix J. The following plots include the correction formulas for the sensitivity of the Microflown particle velocity elements as described previously in section 2.1.2 (The plots excluding the correction formulas can be found in appendix K. The influence of the BGN can clearly be identified for a frequency range to 1kHz (blue curve always above the red and green curve). Looking at 200Hz it can be noticed that the Microflown measures 10dB less if the level of BGN is 82dB and around 8dB less if the level of BGN is 68dB. Without any background noise, the difference is 6.7dB. The deflections belong to those frequencies where the exciter was unable to excite the structure (see figure 3-23) and the cavity got exited in acoustical resonances (see figure 3-28).

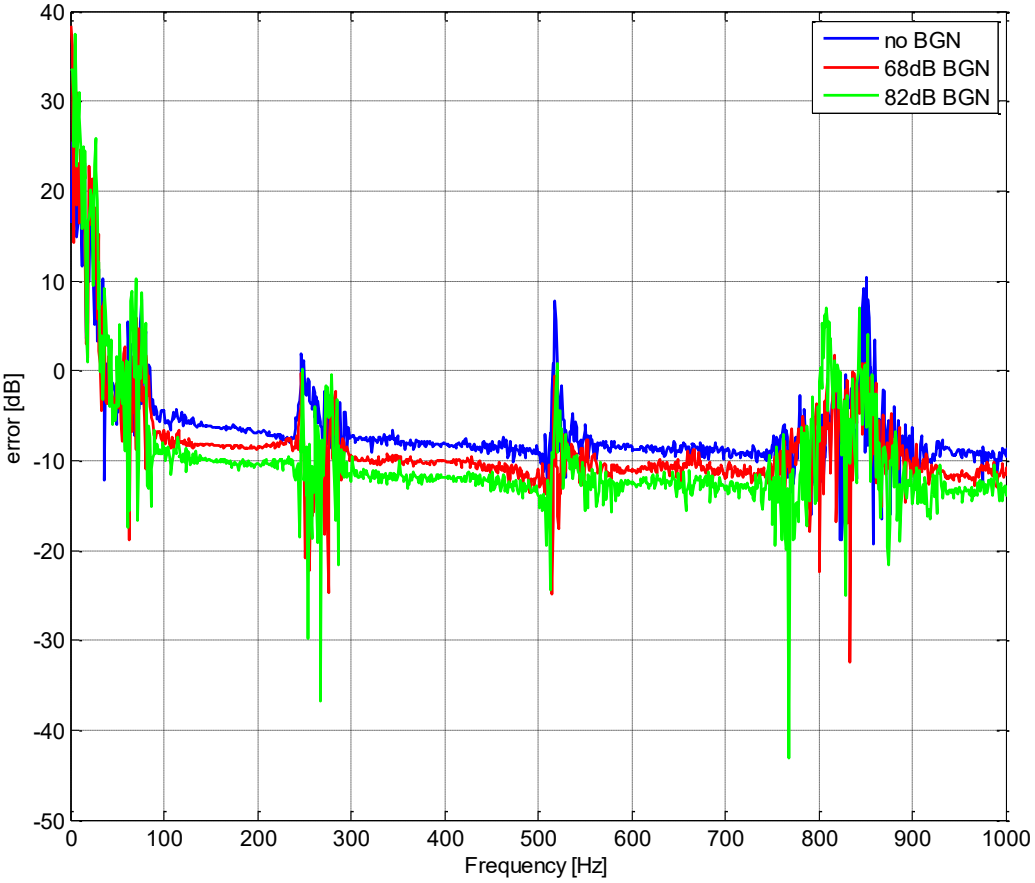

Figure 4-16 Error for measurements with/without BGN filter on

To be able to compare the error to the one determined for the analytical model (figure 2-20 to figure 2-22), the relative error has to be calculated (equation [4-7]). The comparison has been done for the nominal case (1mm distance between structure and Microflown, no BGN). The results can be seen in figure 4-17. A slightly increasing relative error of 7dB for 100Hz and around 3dB for 1kHz can be noticed.

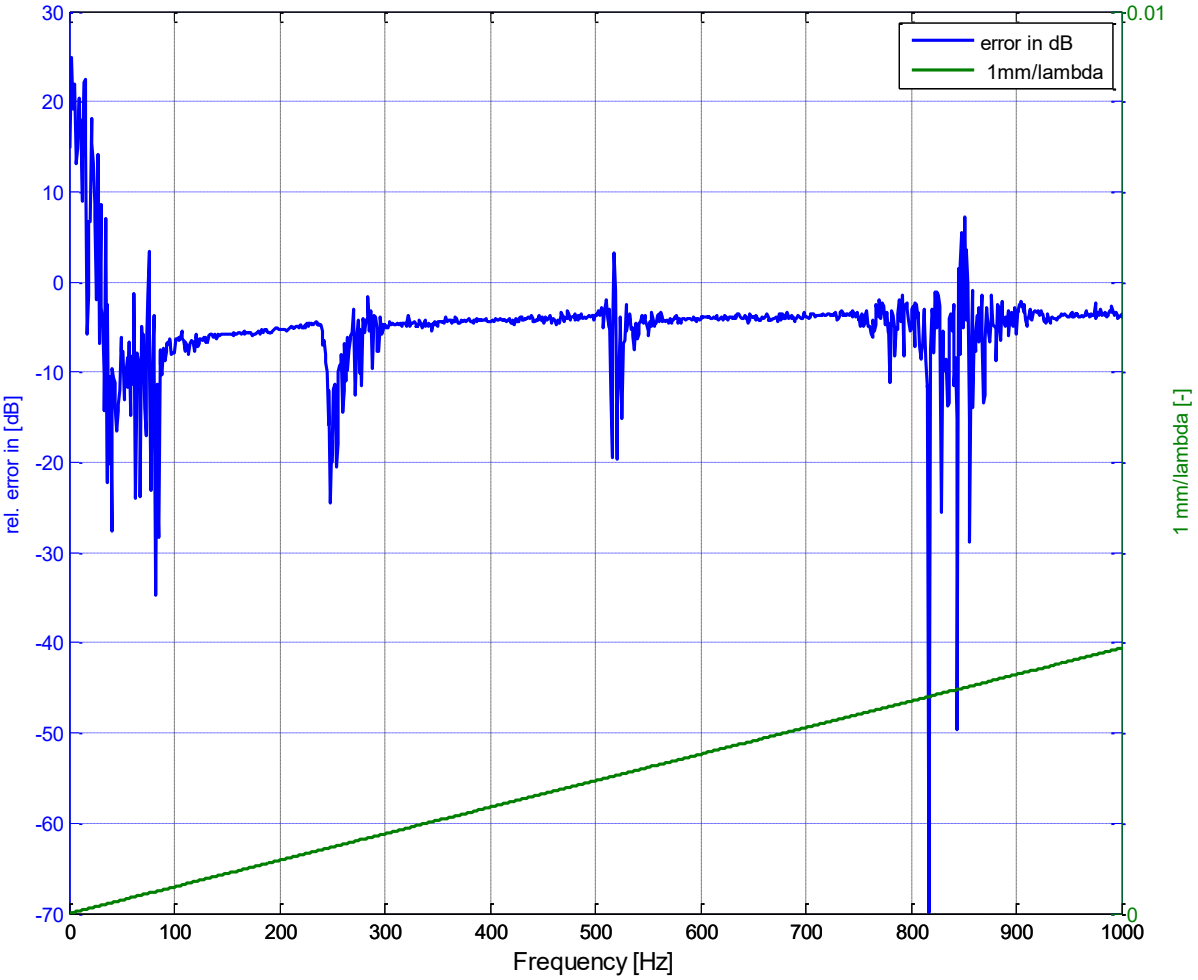

Figure 4-17 Relative error for nominal case

At first it is important to know that the vibro-acoustic test rig is a two dimensional sound tube whereas the solution for the analytical model is for one dimension only. Of course the calculated error of measurement data is bigger than the error calculated in the analytical model (around 5dB compared to a maximum of 1dB in the analytical model). This belongs to the fact that the analytical model is calculated without absorption and for perfect conditions. Moreover the analytical model is over- or underestimating the error whereas the calculated relative error of the measurement data is just underestimating the error.

5 Guidelines for an appropriate use of the acoustic sensor

After the investigations on the measurement of the structural vibration using particle velocity probes, the following guidelines for an appropriate use the acoustic sensor have been formulated below:

(1) Have a good knowledge about how the structural behaves (amplitudes at resonant frequencies)
   - Important for the measurement distance between Microflown and structure

(2) Definition of the measurement setting (high/low gain, correction on/off)

(3) Be careful with sensitivities!
   - Every element (blue, red and green) has its particular sensitivity
     - Calibration report
   - Apply filters in the post-processing if necessary (e.g. using MATLAB)
     - Formulas out of calibration report

(4) Pay attention to the SPL
   - No overload on the microphone or particle velocity sensor
     - Distortion of the measured signal
   - Dynamic ranges can be taken out of calibration sheet

(5) Measure the normal and tangential particle velocity and calculate the coherence function
   - Information about where the structure and the fluid couple well or worse

(6) Measure the background noise (Microflown microphone)
   - Important for the influence on the coherence function

(7) Measure the transfer paths and calculate the auto spectral density
   - Idea about the level for the measurement and the SNR at certain frequencies

6 Summary

In this master's thesis, the ability to use particle velocity probes for contact-free vibration measurements has been reviewed. Some investigations on a coherence based measurement technique have been done as well as a method for the qualification of an acceptable signal-to-noise ratio developed. Furthermore the optimal measurement distance has been derived from an analytical model first and verified in measurements afterwards. Finally a set of guidelines for an appropriate use of the sensor have been formulated.

At first, the theoretical background has been elucidated before the vibro acoustic test environment is described. An analytical model has been discussed in detail due to the fact that the measurement distance between the object and particle velocity probe plays an important role for good measurement results.

Some investigations on the self-noise of the used sensors and the acoustic and mechanical resonances have been performed. Afterwards, the measurement of the structural vibration using particle velocity sensors have been reviewed.

From the analysis of the data coming from the Microflown particle velocity sensors, some important information concerning the measurement settings have been gained. Independent of the direction of the velocity sensors (blue, red or green), the same trends in the self-noise curves have been found.

The self-noise of the Microflown particle velocity sensors is even higher, if the *low gain* settings are used. The correction settings (on/off) have an influence when a constant sensitivity for the particle velocity sensors is assumed (figure 3-13). If a frequency dependent sensitivity for the Microflown is assumed, there is no influence of those settings (figure 3-16, just a little influence in the low gain settings for higher frequencies).

For a constant sensitivity, there is a significant influence in the self-noise for the high gain settings above 300Hz (figure 3-13). As also shown in table 3-5, the smallest equivalent noise level can be found for the settings: *high gain correction off* in both frequency bands.

The curves for high gain and correction on/off are almost congruent in the case of the frequency dependent sensitivity for the Microflown (figure 3-16). Table 3-6 indicates the smallest equivalent noise level for those cases as well.

In summary the Microflown shows a different behavior in the self-noise if a constant, or frequency dependent sensitivity is assumed. Especially for the low frequency range the self-noise is e.g. for 5Hz - 55dB (constant sensitivity) and 80dB (frequency dependent sensitivity).

The mechanical and the acoustic resonances could have been determined during the measurements described in section 3.4.2 and 3.5.2. An approach of the determination of the damping ratio out of the reverberation time out the measurement data has been given in section 2.3.4.

The measurement of the mechanical resonances has been more difficult compared to the acoustic measurement due to the fact that the broadband excitation of the beam structure resulted in an unacceptable coherence below 100 Hz. This is exactly the frequency range where the beam has his first couple of eigenfrequencies. The tonal excitation of the beam structure worked out well for the lower frequencies because the mode shapes could easily

been allocated to the theoretical imagination. A comparison between the measured mechanical resonances and the theory is given in table 6-1.

Table 6-1 Comparison of the mechanical resonances

mode	theory	LMS		ELAC Exciter		LDS minishaker	
	f_n [Hz]	f_n [Hz]	D[%]	f_n [Hz]	D[%]	f_n [Hz]	D[%]
1	5.9	10.4	2.29	9. 8	0.21	12.1	0.23
2	23.5	21.5	2.22	17.8	0.63	26.5	0.39
3	52.8	55.2	1.8	47.5	0.91	64.8	0.26
4	93.9	94.1	1.55	94.8	0.67	110.5	0.10
5	146.6	138.4	1.5	148.5	0.43		
6	211.2	193.2	1.21				
7	287.4	253.5	1.01				

The deviation of the eigenfrequencies measured and calculated using the theoretical approach belong to the extra weight added to the structure. The edges on both sides of the beam structure are not completely stiff like the simply supported approach of the theory suggests.

Comparing the damping ratios of the three measurements of the structural resonances, it can be noticed, that the overall damping ratios of the ELAC and the LDS shaker measurement are one to the power of ten less that the LMS measurement (table 6-1). Both curves assumed an equivalent trend through the measurement data in figure 3-31 and figure 3-32.

Compared to the damping of the mechanical resonances, the acoustic resonances are one to the power of ten less damped then the LMS measurement but in the same range like the ELAC and LDS measurement (table 3-16 and table 6-1). This is a good indication for the walls of the test rig to be reverberant and that the acrylic plate does not have a big influence on the measurement.

The theoretical and measured acoustic eigenfrequencies (table 3-14 and table 3-15) show some deviations. A reason might be that the theoretical approach assumes a test rig without any installations. The resonant frequencies are not separated for each direction in the measurement so it is possible that a resonant peak might not only be the mode of one direction but a superposition of two directions. Moreover the acrylic plate on top of the test rig is not completely stiff and is excited as well in the broadband excitation.

The resulting MAC matrices for the fluid structure interaction given in section 3.6 show that the way the excitation acts on the structure (punctually using exciter or shaker or as a distributed load using the loudspeaker), has to be considered. The de-tuning of the eigenfrequencies due to the mass of the exciter is important. The transmission paths have been figured out (figure 3-33).

The coherence based measurement technique brought some interesting insights concerning the need of a measurement signal coming directly from the structure. The position of the accelerometer and Microflown has been varied for different cases which have been reviewed (figure 4-3). The influence of absorbing materials on both sides of the vibro-acoustic test rig has been figured out for the coherence function (figure H-2 and figure H-5).

The study has shown that the calculated coherence between the normal and tangential particle velocity has the same statements as if the coherence would have been calculated between a signal of an accelerometer and one component (either normal or tangential) of the Microflown (figure 4-4 to figure 4-6).

This allows a determination of frequencies where the acoustic sensor can be used to perform accurate measurements.

Moreover the influence of background noise to measurements with the particle velocity has been reviewed. From a certain SPL an influence on the coherence can be figured out. If the SPL is too low, there is now remarkable influence on the coherence function.

With a high background noise it is essential to measure as close as possible to the structure to really measure the vibration coming from the oscillating structure and not from the air surrounding the probe (figure 4-9). The relation between background noise and measurement distance has been figured out successfully.

The same trends for the measurement distance according to the results of the analytical model have been identified (figure 2-19 and figure 4-9).

A method to quantify the signal-to-noise ratio has been presented using the transfer function and the auto spectral density to be able to verify the influence of the SNR of the system itself and the SNR of the inputs (section 4.2.1).

The study has shown that the resonances can clearly be detected after the measurement of both transfer paths (exciter for the structure and the loudspeaker for the cavity). At certain frequencies the structure has a resonance where the acoustic does not. Here the acoustic was unable to excite the structure. The same situation can be vice versa and of course there are situations where both transfer functions show a resonance peak.

If the SNR is calculated with both parts (one for the system influence and the other one for the input influence (equation [4-4]), it could be shown that the SNR has been sufficient if the loudspeaker could not excite the structural resonance (Figure 4-14). Furthermore this method is a good indication for the excitation level if the SNR is too small.

Thinking about a set of measurement points, this technique can be used to verify if it is possible to perform measurements at these points or not.

The measurement error has been calculated according to the measurement data to see if a link to the analytical model can be set (section 4.2.1). The calculated error was higher than the one of the analytical model. This belongs to the fact that the analytical model provides only the solution for a one dimensional sound tube and is calculated without absorption. The distance is smaller (with regards to the wavelength) than the one of the analytical model. However the same trends could be found in the analytical model and the evaluation of the measurement data.

Finally some guidelines for an appropriate use of the sensor have been formulated (chapter 5).

For this configuration of the vibro-acoustic test environment the methods for the coherence function and the signal-to-noise ratio have been applied successfully. The identification of the structural vibration worked out for areas with a good coherence and a good SNR. For further investigations it would be interesting to perform a measurement with a more complex

structure and see if the methods still work (even with a two dimensional analytical model which represents the vibro-acoustic test rig in a better way).

An analytical model for a two-dimensional case could be used to see if the test-rig gets represented in a more accurate way without simplifications.

Moreover it would be interesting in terms of modal parameters, if a comparison between a full experimental modal analysis of a complex structure and an array of USP probes provides the same results. Like previously described it would help the engineer to have a software which will apply these methods to verify if measurement points are acceptable or not. After the generation of a geometrical model including the measurement points the transfer paths and the normal and tangential velocity have to be measured. If this is completed, the software calculates the coherence functions and the auto spectral density and gives an indication about the possible frequency range to measure at each point and the level of excitation needed to have an acceptable SNR.

References

[1]. **Chargin, M. , Gartmeier, O.** *A Finite Element Procedure For Calculating Fluid-Structure Interaction Using MSC/NASTRAN.* California : NASA, December 1990. NASA Technical Memorandum 102857.
[2]. **de Bree, H.-E.** *The Microflown - An Acoustic Particle Velocity Sensor.* s.l. : Acoustics Australia, December 2003. pp. 91-94. Vol. 31 No.3.
[3]. **Microflown Technologies.** [Online] [Cited: June 20, 2013.] USP Probe. http://www.microflown.com/products/accessories/usp-orientation-tool.html.
[4]. **Microflown, Technologies.** *Datasheet of the USP Probe.* Arnhem : s.n., 07-2012. V1.0.
[5]. **de Bree, H.-E., Leussink, P., Korhorst, T.** *The y-flown: a novel device for measuring acoustic flows.* MESA Research Institute, University of Twente : Elsevier, 1996. pp. 552-557. SSDI 0942-4247 (95) 01202-8.
[6]. **Microflown Technologies.** *Datasheet of the 4 Channels signal conditioner.* Arnhem : s.n., 01-2013. V1.0.
[7]. **Brommund, E. , Sachau, D.** *Schwingugslehre mit Maschinendynamik.* 1. Auflage. 2008 : Teuber Verlag. 978-3-8351-0151-7.
[8]. **Grothe, K.-H. , Feldhusen, J.** *Dubbel - Taschenbuch für den Maschinenbau.* Heidelberg : Springer Verlag, 2007. Vol. 22.Auflage. 978-3-540-49714-1.
[9]. **Sengpielaudio.** [Online] [Cited: May 23, 2013.] Excel Datasheet for the calculation of acoustic modes. www.sengpielaudio.com/EBS-RaumModen.xls.
[10]. **Möser, M.** *Technische Akustik.* 9. aktualisierte Auflage. s.l. : Springer Verlag, 2012. 978-3-642-30932-8.
[11]. **Hunecke, J.** Hunecke Raumakustik. [Online] [Cited: June 20, 2013.] http://www.hunecke.de/de/wissen/absorber/poroese-absorber.html.
[12]. **Binda, M., Pastor, M.** *Modal Assurance Criterion.* MMaMS. s.l. : Elsevier, 2012. pp. 543-548.
[13]. **Allemang, R.** *The Modal Assurance Criterion - Twenty Years of Use and Abuse.* Cincinetti, Ohio : Sound and Virabtion, August 2003. pp. 14-21.
[14]. **Kletschkowski, T.** *Identification of Structural Parameters Based on Acoustic Measurements.* Merano, Italy : AIA-DAGA, Conference on Acoustics, March 2013. pp. 1549-1552.
[15]. **Zeller, P.** *Handbuch Fahrzeugakustik.* Heidelberg : Vieweg+Teubner, 2012. p. 362. Vol. 2. überarbeitete Auflage. 978-3-8348-1443-2.
[16]. **Kletschkowski, T.** *Adaptive Feed-Forward Control Of Low Frequency Interior Noise.* Heidelberg : Springer Verlag, Oktober 2011. Vol. Auflage: 2012. 978-94-007-2536-2.

Appendix A: Self-noise level without Microflown filters

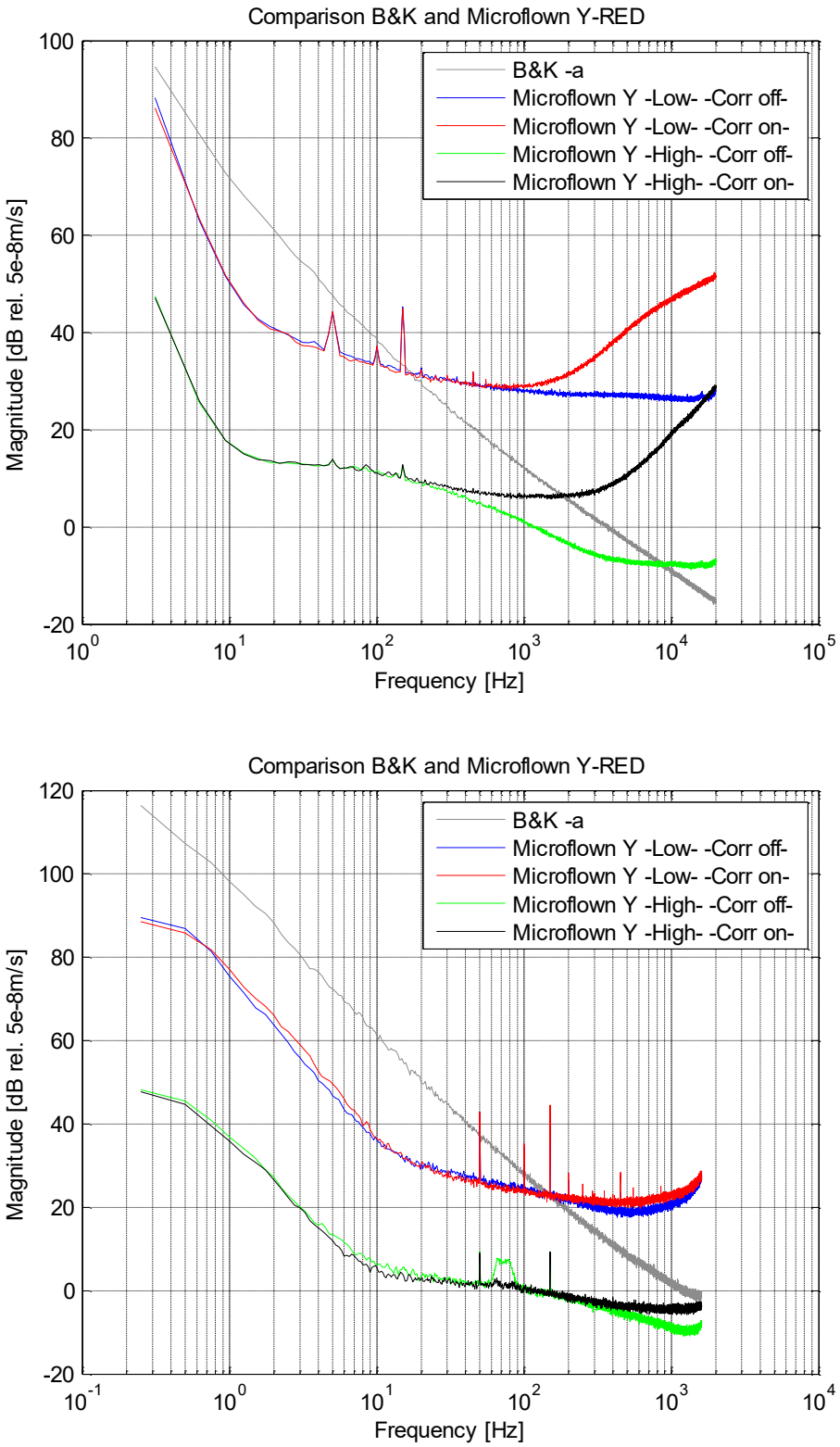

Figure A-1 Comparison between the accelerometer and the Y-RED element of the Microflown fullband (top) and lowband (bottom)

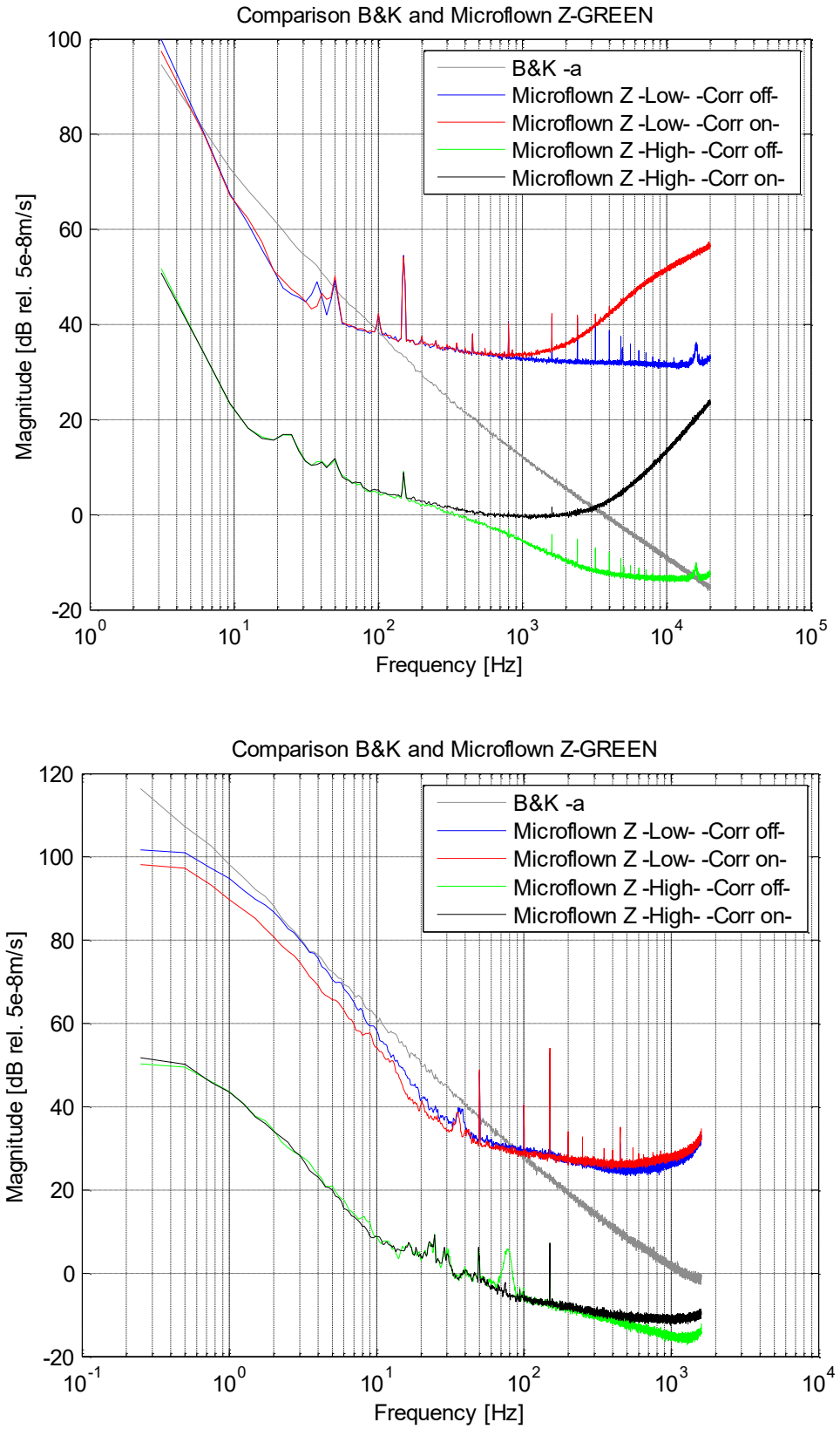

Figure A-2 Comparison between the accelerometer and the Z-GREEN element of the Microflown fullband (top) and lowband (bottom)

Appendix B: Self-noise level with Microflown filters

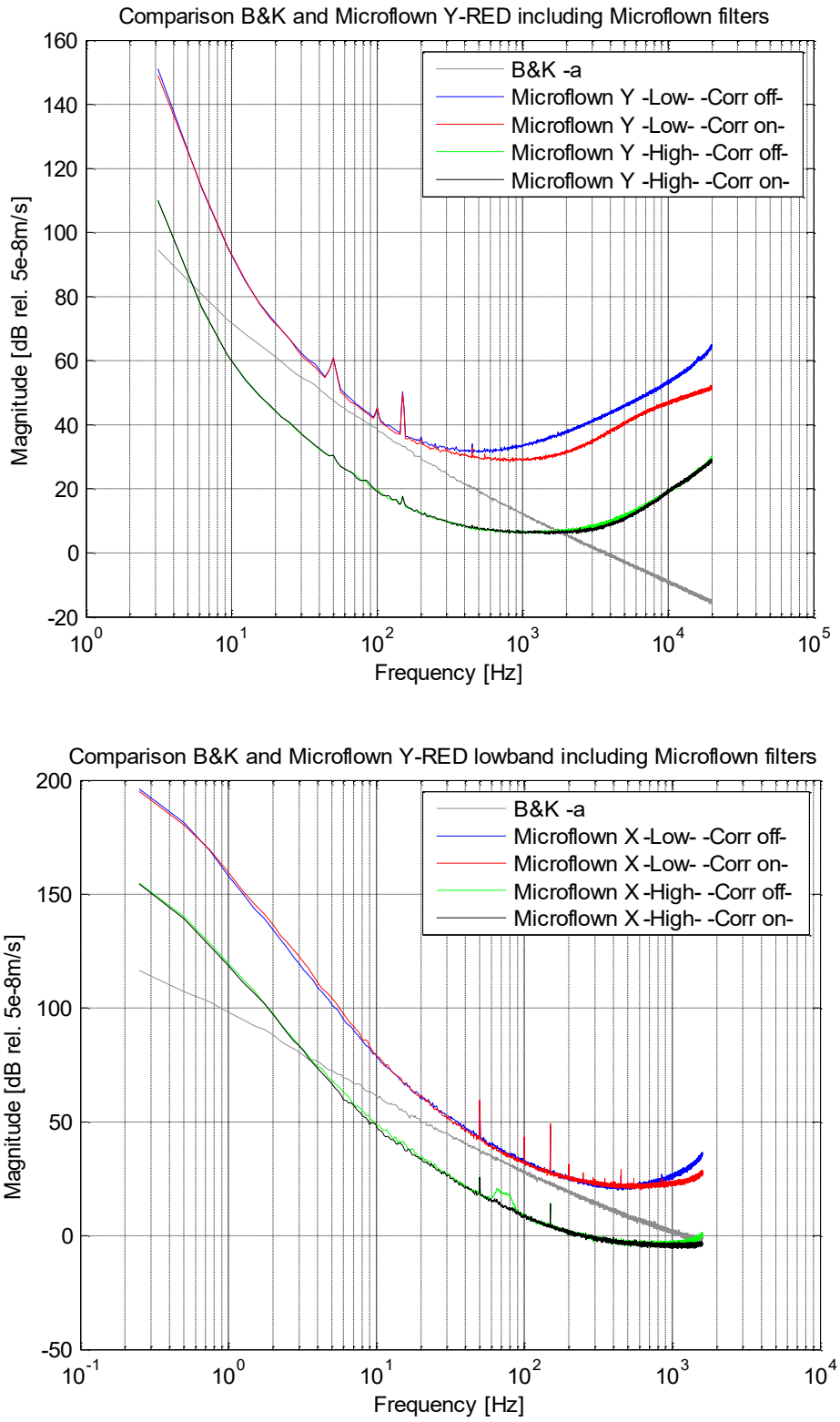

Figure B-1 Comparison between the accelerometer and the Y-RED element of the Microflown fullband (top) and lowband (bottom) including the Microflown filters

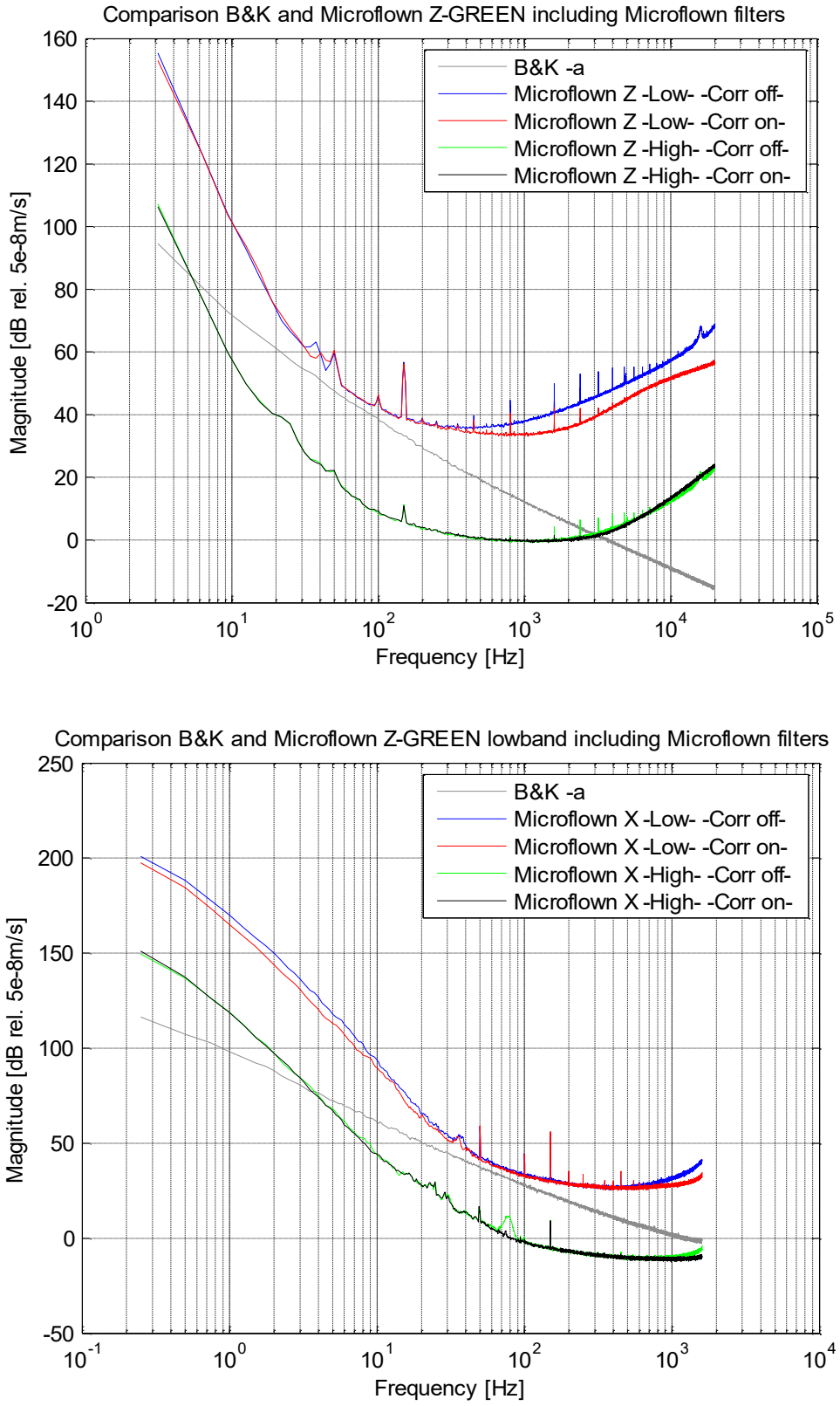

Figure B-2 Comparison between the accelerometer and the Z-GREEN element of the Microflown fullband (top) and lowband (bottom) including the Microflown filters

Appendix C: Scatter plots of the self-noise measurement

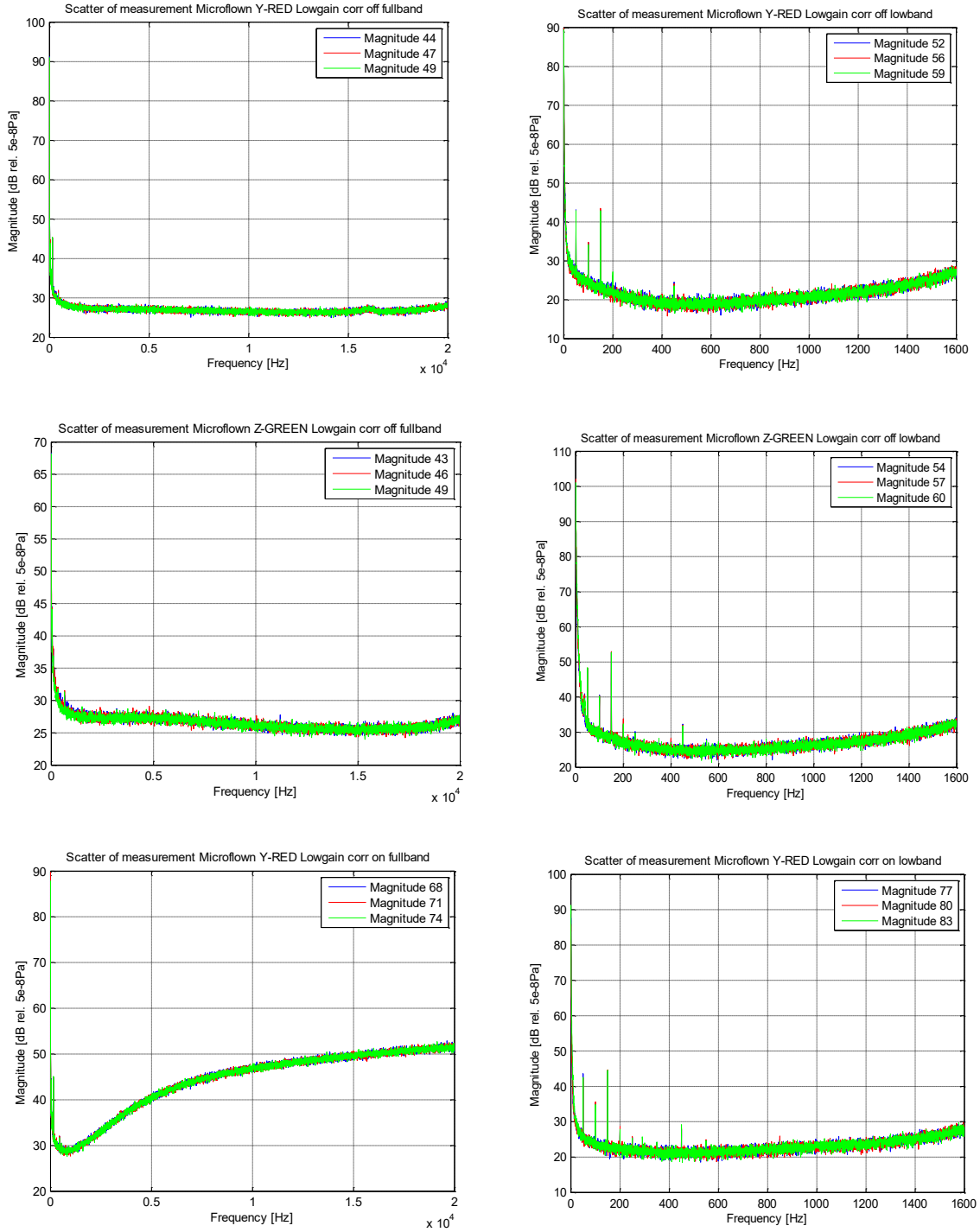

Figure C-1 Scatter plots of Microflown particle velocity (Y-Red) low gain correction off (top), Microflown particle velocity low gain correction off (Z-Green) (middle) and Microflown particle velocity low gain correction on (Y-Red) (bottom)

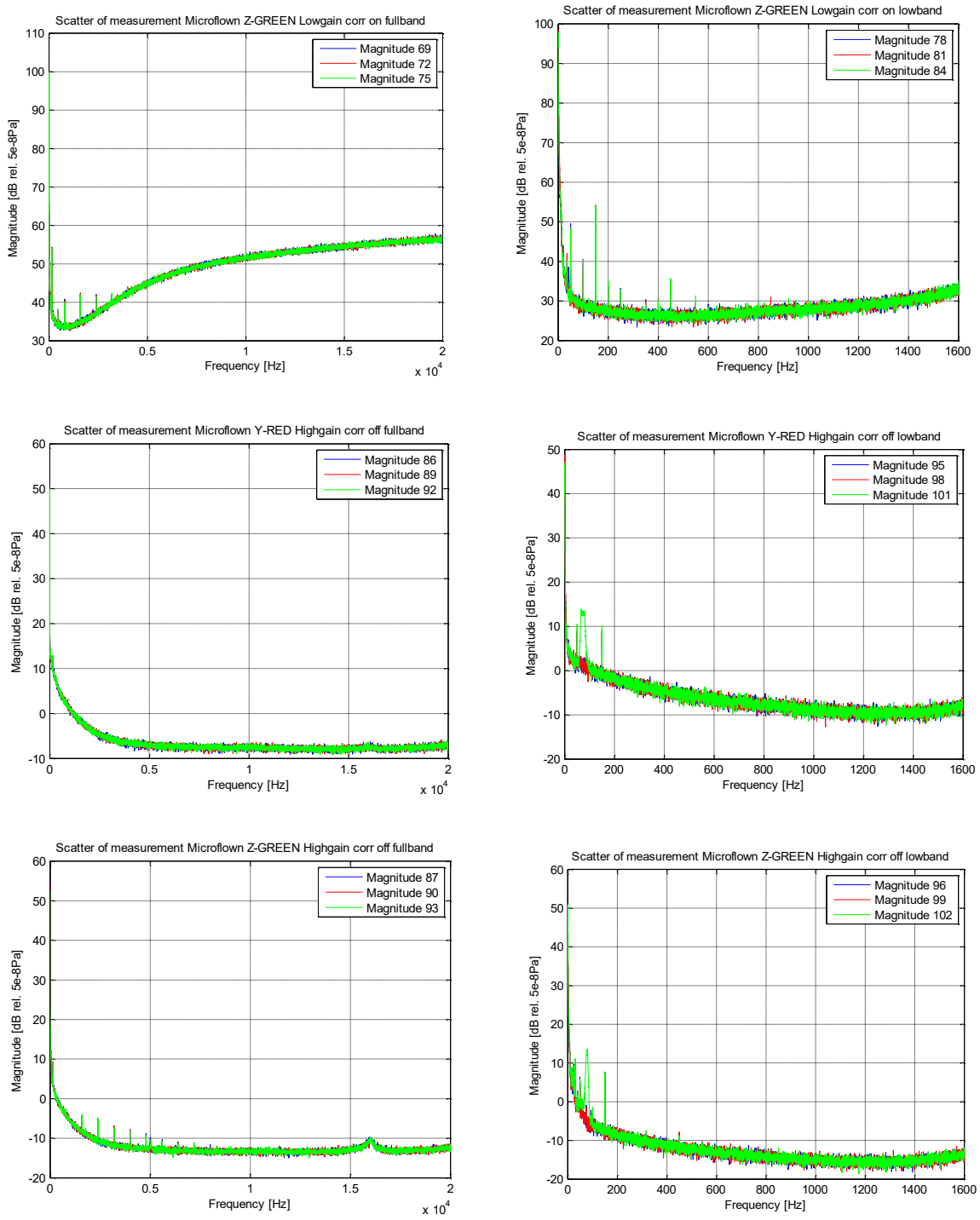

Figure C-2 Scatter plots of Microflown particle velocity (Z-Green) low gain correction on (top), Microflown particle velocity high gain correction off (Y-Red) (middle) and Microflown particle velocity high gain correction off (Z-Green) (bottom)

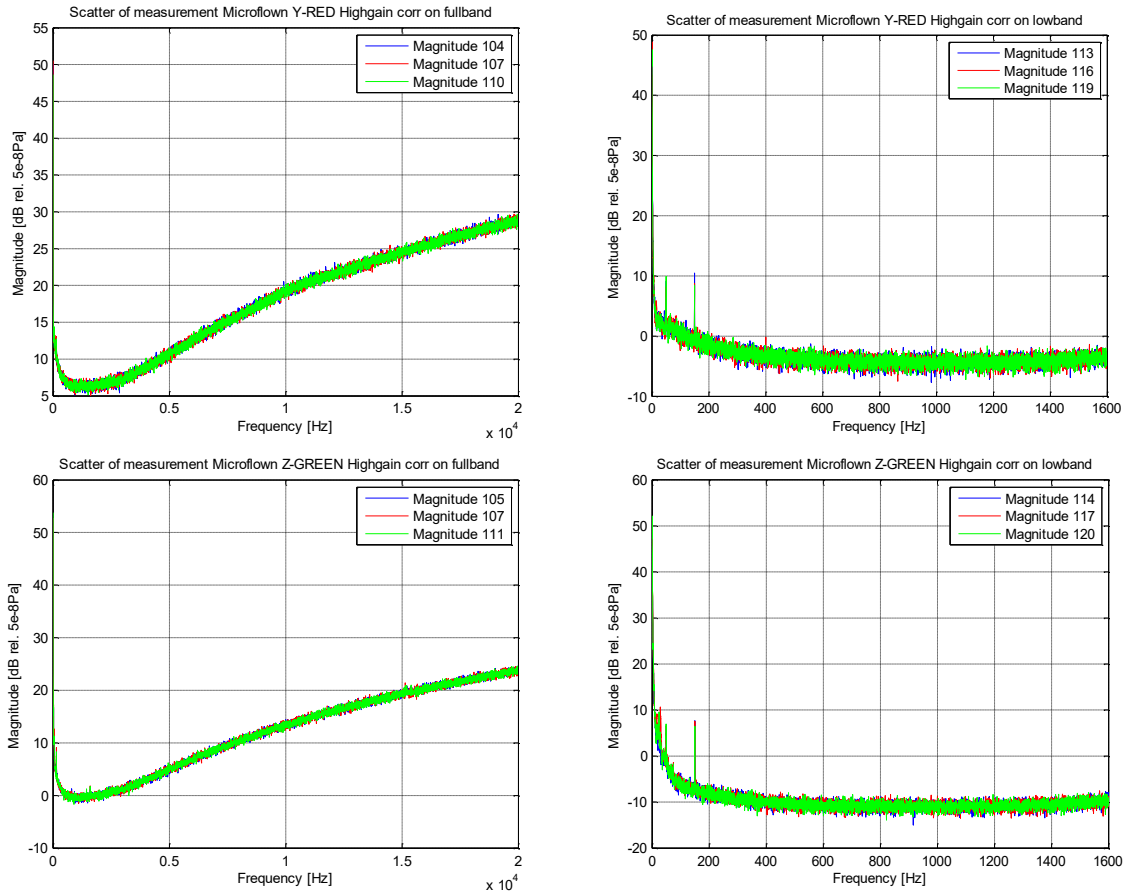

Figure C-3 Scatter plots of Microflown particle velocity (Y-Red) high gain correction on (top), Microflown particle velocity high gain correction on (Z-Green) (bottom)

Appendix D: MATLAB Code – Validation using FEM

```
clc
close all
clear all

%%FEM für BiegeBalken (Nach Strukturdynamik II)

%%Eingabefeld--------------------------
Emod = 70.0e9; %Emodul Aluminium N/m²
rho  = 2700.0; %Dichte in kg/m³

Lges = 0.895;  %Balkenlänge in m
Bges = 0.03;   %Balkenbreite in m
Hges = 0.002035; %Balkenhöhe in m

ML = 0.0*(0.159+0.010);    %Linke Einzelmasse in kg + Aufnahemer in kg
MM = 0.0*(0.290+0.015);    %Linke Einzelmasse in kg + Aufnahemer in kg
MR = 0.0*(0.159+0.010);    %Linke Einzelmasse in kg + Aufnahemer in kg

%%Berechnung der Massebelegung
mue = rho*Bges*Hges;

%%Berechnung der Biegesteifigkeit
BSt = Emod*Bges*Hges^3/12.0;

%%Aufbau der Massenmatrizen mit Einzelmassen (Spaltenweise eingegeben)
Lele=Lges/4.0;
mvor=mue*Lele/420.0;
M1mat = mvor*[[156.0 -22.0*Lele 54.0 13.0*Lele];[-22.0*Lele 4.0*Lele^2 -
13.0*Lele -3.0*Lele^2];[54.0 -13.0*Lele 156.0+ML/mvor 22.0*Lele];[13.0*Lele
-3.0*Lele^2 22.0*Lele 4.0*Lele^2]]';
M2mat = mvor*[[156.0 -22.0*Lele 54.0 13.0*Lele];[-22.0*Lele 4.0*Lele^2 -
13.0*Lele -3.0*Lele^2];[54.0 -13.0*Lele 156.0+MM/mvor 22.0*Lele];[13.0*Lele
-3.0*Lele^2 22.0*Lele 4.0*Lele^2]]';
M3mat = mvor*[[156.0 -22.0*Lele 54.0 13.0*Lele];[-22.0*Lele 4.0*Lele^2 -
13.0*Lele -3.0*Lele^2];[54.0 -13.0*Lele 156.0+MR/mvor 22.0*Lele];[13.0*Lele
-3.0*Lele^2 22.0*Lele 4.0*Lele^2]]';
M4mat = mvor*[[156.0 -22.0*Lele 54.0 13.0*Lele];[-22.0*Lele 4.0*Lele^2 -
13.0*Lele -3.0*Lele^2];[54.0 -13.0*Lele 156.0 22.0*Lele];[13.0*Lele -
3.0*Lele^2 22.0*Lele 4.0*Lele^2]]';

%%Aufbau der Steifigkeitsmatrizen (Spaltenweise eingegeben)
lvor=BSt/Lele^3;
K1mat = lvor*[[12.0 -6.0*Lele -12 -6.0*Lele];[-6.0*Lele 4.0*Lele^2 6.0*Lele
2.0*Lele^2];[-12.0 6.0*Lele 12 6.0*Lele];[-6.0*Lele 2.0*Lele^2 6.0*Lele
4.0*Lele^2]]';
K2mat = lvor*[[12.0 -6.0*Lele -12 -6.0*Lele];[-6.0*Lele 4.0*Lele^2 6.0*Lele
2.0*Lele^2];[-12.0 6.0*Lele 12 6.0*Lele];[-6.0*Lele 2.0*Lele^2 6.0*Lele
4.0*Lele^2]]';
K3mat = lvor*[[12.0 -6.0*Lele -12 -6.0*Lele];[-6.0*Lele 4.0*Lele^2 6.0*Lele
2.0*Lele^2];[-12.0 6.0*Lele 12 6.0*Lele];[-6.0*Lele 2.0*Lele^2 6.0*Lele
4.0*Lele^2]]';
K4mat = lvor*[[12.0 -6.0*Lele -12 -6.0*Lele];[-6.0*Lele 4.0*Lele^2 6.0*Lele
2.0*Lele^2];[-12.0 6.0*Lele 12 6.0*Lele];[-6.0*Lele 2.0*Lele^2 6.0*Lele
4.0*Lele^2]]';

%Aufbau der Verknüpfungsmatritzen (zeilenweise)
A1 = [[0 0 0 0 0 0 0 0 0 0];[0 1 0 0 0 0 0 0 0 0];[0 0 1 0 0 0 0 0 0 0];[0
0 0 1 0 0 0 0 0 0]];
```

```
A2 = [[0 0 1 0 0 0 0 0 0 0];[0 0 0 1 0 0 0 0 0 0];[0 0 0 0 1 0 0 0 0 0];[0
0 0 0 0 1 0 0 0 0]];
A3 = [[0 0 0 0 1 0 0 0 0 0];[0 0 0 0 0 1 0 0 0 0];[0 0 0 0 0 0 1 0 0 0];[0
0 0 0 0 0 0 1 0 0]];
A4 = [[0 0 0 0 0 0 1 0 0 0];[0 0 0 0 0 0 0 1 0 0];[0 0 0 0 0 0 0 0 1 0];[0
0 0 0 0 0 0 0 0 1]];

%%Berechnung der Globalmatritzen
Mmatges = A1'*M1mat*A1+A2'*M2mat*A2+A3'*M3mat*A3+A4'*M4mat*A4;
Kmatges = A1'*K1mat*A1+A2'*K2mat*A2+A3'*K3mat*A3+A4'*K4mat*A4;

%%Streichen von Spalten und Zeilen (gelenkige Lager)
Mges = Mmatges;
Mredzeile = [Mges(2,:); Mges(3,:); Mges(4,:); Mges(5,:); Mges(6,:);
Mges(7,:); Mges(8,:); Mges(10,:)];
Mred = [Mredzeile(:,2), Mredzeile(:,3), Mredzeile(:,4), Mredzeile(:,5),
Mredzeile(:,6), Mredzeile(:,7), Mredzeile(:,8), Mredzeile(:,10)];

Mges = Kmatges;
Mredzeile = [Mges(2,:); Mges(3,:); Mges(4,:); Mges(5,:); Mges(6,:);
Mges(7,:); Mges(8,:); Mges(10,:)];
Kred = [Mredzeile(:,2), Mredzeile(:,3), Mredzeile(:,4), Mredzeile(:,5),
Mredzeile(:,6), Mredzeile(:,7), Mredzeile(:,8), Mredzeile(:,10)];

Mred0=Mred;

[EVw0,f0]=eig(Kred,Mred);

EVwn(:,1)=EVw0(:,1)/EVw0(2,1);
EVwn(:,2)=EVw0(:,2)/EVw0(2,2);
EVwn(:,3)=EVw0(:,3)/EVw0(2,3);

EVw = [[EVwn(2,1) EVwn(4,1) EVwn(6,1)];[EVwn(2,2) EVwn(4,2)
EVwn(6,2)];[EVwn(2,3) EVwn(4,3) EVwn(6,3)]]';

f0mat(1)=f0(1,1).^0.5/2/pi;
f0mat(2)=f0(2,2).^0.5/2/pi;
f0mat(3)=f0(3,3).^0.5/2/pi;

f0mat'
EVw
```

Appendix E: MATLAB Code – Calculation of the MAC value

```
% ------------------------------------------------------------------------
% --------------------- MAC WERT ANALYSE ---------------------------------
% MA-Thesis betreut durch Herrn Prof. Dr-Ing. (habil.) Thomas Kletschkowski
% ------------------- author: D.Sadra, B.Eng.  ---------------------------
% --------------------------HAW HAMBURG ---------------------------------
% ------------------------------------------------------------------------
clear all
clc
%% Einlesen der normierten Eigenvectoren (übernommen aus XLS-Sheet:
Calculation-Masterthesis)
%%
%% ------------------------------------------------------------------------
%  ----------------------------- EXCITER ----------------------------------
%  ------------------------------------------------------------------------
%Vectoren auf die erster Konmponenten normiert:
Vec_EXC_I   = [ 1.000*exp(1i*0) 6.009*exp(1i*(-1.305)) 4.275*exp(1i*(-
1.159)) 2.679*exp(1i*(+1.523)) 0.771*exp(1i*(-0.199))].';
Vec_EXC_II  = [ 1.000*exp(1i*0) 0.302*exp(1i*(-1.586))
1.320*exp(1i*(+0.178)) 1.039*exp(1i*(-3.271)) 0.255*exp(1i*(-5.375))].';
Vec_EXC_III = [ 1.000*exp(1i*0) 0.221*exp(1i*(-1.042))
0.238*exp(1i*(+0.018)) 0.633*exp(1i*(+0.389)) 0.073*exp(1i*(-1.176))].';
Vec_EXC_IV  = [ 1.000*exp(1i*0) 0.053*exp(1i*(+2.247))
0.245*exp(1i*(+2.602)) 0.310*exp(1i*(+3.260)) 0.085*exp(1i*(+1.823))].';

%% ------------------------------------------------------------------------
%  --------------------------- LAUTSPRECHER----------------------------------
%  ------------------------------------------------------------------------
%Vectoren auf die erster Konmponenten normiert:
Vec_LS_I   = [ 1.000*exp(1i*0) 1.023*exp(1i*(-0.107))
0.530*exp(1i*(+0.184)) 0.668*exp(1i*(+0.258)) 0.951*exp(1i*(+0.409))].';
Vec_LS_II  = [ 1.000*exp(1i*0) 0.723*exp(1i*(-0.439)) 3.601*exp(1i*(-
0.574)) 2.076*exp(1i*(-0.116)) 2.929*exp(1i*(-1.642))].';
Vec_LS_III = [ 1.000*exp(1i*0) 0.184*exp(1i*(+1.089)) 1.417*exp(1i*(-
2.938)) 2.418*exp(1i*(-3.913)) 0.348*exp(1i*(+1.175))].';
Vec_LS_IV  = [ 1.000*exp(1i*0) 0.804*exp(1i*(-0.127)) 0.383*exp(1i*(-
1.821)) 0.813*exp(1i*(-3.130)) 0.643*exp(1i*(-2.940))].';
%% ------------------------------------------------------------------------
%  ---------------------------- SHAKER ------------------------------------
%  ------------------------------------------------------------------------
%Vectoren auf die erster Konmponenten normiert:
Vec_SH_I   = [ 1.000*exp(1i*0) 0.874*exp(1i*(+3.685))
2.348*exp(1i*(+0.737)) 0.956*exp(1i*(+3.737)) 0.656*exp(1i*(+0.017))].';
Vec_SH_II  = [ 1.000*exp(1i*0) 1.710*exp(1i*(-2.760)) 2.348*exp(1i*(-
3.429)) 1.263*exp(1i*(-4.550)) 0.677*exp(1i*(-2.222))].';
Vec_SH_III = [ 1.000*exp(1i*0) 0.380*exp(1i*(+0.231)) 1.001*exp(1i*(-
2.570)) 0.522*exp(1i*(+0.066)) 1.401*exp(1i*(+0.324))].';
Vec_SH_IV  = [ 1.000*exp(1i*0) 2.883*exp(1i*(+0.239))
2.970*exp(1i*(+0.058)) 0.650*exp(1i*(-2.776)) 1.386*exp(1i*(-3.050))].';

%% BILDEN DER MAC MATRIX EXC_LS
 MACt(1,1) = (abs(Vec_EXC_I'*Vec_LS_I))^2./(
(Vec_EXC_I'*Vec_EXC_I)*(Vec_LS_I'*Vec_LS_I) );
MACt(1,2) = (abs(Vec_EXC_I'*Vec_LS_II))^2./(
(Vec_EXC_I'*Vec_EXC_I)*(Vec_LS_II'*Vec_LS_II) );
MACt(1,3) = (abs(Vec_EXC_I'*Vec_LS_III))^2./(
(Vec_EXC_I'*Vec_EXC_I)*(Vec_LS_III'*Vec_LS_III) );
MACt(1,4) = (abs(Vec_EXC_I'*Vec_LS_IV))^2./(
(Vec_EXC_I'*Vec_EXC_I)*(Vec_LS_IV'*Vec_LS_IV) );
```

```
MACt(2,1) = (abs(Vec_EXC_II'*Vec_LS_I))^2./(
(Vec_EXC_II'*Vec_EXC_II)*(Vec_LS_I'*Vec_LS_I) );
MACt(2,2) = (abs(Vec_EXC_II'*Vec_LS_II))^2./(
(Vec_EXC_II'*Vec_EXC_II)*(Vec_LS_II'*Vec_LS_II) );
MACt(2,3) = (abs(Vec_EXC_II'*Vec_LS_III))^2./(
(Vec_EXC_II'*Vec_EXC_II)*(Vec_LS_III'*Vec_LS_III) );
MACt(2,4) = (abs(Vec_EXC_II'*Vec_LS_IV))^2./(
(Vec_EXC_II'*Vec_EXC_II)*(Vec_LS_IV'*Vec_LS_IV) );

MACt(3,1) = (abs(Vec_EXC_III'*Vec_LS_I))^2./(
(Vec_EXC_III'*Vec_EXC_III)*(Vec_LS_I'*Vec_LS_I) );
MACt(3,2) = (abs(Vec_EXC_III'*Vec_LS_II))^2./(
(Vec_EXC_III'*Vec_EXC_III)*(Vec_LS_II'*Vec_LS_II) );
MACt(3,3) = (abs(Vec_EXC_III'*Vec_LS_III))^2./(
(Vec_EXC_III'*Vec_EXC_III)*(Vec_LS_III'*Vec_LS_III) );
MACt(3,4) = (abs(Vec_EXC_III'*Vec_LS_IV))^2./(
(Vec_EXC_III'*Vec_EXC_III)*(Vec_LS_IV'*Vec_LS_IV) );

MACt(4,1) = (abs(Vec_EXC_IV'*Vec_LS_I))^2./(
(Vec_EXC_IV'*Vec_EXC_IV)*(Vec_LS_I'*Vec_LS_I) );
MACt(4,2) = (abs(Vec_EXC_IV'*Vec_LS_II))^2./(
(Vec_EXC_IV'*Vec_EXC_IV)*(Vec_LS_II'*Vec_LS_II) );
MACt(4,3) = (abs(Vec_EXC_IV'*Vec_LS_III))^2./(
(Vec_EXC_IV'*Vec_EXC_IV)*(Vec_LS_III'*Vec_LS_III) );
MACt(4,4) = (abs(Vec_EXC_IV'*Vec_LS_IV))^2./(
(Vec_EXC_IV'*Vec_EXC_IV)*(Vec_LS_IV'*Vec_LS_IV) );

disp('MAC MATRIX EXC_LS:')
MACt()
disp('-------------------------------------------------------------------------')

%% BILDEN DER MAC MATRIX EXC_SH
 MACt(1,1) = (abs(Vec_EXC_I'*Vec_SH_I))^2./(
(Vec_EXC_I'*Vec_EXC_I)*(Vec_SH_I'*Vec_SH_I) );
MACt(1,2) = (abs(Vec_EXC_I'*Vec_SH_II))^2./(
(Vec_EXC_I'*Vec_EXC_I)*(Vec_SH_II'*Vec_SH_II) );
MACt(1,3) = (abs(Vec_EXC_I'*Vec_SH_III))^2./(
(Vec_EXC_I'*Vec_EXC_I)*(Vec_SH_III'*Vec_SH_III) );
MACt(1,4) = (abs(Vec_EXC_I'*Vec_SH_IV))^2./(
(Vec_EXC_I'*Vec_EXC_I)*(Vec_SH_IV'*Vec_SH_IV) );

MACt(2,1) = (abs(Vec_EXC_II'*Vec_SH_I))^2./(
(Vec_EXC_II'*Vec_EXC_II)*(Vec_SH_I'*Vec_SH_I) );
MACt(2,2) = (abs(Vec_EXC_II'*Vec_SH_II))^2./(
(Vec_EXC_II'*Vec_EXC_II)*(Vec_SH_II'*Vec_SH_II) );
MACt(2,3) = (abs(Vec_EXC_II'*Vec_SH_III))^2./(
(Vec_EXC_II'*Vec_EXC_II)*(Vec_SH_III'*Vec_SH_III) );
MACt(2,4) = (abs(Vec_EXC_II'*Vec_SH_IV))^2./(
(Vec_EXC_II'*Vec_EXC_II)*(Vec_SH_IV'*Vec_SH_IV) );

MACt(3,1) = (abs(Vec_EXC_III'*Vec_SH_I))^2./(
(Vec_EXC_III'*Vec_EXC_III)*(Vec_SH_I'*Vec_SH_I) );
MACt(3,2) = (abs(Vec_EXC_III'*Vec_SH_II))^2./(
(Vec_EXC_III'*Vec_EXC_III)*(Vec_SH_II'*Vec_SH_II) );
MACt(3,3) = (abs(Vec_EXC_III'*Vec_SH_III))^2./(
(Vec_EXC_III'*Vec_EXC_III)*(Vec_SH_III'*Vec_SH_III) );
MACt(3,4) = (abs(Vec_EXC_III'*Vec_SH_IV))^2./(
(Vec_EXC_III'*Vec_EXC_III)*(Vec_SH_IV'*Vec_SH_IV) );

MACt(4,1) = (abs(Vec_EXC_IV'*Vec_SH_I))^2./(
(Vec_EXC_IV'*Vec_EXC_IV)*(Vec_SH_I'*Vec_SH_I) );
```

```
MACt(4,2) = (abs(Vec_EXC_IV'*Vec_SH_II))^2./(
(Vec_EXC_IV'*Vec_EXC_IV)*(Vec_SH_II'*Vec_SH_II) );
MACt(4,3) = (abs(Vec_EXC_IV'*Vec_SH_III))^2./(
(Vec_EXC_IV'*Vec_EXC_IV)*(Vec_SH_III'*Vec_SH_III) );
MACt(4,4) = (abs(Vec_EXC_IV'*Vec_SH_IV))^2./(
(Vec_EXC_IV'*Vec_EXC_IV)*(Vec_SH_IV'*Vec_SH_IV) );

disp('MAC MATRIX EXC_SH:')
MACt()
disp('-------------------------------------------------------------------')

%% BILDEN DER MAC MATRIX SH_LS
MACt(1,1) = (abs(Vec_SH_I'*Vec_LS_I))^2./(
(Vec_SH_I'*Vec_SH_I)*(Vec_LS_I'*Vec_LS_I) );
MACt(1,2) = (abs(Vec_SH_I'*Vec_LS_II))^2./(
(Vec_SH_I'*Vec_SH_I)*(Vec_LS_II'*Vec_LS_II) );
MACt(1,3) = (abs(Vec_SH_I'*Vec_LS_III))^2./(
(Vec_SH_I'*Vec_SH_I)*(Vec_LS_III'*Vec_LS_III) );
MACt(1,4) = (abs(Vec_SH_I'*Vec_LS_IV))^2./(
(Vec_SH_I'*Vec_SH_I)*(Vec_LS_IV'*Vec_LS_IV) );

MACt(2,1) = (abs(Vec_SH_II'*Vec_LS_I))^2./(
(Vec_SH_II'*Vec_SH_II)*(Vec_LS_I'*Vec_LS_I) );
MACt(2,2) = (abs(Vec_SH_II'*Vec_LS_II))^2./(
(Vec_SH_II'*Vec_SH_II)*(Vec_LS_II'*Vec_LS_II) );
MACt(2,3) = (abs(Vec_SH_II'*Vec_LS_III))^2./(
(Vec_SH_II'*Vec_SH_II)*(Vec_LS_III'*Vec_LS_III) );
MACt(2,4) = (abs(Vec_SH_II'*Vec_LS_IV))^2./(
(Vec_SH_II'*Vec_SH_II)*(Vec_LS_IV'*Vec_LS_IV) );

MACt(3,1) = (abs(Vec_SH_III'*Vec_LS_I))^2./(
(Vec_SH_III'*Vec_SH_III)*(Vec_LS_I'*Vec_LS_I) );
MACt(3,2) = (abs(Vec_SH_III'*Vec_LS_II))^2./(
(Vec_SH_III'*Vec_SH_III)*(Vec_LS_II'*Vec_LS_II) );
MACt(3,3) = (abs(Vec_SH_III'*Vec_LS_III))^2./(
(Vec_SH_III'*Vec_SH_III)*(Vec_LS_III'*Vec_LS_III) );
MACt(3,4) = (abs(Vec_SH_III'*Vec_LS_IV))^2./(
(Vec_SH_III'*Vec_SH_III)*(Vec_LS_IV'*Vec_LS_IV) );

MACt(4,1) = (abs(Vec_SH_IV'*Vec_LS_I))^2./(
(Vec_SH_IV'*Vec_SH_IV)*(Vec_LS_I'*Vec_LS_I) );
MACt(4,2) = (abs(Vec_SH_IV'*Vec_LS_II))^2./(
(Vec_SH_IV'*Vec_SH_IV)*(Vec_LS_II'*Vec_LS_II) );
MACt(4,3) = (abs(Vec_SH_IV'*Vec_LS_III))^2./(
(Vec_SH_IV'*Vec_SH_IV)*(Vec_LS_III'*Vec_LS_III) );
MACt(4,4) = (abs(Vec_SH_IV'*Vec_LS_IV))^2./(
(Vec_SH_IV'*Vec_SH_IV)*(Vec_LS_IV'*Vec_LS_IV) );

disp('MAC MATRIX SH_LS:')
MACt()
disp('-------------------------------------------------------------------')
```

Appendix F: MATLAB Code – Analytical model (NASA Paper)

```
clear all;
close all;
clc;
%Vibro-Acoustic-Copuling According to NASA Paper
%
%Thomas Kletschkowski
%
%7. August 2013
%
%================================================
%Parameter
%================================================
A = 0.000625;                %piston cross section in m*m
Ks= 7474.75;                 %spring stiffness in N/m
Ms= 0.01;                    %piston mass in kg
nues =sqrt(Ks/Ms)/2.0/pi;    %natural frequency
Ds= 0.5;                     %viscous damping in kg/s
Fs= 2.1885;                  %structural load amplitude in N
%nue=128.3;
l = 1.25;                    %length of tube in m
cf= 344.0;                   %speed of sound in m/s
rf= 1.205;                   %air density in kg/m³
Z0 =rf*cf;                   %specific Impedance
chi=Z0*cf;                   %bulk modulus
Z1 =228.0;                   %specific acoustic resistance (Re(Z)) in kg/m²s
Z2 =-1456.0;                 %specific acoustic reactance (Im(Z)) in kg/m²s
% Z1 =rf*cf;                   %specific acoustic resistance (Re(Z)) in
kg/m²s
% Z2 =0.0;                 %specific acoustic reactance (Im(Z)) in kg/m²s
Ref = (Z1+j*Z2-Z0)/(Z1+j*Z2+Z0); %reflection coefficient at x = l [16],p.44

Absorb = 1.0-abs(Ref)^2;            %acoustic absorption at x = l
%Evaluation points in duct
%================================================
x = [0:0.00125:l];

%Definition of abbrevations needed for solution
%================================================
gamma =  Z0*Z1/(Z1^2+Z2^2);
sigma = -Z0*Z2/(Z1^2+Z2^2);

%alpha = 1.0;                 %absorbing boundary at x = l
alpha = 0.0;                 %rigid boundary at x = l

%% Frequenzschleife author: D.Sadra,B.Eng.
%%%%%%%%%%%%%%%%%%%%%%%%%%%%%%%%%%%%%%%%%%%%%%%%%%%%%%%%%%%%%%%%%%%%%%%%%%%%
Nf=500;                      %Number of freq.
Fstep=1;                     %Frequency steps
%%%%%%%%%%%%%%%%%%%%%%%%%%%%%%%%%%%%%%%%%%%%%%%%%%%%%%%%%%%%%%%%%%%%%%%%%%%%

FreqV=1:Fstep:Nf*Fstep;      %Frequenzvector
for i=1:Nf;
  nue=FreqV(i)     ;               %excitation frequency in Hz

G1z = 0.5*(1.0-
lpha^2*(sigma^2+gamma^2))*sin(4.0*pi*l*nue/cf)+alpha*sigma*cos(4.0*pi*l*nue
/cf);
G1n =
(sin(2.0*pi*l*nue/cf)+alpha*sigma*cos(2.0*pi*l*nue/cf))^2+alpha^2*gamma^2*(
cos(2.0*pi*l*nue/cf))^2;
```

```
G1  = G1z/G1n;
G2  = alpha*gamma/G1n;

xsi1 = (nues^2-nue^2)+A*Z0*G1*nue/2.0/pi/Ms;
xsi2 = (Ds+A*Z0*G2)*nue/2.0/pi/Ms;

fMs = Fs/4.0/pi/pi/Ms;

%Definition der komplexen Strukturverschiebung
%================================================
us(i) = fMs*(xsi1-j*xsi2)/(xsi1^2+xsi2^2);
absus(i)=abs(us(i));

%Definition der komplexen Strukturschnelle
%================================================
vs(i) = j*(2.0*pi*nue)*us(i);
absvs(i) = abs(vs(i));
for ii=1:length(x);
    absvsplot(ii) = absvs(i);
end

%Definition des komplexen Schalldruckes
%================================================
philf1 = xsi1*(G1*cos(2.0*pi*nue*x/cf)+sin(2.0*pi*nue*x/cf));
philf2 = xsi2*G2*cos(2.0*pi*nue*x/cf);
philf3 = xsi1*G2*cos(2.0*pi*nue*x/cf);
philf4 = xsi2*(G1*cos(2.0*pi*nue*x/cf)+sin(2.0*pi*nue*x/cf));
p =2.0*pi*Z0*nue*(fMs/(xsi1^2+xsi2^2))*(philf1+philf2+j*philf3-j*philf4);
absp = abs(p);

%Definition der komplexen Schallschnelle
%================================================
vhilf1 = xsi1*(-
G1*sin(2.0*pi*nue*x/cf)+cos(2.0*pi*nue*x/cf))*(2.0*pi*nue/cf);
vhilf2 = -xsi2*G2*sin(2.0*pi*nue*x/cf)*(2.0*pi*nue/cf);
vhilf3 = -xsi1*G2*sin(2.0*pi*nue*x/cf)*(2.0*pi*nue/cf);
vhilf4 = xsi2*(-
G1*sin(2.0*pi*nue*x/cf)+cos(2.0*pi*nue*x/cf))*(2.0*pi*nue/cf);
v
=(j/rf/(2.0*pi*nue))*2.0*pi*Z0*nue*(fMs/(xsi1^2+xsi2^2))*(vhilf1+vhilf2+j*v
hilf3-j*vhilf4);
absv = abs(v);

%Definition des komplexen Schallschnelle Gradienten
%================================================
gvhilf1 = xsi1*(-G1*cos(2.0*pi*nue*x/cf)-
sin(2.0*pi*nue*x/cf))*(2.0*pi*nue/cf)^2;
gvhilf2 = -xsi2*G2*cos(2.0*pi*nue*x/cf)*(2.0*pi*nue/cf)^2;
gvhilf3 = -xsi1*G2*cos(2.0*pi*nue*x/cf)*(2.0*pi*nue/cf)^2;
gvhilf4 = xsi2*(-G1*cos(2.0*pi*nue*x/cf)-
sin(2.0*pi*nue*x/cf))*(2.0*pi*nue/cf)^2;
gv
=(j/rf/(2.0*pi*nue))*2.0*pi*Z0*nue*(fMs/(xsi1^2+xsi2^2))*(gvhilf1+gvhilf2+j
*gvhilf3-j*gvhilf4);
absgv = abs(gv);

%Relativer Schnellefehler Betrag
abs_feh(i)=1.0-abs(v(1)/vs(i));
abs_feh2(i)=1.0-abs(v(5)/vs(i));
abs_feh3(i)=1.0-abs(v(10)/vs(i));
abs_feh4(i)=1.0-abs(v(50)/vs(i));
```

```
%Relativer Schnellefehler Phase
angle_feh(i)=angle(v(1)/vs(i))*180.0/pi;
angle_feh2(i)=angle(v(5)/vs(i))*180.0/pi;
angle_feh3(i)=angle(v(10)/vs(i))*180.0/pi;
angle_feh4(i)=angle(v(50)/vs(i))*180.0/pi;
end
% disp (abs_feh);
% disp (angle_feh);
%plots
%Frequenz über Verschiebung
figure;
plot(FreqV,absus)
title ('Frequency over displacement','Fontsize',12);
xlabel('Frequency [Hz]','Fontsize',10);
ylabel('displacement,','Fontsize',10');
legend ('Frequency over displacement','Location','SouthOutside');
grid on;
% print('-dmeta','-r400',['Frequency over displacement' '.emf']);
%schnellefehler Betrag
figure;
plot(FreqV,abs_feh,'b')
hold on;
plot(FreqV,abs_feh2,'r')
hold on;
plot(FreqV,abs_feh3,'g')
hold on;
plot(FreqV,abs_feh4,'k')
title ('Velocity failure - absolute magnitude','Fontsize',12);
xlabel('Frequency [Hz]','Fontsize',10);
ylabel('velocity failure absolute magnitude [Hz??],','Fontsize',10');
legend ('1.25mm','6.25mm','12.50mm','62.50mm','Location','BestOutside');
grid on;
% print('-dmeta','-r400',['velocity_failure_absolute_magnitude' '.emf']);
%schnellefehler Phase
figure;
plot(FreqV,angle_feh)
hold on;
plot(FreqV,angle_feh2,'r')
hold on;
plot(FreqV,angle_feh3,'g')
hold on;
plot(FreqV,angle_feh4,'k')
title ('Velocity failure - absolute phase','Fontsize',12);
xlabel('Frequency [Hz]','Fontsize',10);
ylabel('velocity failure absolute phase [deg]','Fontsize',10);
legend ('1.25mm','6.25mm','12.50mm','62.50mm','Location','BestOutside');
grid on;
% print('-dmeta','-r400',['velocity_failure_absolute_phase' '.emf']);
%Visualization of sound pressure
%================================================
figure;
plot(x,absp/1000.0^2,'LineWidth',3);
grid on;
xlabel 'Frequency in Hz';
ylabel 'pressure magnitude in N/mm²';
xlim([0 1.25])

%Visualization of particle velocity
%================================================
figure;
plot(x,absv,'LineWidth',3); hold on; plot
(x,absvsplot,'LineWidth',3,'Color','red'); hold off;
grid on;
```

```
xlabel 'Frequency in Hz';
ylabel 'velocity magnitude in m/s';
xlim([0 1.25])

%Vizualization of results
%=================================================
figure;
subplot(2,1,1,'FontSize',16);
plot(x,absp/1000.0^2/Fs,'LineWidth',3);
grid on;
xlabel ('Lenght in m','fontsize',16);
ylabel ('normalized pressure in N/mm²/N','fontsize',16);
xlim([0 1.25]);
subplot(2,1,2,'FontSize',16);
plot(x,absv/Fs,'LineWidth',3); hold on; plot
(x,absvsplot/Fs,'LineWidth',3,'Color','red'); hold off;
grid on;
xlabel ('Lenght in m','fontsize',16);
ylabel ('normalized velocity in m/s/N','fontsize',16);
xlim([0 1.25]);

%Vizualization of results
%=================================================
figure;
subplot(2,1,1,'FontSize',16);
plot(x,absp/1000.0^2/Fs,'LineWidth',3);
grid on;
xlabel ('Lenght in m','fontsize',16);
ylabel ('normalized pressure in N/mm²/N','fontsize',16);
xlim([0 1.25]);
subplot(2,1,2,'FontSize',16);
plot(x,absv/Fs,'LineWidth',3); hold on; plot
(x,absvsplot/Fs,'LineWidth',3,'Color','red'); hold on;...
    plot (x,abs(v(1)+gv(1)*x)/Fs,'LineWidth',3,'Color','green'); hold off;
grid on;
xlabel ('Lenght in m','fontsize',16);
ylabel ('normalized velocity in m/s/N','fontsize',16);
xlim([0 1.25]);
%ylim([0 50]);

%Vizualization of results
%=================================================
figure;
subplot(2,1,1,'FontSize',16);
plot(x,absp/1000.0^2/Fs,'LineWidth',3);
grid on;
xlabel ('Lenght in m','fontsize',16);
ylabel ('normalized pressure in N/mm²/N','fontsize',16);
xlim([0 1.25]);
subplot(2,1,2,'FontSize',16);
plot(x,absgv/Fs,'LineWidth',3);
grid on;
xlabel ('Lenght in m','fontsize',16);
ylabel ('normalized velocity gradient in 1/s/N','fontsize',16);
xlim([0 1.25]);
```

Appendix G: MATLAB Code – analytical model (NASA Paper) iterative solver

```
close all;
clc;
clear all;
%Vibro-Acoustic-Copuling According to NASA Paper
%Iterative solver
%D.Sadra
%================================================
%Parameter
%================================================
A = 0.000625;               %piston cross section in m*m
Ks= 7474.75;                %spring stiffness in N/m
Ms= 0.01;                   %piston mass in kg
nues =sqrt(Ks/Ms)/2.0/pi;   %natural frequency
Ds= 0.5;                    %viscous damping in kg/s
Fs= 2.1885;                 %structural load amplitude in N
l = 1.25;                   %length of tube in m
cf= 344.0;                  %speed of sound in m/s
rf= 1.205;                  %air density in kg/m³
Z0 =rf*cf;                  %specific Impedance
chi=Z0*cf;                  %bulk modulus
Z1 =228.0;                  %specific acoustic resistance (Re(Z)) in kg/m²s
Z2 =-1456.0;                %specific acoustic reactance (Im(Z)) in kg/m²s
% Z1 =rf*cf;                  %specific acoustic resistance (Re(Z)) in
kg/m²s
% Z2 =0.0;                 %specific acoustic reactance (Im(Z)) in kg/m²s

Ref = (Z1+j*Z2-Z0)/(Z1+j*Z2+Z0);    %reflection coefficient at x = l kle
p.44
Absorb = 1.0-abs(Ref)^2;            %acoustic absorption at x = l

%Evaluation points in duct
%================================================
x = [0:0.001:l];

%Definition of abbrevations needed for solution
%================================================
gamma =  Z0*Z1/(Z1^2+Z2^2);
sigma = -Z0*Z2/(Z1^2+Z2^2);

% alpha = 1.0;                %absorbing boundary at x = l
alpha = 0.0;                %rigid boundary at x = l

%% Frequenzschleife
%%%%%%%%%%%%%%%%%%%%%%%%%%%%%%%%%%%%%%%%%%%%%%%%%%%%%%%%%%%%%%%%%%%%%%%%%%%%
Nf=500;                     %Number of freq.
Fstep=1;                    %Frequency steps
%%%%%%%%%%%%%%%%%%%%%%%%%%%%%%%%%%%%%%%%%%%%%%%%%%%%%%%%%%%%%%%%%%%%%%%%%%%%
FreqV=1:Fstep:Nf*Fstep;      %Frequentvector
xd_1=zeros(Nf,1);               %Vektor for fehler 1%
xd_5=zeros(Nf,1);               %Vektor for fehler 5%
xd_10=zeros(Nf,1);               %Vektor for fehler 10%
vvec=zeros(Nf,1);
pvec=zeros(Nf,1);
vsvec=zeros(Nf,1);

% Schleife für die iterative Berechnung des Abstandes
delta=0.0001;
MeasureErr=0.1;
```

```
for i=1:Nf;
    weiter =1;
    disp(i);
    xn=delta;

    nue=FreqV(i);               %excitation frequency in Hz

    G1z = 0.5*(1.0-
alpha^2*(sigma^2+gamma^2))*sin(4.0*pi*l*nue/cf)+alpha*sigma*cos(4.0*pi*l*nu
e/cf);
    G1n =
(sin(2.0*pi*l*nue/cf)+alpha*sigma*cos(2.0*pi*l*nue/cf))^2+alpha^2*gamma^2*(
cos(2.0*pi*l*nue/cf))^2;
    G1  = G1z/G1n;
    G2  = alpha*gamma/G1n;

    xsi1 = (nues^2-nue^2)+A*Z0*G1*nue/2.0/pi/Ms;
    xsi2 = (Ds+A*Z0*G2)*nue/2.0/pi/Ms;

    fMs = Fs/4.0/pi/pi/Ms;

    %Definition der komplexen Strukturverschiebung
    %=================================================
    us(i) = fMs*(xsi1-j*xsi2)/(xsi1^2+xsi2^2);
    absus(i)=abs(us(i));

     %Definition der komplexen Strukturschnelle
    %=================================================
    vs(i) = j*(2.0*pi*nue)*us(i);
    absvs(i) = abs(vs(i));
    for ii=1:length(x);
        absvsplot(ii) = absvs(i);
    end
    vsvec(i)=vs(i);

    Zielfunktion=5;
    while weiter > 0
         %Definition des komplexen Schalldruckes
        %=================================================
        philf1 = xsi1*(G1*cos(2.0*pi*nue*xn/cf)+sin(2.0*pi*nue*xn/cf));
        philf2 = xsi2*G2*cos(2.0*pi*nue*xn/cf);
        philf3 = xsi1*G2*cos(2.0*pi*nue*xn/cf);
        philf4 = xsi2*(G1*cos(2.0*pi*nue*xn/cf)+sin(2.0*pi*nue*xn/cf));
        p =2.0*pi*Z0*nue*(fMs/(xsi1^2+xsi2^2))*(philf1+philf2+j*philf3-
j*philf4);
        absp = abs(p);
        pvec(i)=p;
         %Definition der komplexen Schallschnelle
        %=================================================
        vhilf1 = xsi1*(-
G1*sin(2.0*pi*nue*xn/cf)+cos(2.0*pi*nue*xn/cf))*(2.0*pi*nue/cf);
        vhilf2 = -xsi2*G2*sin(2.0*pi*nue*xn/cf)*(2.0*pi*nue/cf);
        vhilf3 = -xsi1*G2*sin(2.0*pi*nue*xn/cf)*(2.0*pi*nue/cf);
        vhilf4 = xsi2*(-
G1*sin(2.0*pi*nue*xn/cf)+cos(2.0*pi*nue*xn/cf))*(2.0*pi*nue/cf);
        v
=(j/rf/(2.0*pi*nue))*2.0*pi*Z0*nue*(fMs/(xsi1^2+xsi2^2))*(vhilf1+vhilf2+j*v
hilf3-j*vhilf4);
        absv = abs(v);
        vvec(i) = v;
```

```
         %Definition des komplexen Schallschnelle Gradienten
        %================================================
        gvhilf1 = xsi1*(-G1*cos(2.0*pi*nue*xn/cf)-
sin(2.0*pi*nue*xn/cf))*(2.0*pi*nue/cf)^2;
        gvhilf2 = -xsi2*G2*cos(2.0*pi*nue*xn/cf)*(2.0*pi*nue/cf)^2;
        gvhilf3 = -xsi1*G2*cos(2.0*pi*nue*xn/cf)*(2.0*pi*nue/cf)^2;
        gvhilf4 = xsi2*(-G1*cos(2.0*pi*nue*xn/cf)-
sin(2.0*pi*nue*xn/cf))*(2.0*pi*nue/cf)^2;
        gv
=(j/rf/(2.0*pi*nue))*2.0*pi*Z0*nue*(fMs/(xsi1^2+xsi2^2))*(gvhilf1+gvhilf2+j
*gvhilf3-j*gvhilf4);
        absgv = abs(gv);

        abs_feh(i)=1.0-abs(vvec(i)/vs(i));
%
        if abs_feh(i) > 0
           if abs_feh(i) < MeasureErr
              xn=xn+delta;
              weiter = 1;
           else
              weiter = -1;
           end
        else
           if -MeasureErr < abs_feh(i)
              xn=xn+delta;
              weiter = 1;
           else
              weiter = -1;
           end
        end
    end

    xnd10(i)=xn;
end

%% SUBPLOT 1
figure;
subplot(2,1,1)                                  % erster Subplot
plot(FreqV,abs(vvec));
hold on;
plot(FreqV,abs(vsvec),'r');
hold on;
title ('FRF of cavity and structure','Fontsize',12);
xlabel('Frequency [Hz]','Fontsize',10);
ylabel('displacement[m]','Fontsize',10');
legend ('FRF cavity','FRF structure','Location','NorthEast');
grid on;
subplot(2,1,2);                                 % zweiter Subplot
[AX,H1,H2] = plotyy(FreqV,xnd10,FreqV,abs(pvec)/max(abs(pvec)));
title ('Maximum distance for 10%error and pressure
distribution','Fontsize',12);
xlabel('Frequency [Hz]','Fontsize',10);
set(get(AX(1),'Ylabel'),'String','Maximum distance for 10% error [m]')
set(get(AX(2),'Ylabel'),'String','pressure distribution [Pa]')
legend ('constant measurement error of 10%','pressure
distribution','Location','NorthEast');
grid on;

%% SUBPLOT 1
figure;
subplot(2,1,1)                                  % erster Subplot
plot(FreqV,abs(vvec));
```

```
hold on;
plot(FreqV,abs(vsvec),'r');
hold on;
title ('FRF of cavity and structure','Fontsize',12);
xlabel('Frequency [Hz]','Fontsize',10);
ylabel('displacement[m]','Fontsize',10');
legend ('FRF cavity','FRF structure','Location','NorthEast');
grid on;
subplot(2,1,2);                                    % zweiter Subplot
[AX,H1,H2] =
plotyy(FreqV,xnd10./cf.*FreqV,FreqV,20*log10(abs(vvec)./abs(vsvec)));
title ('Maximum distance for 10%error and error dB-wise','Fontsize',12);
xlabel('Frequency [Hz]','Fontsize',10);
set(get(AX(1),'Ylabel'),'String','Maximum distance for 10% error/lambda [-
]')
set(get(AX(2),'Ylabel'),'String','error in [dB]')
legend ('constant measurement error of 10%/lambda',' error dB-
wise','Location','NorthEast');
grid on;
```

Appendix H: Coherence plots for parameter variation

Only the plots of the measured coherence between the normal and the tangential particle velocity will be shown. For the overview of the different cases see section 4.1.2. The coherence of the tangential particle velocity has been the same like figure 4-4.

Case II – particle velocity measured with the red element (accelerometer and Microflown 300mm off the wall):

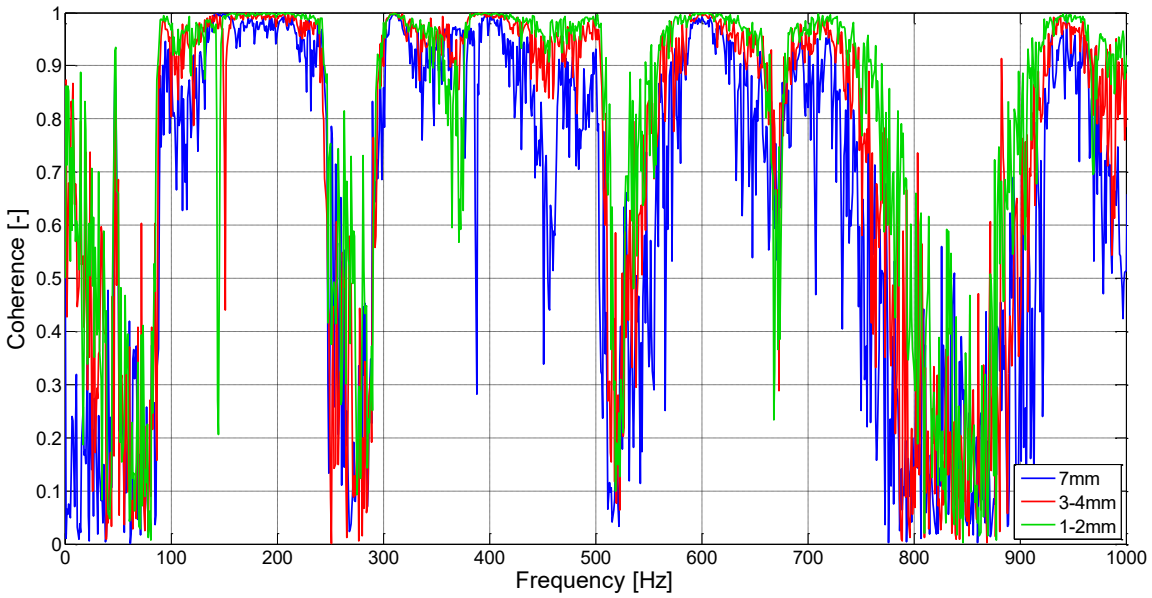

Figure H-1 Case II - coherence

Case III – absorbing material on both walls (accelerometer and Microflown 300mm off the wall):

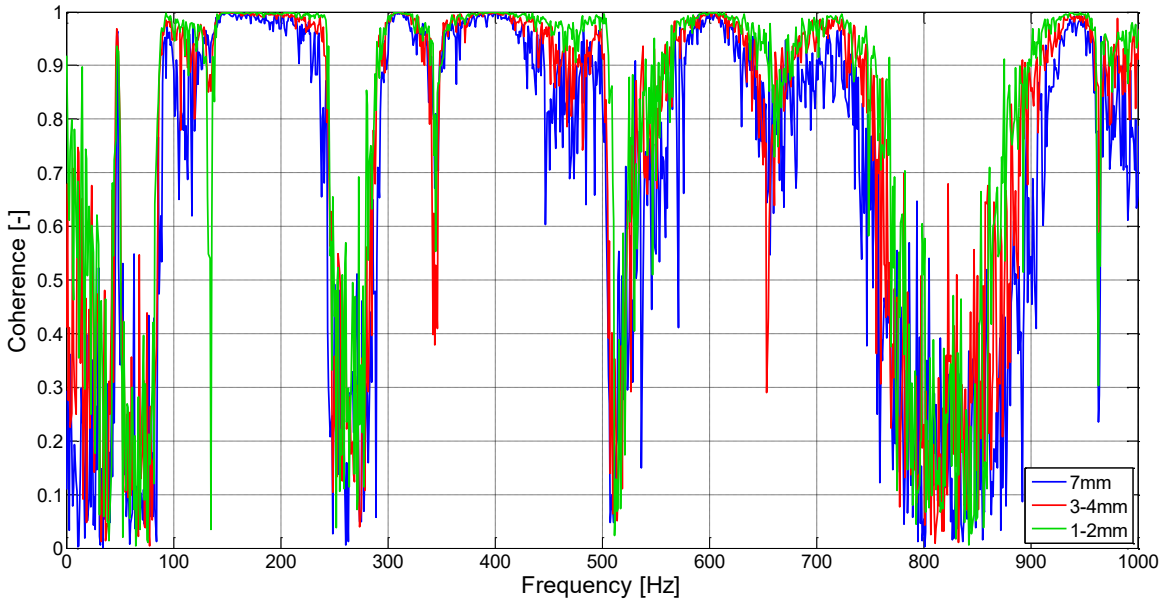

Figure H-2 Case III - coherence

Case IV – different position of accelerometer and Microflown (accelerometer 300mm off the wall and Microflown 400mm off the wall):

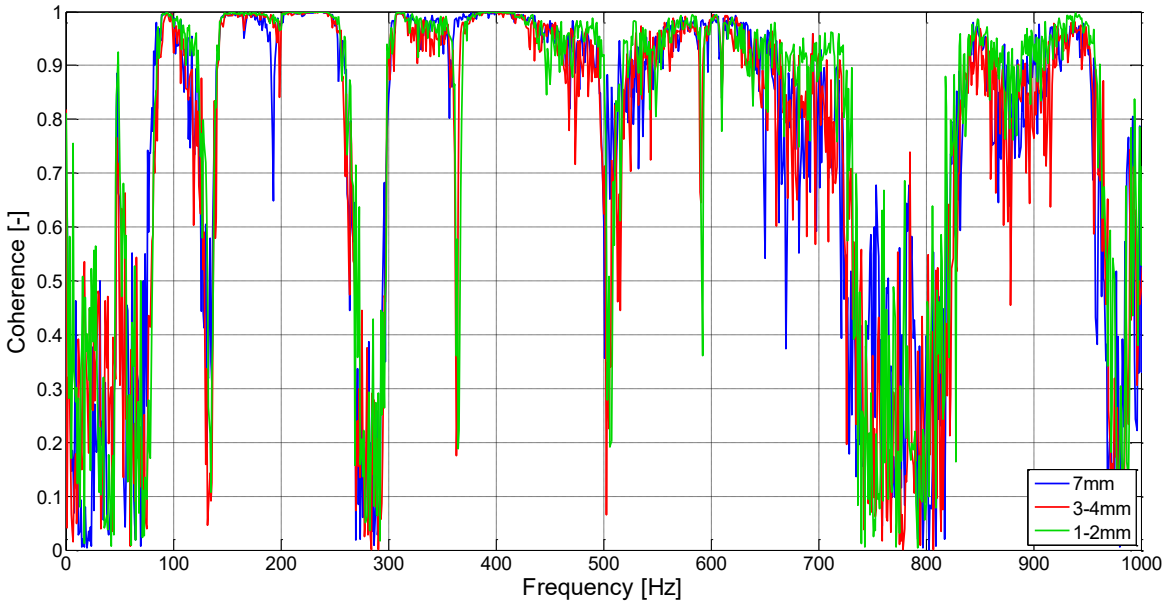

Figure H-3 Case IV - coherence

Case V – accelerometer and Microflown at 400mm of the walls:

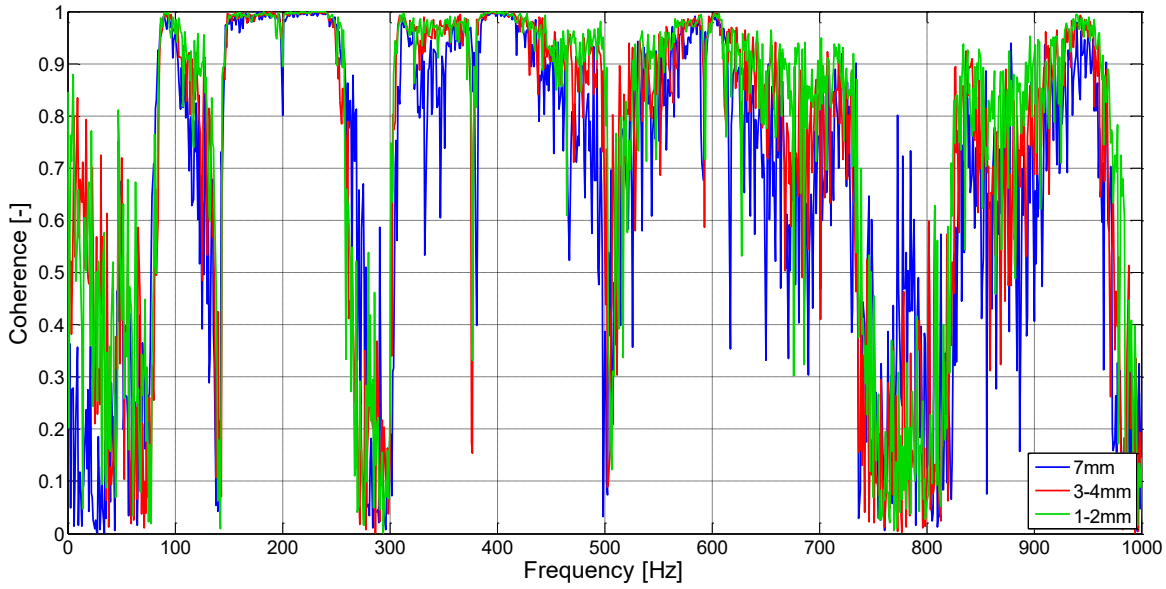

Figure H-4 Case V - coherence

Case VI – absorbing material on both walls (accelerometer and Microflown 400mm off the wall):

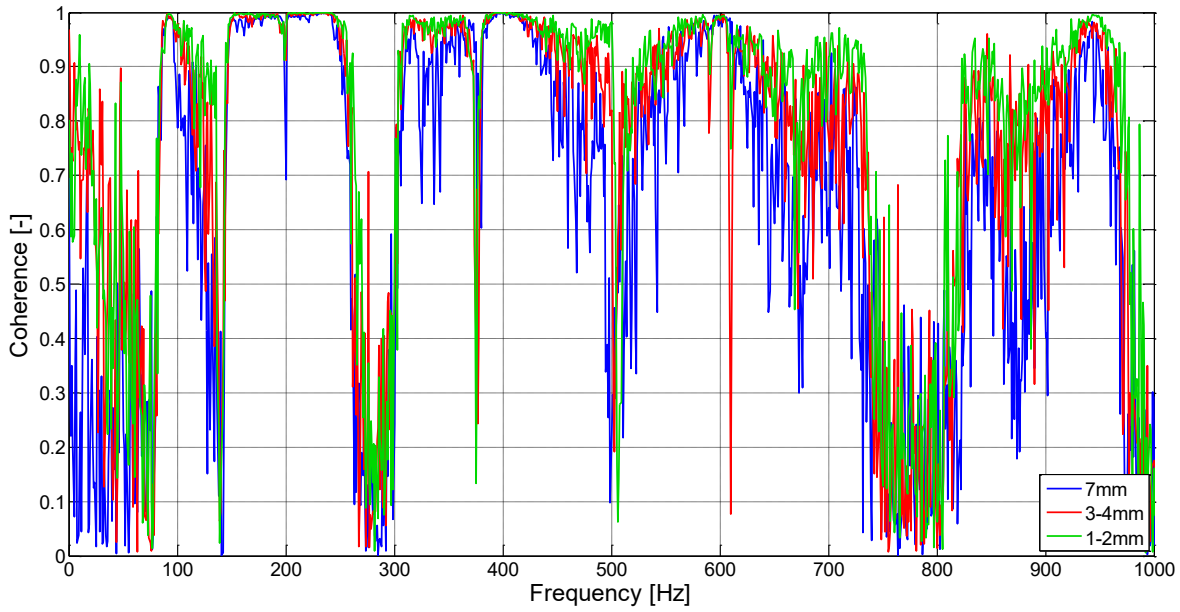

Figure H-5 Case VI - coherence

Appendix I: MATLAB Code – Transfer function and auto spectral density

```
clear all
clc
close all
%% Einlesen der Dateien
% Signal EXC + Signal Schnelle normal 1mm Abstand Struktur
wavread 'expkohrenzmessung101vlt1';          %Signal des Exciters
x1=ans;
wavread 'expkohrenzmessung101vel2';          %Signal der Normalschnelle
y1=ans;
% Signal LS + Signal Schnelle normal 1mm Abstand Struktur
wavread 'expkohrenzmessung96vlt1';          %Signal des Exciters
x2=ans;
wavread 'expkohrenzmessung96vel2';          %Signal der Normalschnelle
y2=ans;

%% Berechnung der beiden Transferfunktionen
%Berechnung der Transferfunktion
[Tx1y1,F]= tfestimate(x1,y1,[],[],44000.0,44000.0);
[Tx2y2,F]= tfestimate(x2,y2,[],[],44000.0,44000.0);

%% Auto spectral desity
[Px1x1,F]= cpsd(x1,x1,[],[],44000.0,44000.0);
[Px2x2,F]= cpsd(x2,x2,[],[],44000.0,44000.0);

%% Bestimmen des SNR
alpha=(abs(Tx1y1)./abs(Tx2y2)).^2;
beta=(Px1x1./Px2x2);

SNR_part1=10*log10(alpha);
SNR_part2=10*log10(beta);

SNR=SNR_part1+SNR_part2;
 %% Plots
figure;
plot(F,abs(Tx1y1)./52.8,'b')
hold on;
plot(F,abs(Tx2y2)./54.9,'r')
ylim([0 0.03]);
xlim([0 1000]);
title ('Transfer Functions Exciter/Loudspeaker - normal velocity
yFlown','Fontsize',12);
xlabel('Frequency [Hz]','Fontsize',10);
ylabel('velocity [m/s/V]','Fontsize',10');
legend ('Transfer Function x1y1 (Exciter)','Transfer Function x2y2
(Loudspeaker)');
grid on;
print('-dmeta','-r400',['Transfer_Function_ExciterLoudspeaker_-
_normal_velocity_yFlown' '.emf']);
figure;
plot(F,SNR_part1,'b')
hold on;
plot(F,SNR_part2,'r')
xlim([0 1000]);
title ('Signal to Noise Ratio','Fontsize',12);
xlabel('Frequency [Hz]','Fontsize',10);
ylabel('SNR [dB] ','Fontsize',10');
legend ('System influence abs(H1)^2/abs(H2)^2','Input influence Sxx/Syy');
grid on;
print('-dmeta','-r400',['Autospectral_density_ExciterLoudspeaker' '.emf']);
```

```
%% SUBPLOT 1
figure;
subplot(2,1,1)                                          % erster Subplot
plot(F,abs(Tx1y1)./52.8);
hold on;
plot(abs(Tx2y2)./54.9,'r');
hold on;
ylim([0 0.03]);
xlim([0 1000]);
title ('Transfer Functions Exciter/Loudspeaker - normal velocity
yFlown','Fontsize',12);
xlabel('Frequency [Hz]','Fontsize',10);
ylabel('velocity [m/s/V]','Fontsize',10');
legend ('Transfer Function x1y1 (Exciter)','Transfer Function x2y2
(Loudspeaker)');
grid on;
subplot(2,1,2);
plot(F,SNR_part1,'b')
hold on;
plot(F,SNR_part2,'r')
xlim([0 1000]);
title ('Signal to Noise Ratio','Fontsize',12);
xlabel('Frequency [Hz]','Fontsize',10);
ylabel('SNR [dB] ','Fontsize',10');
legend ('System influence abs(H1)^2/abs(H2)^2','Input influence
Sxx/Syy');grid on;
grid on;
```

Appendix J: MATLAB CODE – Calculation of the errors

```
close all;
clc;
clear all;
%dB-Plot auto spectral density 3 cases
% - no BGN
% - 68dB BGN
% - 82db BGN
%Daniel Sadra
%
%3. September 2013
%
%================================================
delta_x=0.001;          % 1 mm Abstand
c=340      ;            % 340 m/s schallgeschw.

%% Einlesen der Dateien (distance 1mm)
% 1. Acc - vn -> NO BGN (Measurement 41)
wavread '41_acc';          %Signal des Acc
x1=ans;
wavread '41_vel2';         %Signal der Normalschnelle
y1=ans;
% 2. Acc - vn -> 68dB  BGN (Measurement 80)
wavread '80_acc';          %Signal des Acc
x2=ans;
wavread '80_vel2';          %Signal der Normalschnelle
y2=ans;
% 3. Acc - vn -> 82dB  BGN (Measurement 89)
wavread '89_acc';          %Signal des Acc
x3=ans;
wavread '89_vel2';          %Signal der Normalschnelle
y3=ans;

%% Berechnung der beiden Transferfunktionen
%Berechnung der Transferfunktion 1
[Tx1y1,F]= tfestimate(x1,y1,[],[],44000.0,44000.0);
%Berechnung der Transferfunktion 2
[Tx2y2,F]= tfestimate(x2,y2,[],[],44000.0,44000.0);
%Berechnung der Transferfunktion 3
[Tx3y3,F]= tfestimate(x3,y3,[],[],44000.0,44000.0);

%% Microflown velocity sensor GREEN
fc1u_g=75*ones(22001,1);
fc2u_g=675*ones(22001,1);
fc3u_g=11692*ones(22001,1);
fc4u_g=77*ones(22001,1);
%% Microflown Filters
% Korrektur für 41_vel2
Tx1y1_LP1                =Tx1y1.*(sqrt(1+fc1u_g.^2./F.^2));
Tx1y1_LP1_LP4            =Tx1y1_LP1.*(sqrt(1+fc4u_g.^2./F.^2));
Tx1y1_LP1_LP4_LP3        =Tx1y1_LP1_LP4.*(sqrt(1+F.^2./fc3u_g.^2));
Tx1y1_LP1_LP4_LP3_LP2    =Tx1y1_LP1_LP4_LP3.*(sqrt(1+F.^2./fc2u_g.^2));
Tx1y1_corr = abs(Tx1y1_LP1_LP4_LP3_LP2);
% Korrektur für 80_vel2
Tx2y2_LP1                =Tx2y2.*(sqrt(1+fc1u_g.^2./F.^2));
Tx2y2_LP1_LP4            =Tx2y2_LP1.*(sqrt(1+fc4u_g.^2./F.^2));
Tx2y2_LP1_LP4_LP3        =Tx2y2_LP1_LP4.*(sqrt(1+F.^2./fc3u_g.^2));
Tx2y2_LP1_LP4_LP3_LP2    =Tx2y2_LP1_LP4_LP3.*(sqrt(1+F.^2./fc2u_g.^2));
Tx2y2_corr= abs(Tx2y2_LP1_LP4_LP3_LP2);
% Korrektur für 89_vel2
Tx3y3_LP1                =Tx3y3.*(sqrt(1+fc1u_g.^2./F.^2));
```

```
Tx3y3_LP1_LP4             =Tx3y3_LP1.*(sqrt(1+fc4u_g.^2./F.^2));
Tx3y3_LP1_LP4_LP3         =Tx3y3_LP1_LP4.*(sqrt(1+F.^2./fc3u_g.^2));
Tx3y3_LP1_LP4_LP3_LP2     =Tx3y3_LP1_LP4_LP3.*(sqrt(1+F.^2./fc2u_g.^2));
Tx3y3_corr= abs(Tx3y3_LP1_LP4_LP3_LP2);

%% uncorrected
figure;
plot(F,abs(Tx1y1.*(2*pi.*F))./20000,'b')
hold on;
plot(F,abs(Tx2y2.*(2*pi.*F))./22300,'r')
hold on;
plot(F,abs(Tx3y3.*(2*pi.*F))./25600,'g')
xlim([0 1000]);
% title ('level difference - accelerometer - normal velocity
yFlown','Fontsize',12);
xlabel('Frequency [Hz]','Fontsize',12);
ylabel('error [dB]','Fontsize',12');
legend ('no BGN','68dB BGN','82dB BGN');
grid on;
figure;
plot(F,20*log10(abs(Tx1y1.*(2*pi.*F))./20000),'b')
hold on;
plot(F,20*log10(abs(Tx2y2.*(2*pi.*F))./22300),'r')
hold on;
plot(F,20*log10(abs(Tx3y3.*(2*pi.*F))./25600),'g')
xlim([0 1000]);
% title ('level difference - accelerometer - normal velocity
yFlown','Fontsize',12);
xlabel('Frequency [Hz]','Fontsize',12);
ylabel('error [dB]','Fontsize',12');
legend ('no BGN','68dB BGN','82dB BGN');
grid on;

%% corrected
figure;
plot(F,abs(Tx1y1_corr.*(2*pi.*F))./20000,'b')
hold on;
plot(F,abs(Tx2y2_corr.*(2*pi.*F))./22300,'r')
hold on;
plot(F,abs(Tx3y3_corr.*(2*pi.*F))./25600,'g')
xlim([0 1000]);
ylim ([0 2.5]);
% title ('level difference - accelerometer - normal velocity yFlown
corrected','Fontsize',12);
xlabel('Frequency [Hz]','Fontsize',12);
ylabel('error [dB]','Fontsize',12');
legend ('no BGN','68dB BGN','82dB BGN');
grid on;
figure;
plot(F,20*log10(abs(Tx1y1_corr.*(2*pi.*F))./20000),'b')
hold on;
plot(F,20*log10(abs(Tx2y2_corr.*(2*pi.*F))./22300),'r')
hold on;
plot(F,20*log10(abs(Tx3y3_corr.*(2*pi.*F))./25600),'g')
xlim([0 1000]);
% title ('level difference - accelerometer - normal velocity yFlown
corrected','Fontsize',12);
xlabel('Frequency [Hz]','Fontsize',12);
ylabel('error [dB]','Fontsize',12');
legend ('no BGN','68dB BGN','82dB BGN');
grid on;

%% Frequenzschleife
```

```
%%%%%%%%%%%%%%%%%%%%%%%%%%%%%%%%%%%%%%%%%%%%%%%%%%%%%%%%%%%%%%%%%%%%%%%%%%%%
Nf=22001;                       %Number of freq.
Fstep=1;                      %Frequency steps
%%%%%%%%%%%%%%%%%%%%%%%%%%%%%%%%%%%%%%%%%%%%%%%%%%%%%%%%%%%%%%%%%%%%%%%%%%%%
FreqV=1:Fstep:Nf*Fstep;       %Frequentvector
for i=1:Nf;
  nue=FreqV(i)     ;               %excitation frequency in Hzend

  bez_delta_x(i)=delta_x*nue/c;
end

%% uncorrected
figure
[AX,H1,H2] = plotyy(F,20*log10(1-
abs(Tx1y1.*(2*pi.*F)./20000)),FreqV,bez_delta_x);
xlim(AX(1),[0 1000]);
xlim(AX(2),[0 1000]);
axis([AX(1)],[0 1000 -80 40]);
axis([AX(2)],[0 1000 0 0.01]);
% title ('error in dB for 1mm measurement distance','Fontsize',14);
xlabel('Frequency [Hz]','Fontsize',12);
set(get(AX(1),'Ylabel'),'String','rel. error in [dB]')
set(get(AX(2),'Ylabel'),'String','1 mm/lambda [-]')
legend ('error in dB',' 1mm/lambda','Location','NorthEast');
grid on;

figure
plot(F,20*log10(1-abs(Tx1y1.*(2*pi.*F))./20000));
% axis([AX(2)],[0 1000 -30 -100]);
% title ('error in dB for 1mm measurement distance','Fontsize',14);
xlabel('Frequency [Hz]','Fontsize',12);
ylabel('rel. error [dB]','Fontsize',12');
legend ('rel. error in dB','Location','NorthEast');
grid on;
xlim([0 1000]);

%% corrected
figure
[AX,H1,H2] = plotyy(F,20*log10(1-
abs(Tx1y1_corr.*(2*pi.*F)./20000)),FreqV,bez_delta_x);
xlim(AX(1),[0 1000]);
xlim(AX(2),[0 1000]);
axis([AX(1)],[0 1000 -80 40]);
axis([AX(2)],[0 1000 0 0.01]);
% title ('error in dB for 1mm measurement distance','Fontsize',14);
xlabel('Frequency [Hz]','Fontsize',12);
set(get(AX(1),'Ylabel'),'String','rel. error in [dB]')
set(get(AX(2),'Ylabel'),'String',' 1 mm/lambda [-]')
legend ('error in dB',' 1mm/lambda','Location','NorthEast');
grid on;

figure
plot(F,20*log10(1-abs(Tx1y1_corr.*(2*pi.*F))./20000));
% axis([AX(2)],[0 1000 -30 -100]);
% title ('error in dB for 1mm measurement distance','Fontsize',14);
xlabel('Frequency [Hz]','Fontsize',12);
ylabel('rel. error [dB]','Fontsize',12');
legend ('rel. error in dB','Location','NorthEast');
grid on;
xlim([0 1000]);
```

Appendix K: Plots of errors (SNR and BGN) without filter for Microflown

These plots exclude the filters for the sensitivity of the Microflown compared to figure 4-16 and figure 4-17.

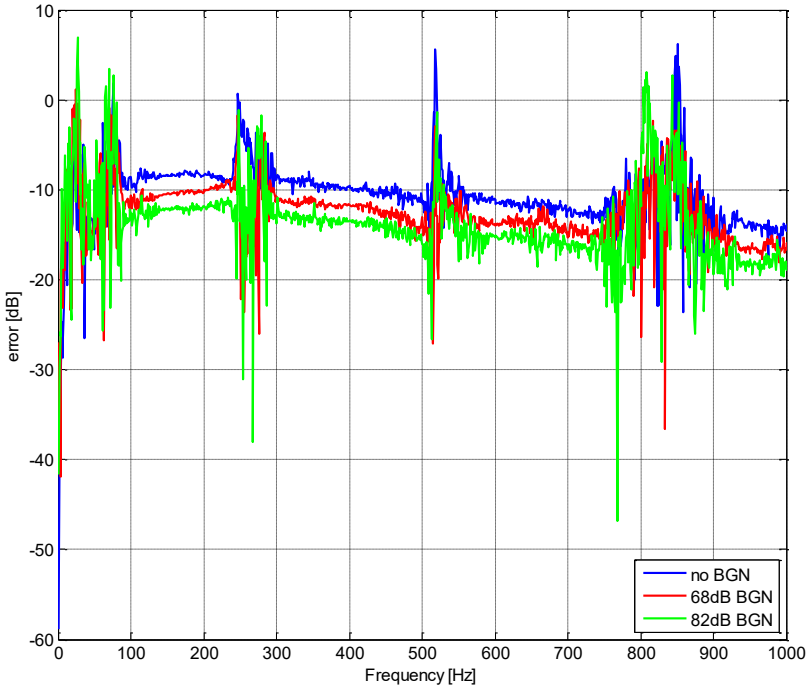

Figure K-1 Error for measurements with/without BGN - no filter

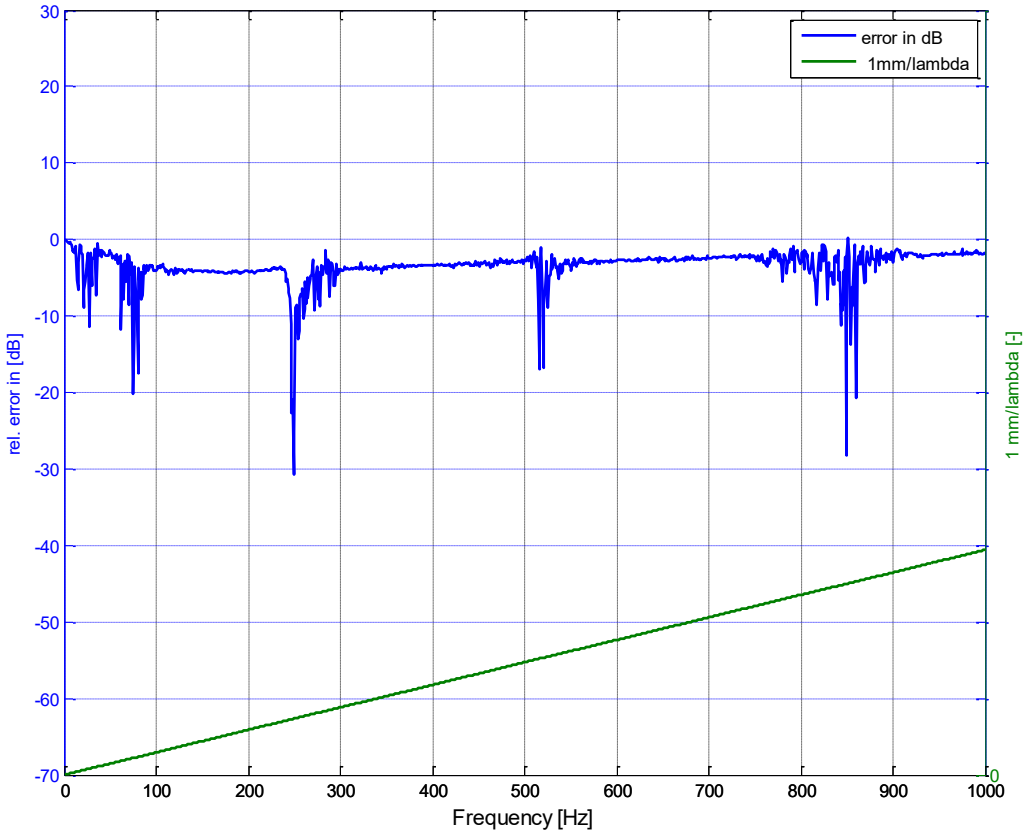

Figure K-2 Relative error for nominal case - no filter

Appendix L: Data disc

The following documents can be found on this data disc:

(1) Master's thesis in .pdf format,

(2) Datasheets of the equipment, which has been used for the various measurements,

(3) References which have been used,

(4) MATLAB Codes.